



METAL AND METAL-SULPHIDE CONTAINING CARBONS FROM SULPHONATED STYRENE-DIVINYLBENZENE COPOLYMER BASED ION-EXCHANGERS

László Kótai^{[a]*}, Tibor Pasinszki^[b], Zsuzsanna Czégény^[a], Szabolcs Bálint^[a],
István Sajó^[a], Zoltán May^[a], Péter Németh^[a], Zoltán Károly^[a], Pradeep K. Sharma^[c],
Vinita Sharma and Kalyan K. Banerji^[d]

Keywords: metal-containing activated carbons; waste ion-exchangers; carbonization; metal/metal compound-carbon composites; sulphonated styrene-divinylbenzene copolymers

A temperature controlled carbonization process (5-800 °C for 1-4 h) of metal forms of different kinds of partially or totally saturated sulphonated styrene-divinylbenzene copolymer based ion-exchangers loaded with various valence state metal ions has been evaluated. The effect of temperature, nature and valence of metal ions, crosslinking and other parameters on the composition and properties of the formed composites have been evaluated. Depending on the ionic form and the saturation degree of the ion exchangers the sulphur content of the ion-exchangers can partially transform into metal sulphides, SO₃ or SO₂. Ni(II), Mn(II) and Zn(II) forms of the ion-exchangers resulted the appropriate MⁿS type metal sulphides (NiS, MnS or ZnS), while copper(II) resulted metallic copper formation at 500 °C in 2 h. Both iron(II) and iron(III) forms of sulphonated styrene-divinylbenzene copolymers resulted Fe_{0.95}S and α-Fe formation at 800 °C for 2 h, however, the ratio of these compounds depended on the valence state of iron and were found to be 8:1 and 7:2 in the case of Fe(III) and Fe(II)-forms, respectively. The shape of the formed carbon particles are bead-like and the hardness of the formed carbon beads proportional with the divinylbenzene content of the starting polymer. The higher divinylbenzene content the harder beads of carbon forms. All the beads have a leak due to evolution of gases which emitted at the weakest part of ball-like bead. The ball-like metal-containing activated carbon beads have low hydrodynamic resistance towards fluid streams and this carbonisation method can be used as an environmentally friendly way for processing of waste ion-exchangers into industrially usable carbon based metallic containing composites.

* Corresponding Authors

Tel: 00-36-70-2440001

E-Mail: kotail@chemres.hu

[a] Research Centre for Natural Sciences, Hungarian Academy of Sciences, Budapest, H-1025, Pusztaszeri u. 59-67.

[b] Department of Inorganic Chemistry, Institute of Chemistry, Eötvös Loránd University of Sciences, Budapest, Pázmány Péter sétány 1/A, H-1117, Hungary

[c] Department of Chemistry, J. N. V. University, Jodhpur, Rajasthan, 342005, India.

[d] Faculty of Science, National Law University, Mandore, Jodhpur 342304, India

experiments performed with sulphonic acid type active group containing styrene-divinylbenzene copolymers loaded with various valence state metal ions and containing different amount of crosslinking agent (divinylbenzene) are presented.

Experimental

Synthesis of metal-loaded ion-exchangers were performed in column experiments with H⁺-forms of the sulphonic acid type ion-exchangers (Varion KS, Varion KSM, Varion KS660 and Lewatit P100). The columns were filled with 100 g of the ion-exchangers and activated with the saturated aqueous solutions of zin(II) sulphate, manganese(II) nitrate, iron(II) chloride, iron(III)-chloride, zinc(II) sulphate, nickel(II) sulphate and copper(II) sulphate until complete saturation. All saturation experiments were performed at room temperature. The activated resins contained homogeneously distributed metal loading at the active groups were washed with distilled water and dried in open air overnight. The partially saturated saturated ion-exchangers were prepared by using method of Somogyi et al.³

The carbonisation experiments were performed between 500 and 800 °C for 1-4 h under flowing N₂ in an 50 cm long quartz tube. Metal content of the composites were determined by inductively coupled plasma (ICP) emission spectrometric measurements with an Atomscan 25 (Thermo Jarrel Ash) spectrometer after digestion of carbonized samples in 3:1 cc. HCl:HNO₃ mixture for 24 h.

X-ray powder diffraction measurements were performed by means of a Philips PW-1050 Bragg-Brentano

Introduction

Numerous metal or metal-compound loaded carbon composites have already been synthesized, and studied in various chemical processes as catalysts, chemisorbents or reactive materials.¹ The preparation of these composites generally based on adsorption/chemisorption of a particular metal compounds which is transformed into the active ingredients on the surface of the carbon, or a mixture of carbon precursors and metal compounds are carbonized together. These processes generally give heterogeneous composites which properties hardly controlled or can be adjusted only in separated processes. In order to solve these problems a simple method has been introduced to prepare metal-loaded activated carbons with unique features and homogeneous metal/metal compound loading.

We have developed a simple method for preparation of iron(II) oxide containing carbon supported catalysts of paracetamol production² based on the temperature controlled carbonization of iron form of a carboxylate type iron(III)-ion saturated ion-exchanger polymer. In this communication, the preliminary results obtained in the analogous

parafocusing goniometer, equipped with a secondary beam graphite monochromator and proportional counter; scans were recorded in step mode by using CuK_α radiation at 40 kV and 35 mA tube power. Evaluation of the diffraction patterns have been obtained by full profile fitting techniques.

TG-MS measurements were accomplished by a STD 2960 Simultaneous DTA/TGA (TA Instruments) + Thermostat GSD 200 Q-MS (Balzers) device with 5 °C heating rate in Ar flow.

SEM measurements were performed with a Hitachi S-570 scanning electron microscope equipped with a Rontec EDR 288 detector.

BET surface areas were determined from N_2 adsorption-desorption isotherms with using a Quantachrome AUTOSORB-1 instrument.

Results and Discussions

Preparation of metal-containing ion-exchangers were performed in an usual way with loading of hydrogen forms of sulphonated ion exchangers with using saturated aqueous metal salt solutions.³ The carbon composites were prepared by controlled temperature carbonization (5-800 °C for 1-4 h) of the metal forms of various styrene-based ion exchangers. The carbonization temperatures were adjusted on the basis of the TG-MS results, and the optimal carbonisation time was found to be 2 h. Depending on the ionic form and the saturation degree of the ion exchanger the sulphur content of the ion-exchangers can partially transform into metal sulphides, SO_3 or SO_2 which could be detected by TG-MS unambiguously. The yield of metal/metal sulphide containing carbon composites strongly depends on the nature of metal, ion-exchanger and the carbonisation conditions as well.

The sulphonated styrene-divinylbenzene copolymers are the most frequently used cation exchangers used which results a large amount of waste ion-exchangers. Fully (100 %) and partially saturated forms (25 and 50 % of their capacity) of Varion KS and Varion KSM resins were carbonised at 500 °C for 2 h. Depending on the nature of metal, sulphide (MnS , NiS and ZnS , $\text{FeS}_{0.95}$) species or elemental metal (Cu , $\alpha\text{-Fe}$) were formed. In case of iron, $\text{Fe}_{0.95}\text{S}$ and $\alpha\text{-Fe}$ were formed together at 800 °C, the sulphide component was the major product, however the ratio of $\text{Fe}_{0.95}\text{S}:\alpha\text{-Fe}$ depended on the valence form (Fe^{II} or Fe^{III}) of the iron loaded onto the ion exchanger resin.

The saturation degree has no important effect on the chemical form of the metal in the composites formed at the studied temperature range. The shape of the formed carbon particles is bead-like (Fig.1.), and the hardness of the formed carbon beads proportional with the divinylbenzene content of the starting polymer, the higher divinylbenzene content the harder beads of carbon formed. All the beads have a leak due to evolution of gases which are emitted at the weakest part of ball-like bead causing leaking. Due to evolution of large amount of gases within the structure of beads which evolve at the moment when the resistance of the resin material becomes lesser than the inner pressure, an "explosion-like" emitting of gases (SO_2 , H_2O , hydrocarbon crack gases) could be observed, and the resin beads "jump"

during the carbonization. The formed ball-like metal-containing activated carbon beads have low hydrodynamic resistance towards fluid streams and these materials are potential candidates for treatment of liquid flows.

The SEM picture of the nickel-carbon composite with ca. 30 % nickel content can be seen in Fig.1.

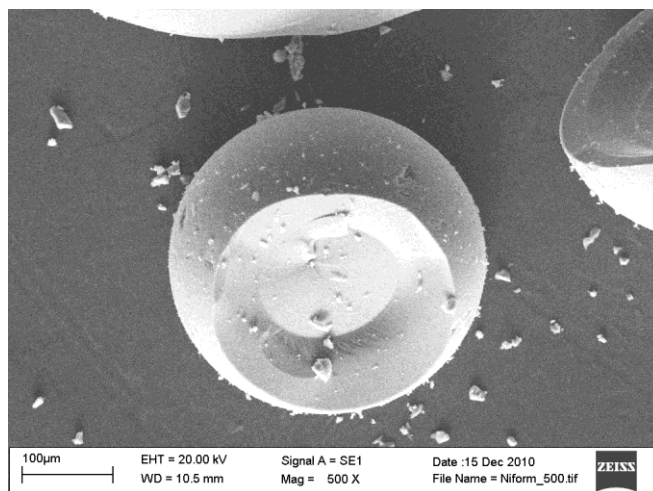


Figure 1. SEM picture of the nickel sulphide containing carbon composite bead prepared from Lewatit S100 (8 % divinylbenzene content) loaded fully with $\text{Ni}(\text{II})$ at 500 °C for 2 h

The bead-like resins formed in the pyrolysis of Lewatit S100 resin contained 2.3 mekv g^{-1} nickel(II) resulted a carbon composite of NiS with 35 % nickel content. The specific surface area was found to be 371 m^2g^{-1} , but the specific surface area strongly depends on the pyrolysis temperature and the divinylbenzene content (porosity) of the starting ion exchanger. The specific surface areas of nickel sulphide containing carbons formed at 500 °C in 2 h in the case of Varion KS and KS660 resins were found to be 172 and 341 m^2g^{-1} , respectively.

Two kinds of iron form (Fe^{II} and Fe^{III} loaded) of Varion KSM resins were carbonised at 800 °C for 2 h. The same products were formed, $\text{Fe}_{0.95}\text{S}$ and metallic iron ($\alpha\text{-Fe}$), however, the ratio of these products depended on the valence of the iron loaded on the ion-exchanger. The approx. ratio of iron sulphide/ $\alpha\text{-Fe}$ were found to be 8:1 and 7:2 in the case of Fe^{III} and Fe^{II} forms of the Varion KSM ion exchanger, respectively. It can be the consequence of the oxidizing nature of Fe^{III} which partially prevents the complete reduction of sulphonic acid group into sulphide.

The metal or metal-compound containing activated carbons can be activated with vapour or other methods and their metal content can also be removed by acidic treatment, e.g. with digestion in dilute HCl or HNO_3 . The formed metallic salt solutions can be recycled into loading new ion exchangers into metallic forms, and the formed carbons can be utilized as simple activated carbons as well.

This method can be candidate as an environmentally friendly way to transform the waste ion-exchangers into useful materials. The acidic or oxidative acidic leaching of the metal-containing species formed during the chemisorption leads to activated carbons with acidic and oxidized surface characteristics.

Conclusion

Ion-exchanger materials, particularly sulphonated styrene-divinylbenzene copolymers can be transformed into metal/metal sulphide composites at 500-800 °C in 1-4 h. These composite materials can be used as catalyst or chemisorbents (with or without further activation) in various technological processes. The systematic investigation of the effect of functional groups, divinylbenzene content, the composition of polymer chain, temperature, reaction time and other factors are in progress. Further studies on the utilization of various metal-containing activated carbon composites prepared in this way, and their transformation with acidic or oxidative acidic leaching into activated carbons are in progress.

Acknowledgement

We express our thanks to the National Development Agency and MAG Zrt. (Magyar Gazdaságfejlesztési Központ Zrt., 1139 Budapest, Váci út 81-83.) who supplied the “Activated Carbon Production from Waste Ion Exchangers at the Axial Chem Ltd.” project (GOP 1.1.1.-09/1-2009-0081) of Kemobil Co. (Tata, 2890, Agostyáni út 81). The project is supported by the European Union and co-financed by the European Regional Development Fund.

References

- ¹Cui, H., Turn, S. Q. *Appl. Catal. B: Environmental* **2009**, 88(1-2), 25-31; Marban, G., Antuna, R., Fuertes, A. B., *Appl. Catal. B: Environmental*, **2003**, 41(3), 323-338; St. Tsoncheva, T., Nickolov, R. N., Neinska, Y. G., Minchev, C. I., Mehandjiev, D. R., *Bulg. Chem. Comm.* **2000**, 32(2), 218-229; Yamamoto, O., Sawai, J., *Bull. Chem. Soc. Japan* **2001**, 74(9), 1761-1765; Mondal, P., Mohanty, B., Majumder, C. B. *Can. J. Chem. Eng.* **2009**, 87(5), 766-778; Chiang, H.-L., Huang, C. P., Chiang, P. C., You, J. H., *Carbon* **1999**, 37(12), 1919-1928; Lee, J.-J., Suh, J.-K., Hong, J.-S., Lee, J.-M., Lee, Y.-S., Park, J.-W., *Carbon* **2008**, 46(13), 1648-1655.
- ²Sreedhar, B., Bhaskar, V., Sridhar, C., Srinivas, T., Kotai, L., Szentmihályi, K., *J. Mol. Catal. A-Chem.*, **2003**, 191(1) 141-147.
- ³Somogyi, I., Kótai, L., Angyal, A. Report **2012**, *Activated Carbon Production from Waste Ion Exchangers at the Axial Chem Ltd*, GOP 1.1.1.-09/1-2009-0081.

Received: 10.10.2012
Accepted 20.10.2012.



INVESTIGATION OF EFFECTS OF TWO ENVIRONMENTAL HEAVY METALS IN A COMBINED EXPOSURE MODEL ON THE NERVOUS SYSTEM IN RATS

A. Papp^{[a]*}, E. Horváth^[a], Zs. Máté^[a], A. Szabó^[a]

This paper was presented at the 4th International Symposium on Trace Elements in the Food Chain, Friends or Foes, 15-17 November, 2012, Visegrád, Hungary

Keywords: Manganese, lead, neurotoxicity, cortical activity, open field, nanoparticles, rat.

In the present study, the interaction of inhalational and oral exposure to manganese and lead was investigated. Young adult male Wistar rats (2 x 10 per group) were treated orally with MnCl₂ (15 and 60 mg/kg b.w.) or Pb acetate (80 and 320 mg/kg) for 3 or 6 weeks. Then, one half of the groups was further treated by intratracheal instillation of nanoparticulate MnO₂ (2.63 mg/kg) or PbO (2 mg/kg) for an equal period of time. Body weight gain and signs of general toxicity were regularly checked. Finally, the rats' motor behavior was tested in an open field box, and their spontaneous and evoked cortical electrical activity was recorded in urethane anesthesia. MnO₂ nanoparticles caused disproportionately strong reduction of body weight gain but with Pb the weight effect was more dependent on dose. In the open field test, Mn caused hypomotility, more strongly after 6 weeks oral plus 6 weeks intratracheal than after 6 weeks oral treatment. Pb-treated rats showed increased ambulation but less rearing and somewhat longer local activity. Spontaneous cortical activity was shifted to higher frequencies after oral Mn application, but this change was not intensified by subsequent nanoparticle application. Oral Pb had an opposite effect. Cortical evoked potentials showed latency lengthening. In several cases, the effect of Mn and Pb was about as strong after 3 weeks oral plus 3 weeks intratracheal as after 6 weeks oral administration, although the summed dose was ca. two times lower in the former case. There can be a more-than-additive interaction between the amounts of heavy metals entering the organism in different routes and chemical forms.

* Corresponding Author

Fax: +36-62-545-120

E-Mail: papp.andras@med.u-szeged.hu

[a] Department of Public Health, University of Szeged Faculty of Medicine, 6720 Szeged, Dóm tér 10.

Introduction

Chemical risk, resulting from application of metal-based and other xenobiotics, is a major problem of our days. Numerous metals are regarded as xenobiotics because they either are completely useless and toxic for the human organism (e.g. mercury, lead or cadmium) or are essential micronutrients but toxic when overdosed (manganese, chromium, copper, etc.).

Exposure to heavy metals is mostly occupational. Metal-containing dusts and fumes are generated along the complete life cycle of metal products (e.g. during welding¹), and can be found in the workplace atmosphere, causing exposure primarily via inhalation. The resulting internal dose is influenced by chemical form and size of the suspended particles. In the last 20 years nanoparticles (NPs) and their interaction with living organisms, raised health concerns². Combustion processes and working on materials at high temperature generate NPs (particles which are smaller than 100 nm at least in one dimension), their composition being determined by the materials worked on or burnt. Likewise, manufactured nanomaterials contain at least one component with at least one dimension in the 1-100 nm range.

Inhaled NPs are either deposited in the nasopharynx or get down to the alveoli³. NPs are not held back by biological barriers like alveolar and capillary wall, are distributed throughout the body by blood circulation, and reach distant target organs including the central nervous system. The NPs' small size and large specific surface area, together with the high numbers of NPs entering the organism in a typical exposure situation, result in great biological and pathogenetical activity².

Apart from inhalation, the second most important route of exposure to heavy metals is ingestion. Airborne particles can be ingested directly; dust can contaminate food or drink, etc. Metals from the sedimenting dust can be incorporated into edible parts of cultivated plants, either directly or via soil pollution (as it happened near the metal reprocessing plant Metallokémia in Budapest⁴). Ingested heavy metals are absorbed in the intestine mostly to ca. 10%. Common metal transport mechanisms, responsible for the uptake of essential metals, are involved, which explains that individuals with increased calcium or iron demand absorb more of the toxic metals. Toxic metals are transported as "free-riders" not only from the intestine to the blood but also from the blood to the central nervous system (CNS). Trivalent metal ions, like Mn³⁺ use transferrin to pass the blood-brain barrier.

Based on practical importance and on previous experiences of our research group^{5,6,7}, lead and manganese were chosen for the present study.

Lead (Pb) has been a ubiquitous environmental pollutant for centuries, and is toxic even in low concentrations⁸. Primary production and reprocessing of Pb causes substantial emission of metal fumes. Neurological effects were observed in workers with chronic Pb exposure: headache, lethargy, dizziness, diminished reaction time, worsened cognitive and visuomotor performance, and reduced nerve conduction velocity⁹. The general population is exposed mainly by contaminated drinking water or food. Pb is accumulated in the central nervous system, first in the cortex and hippocampus¹⁰, and produces encephalopathy. Exposure to low concentrations of Pb has been associated with behavioral abnormalities, learning and hearing impairment and impaired cognitive functions in humans and in experimental animals¹¹. Some approximations suggest that, in exposed children, every 100 µg/L increase in blood Pb level is associated with a 1-5 point decrease in the IQ level¹², such an effect was observed also in Hungary¹³. Pb can also pass the placenta and cause serious damage to the nervous system before birth.

Manganese (Mn) is an essential micronutrient, e.g. as cofactor in metallo-enzymes. The human body contains about 10 mg Mn, stored mainly in the liver and kidneys. The daily demand is 2-3 mg¹⁴. Mn is used in many important alloys, so welding fumes and similar industrial emissions are also a source of Mn-containing NPs. Chronic inhalation of Mn-containing dust and fumes is the typical form of occupational exposure. The Mn-related chronic neurological disorder (manganism) starts with apathy, anorexia, headache, hypersomnia, weakness of the legs etc. and progresses to a Parkinson-like syndrome¹⁵. Such disorder was also observed in patients undergoing maintenance hemodialysis¹⁶ or in inadvertent oral overdosing of Mn. Thus, other physicochemical forms of Mn and other routes of exposure are also relevant to the health of the CNS. In several regions of the USA with Mn-rich drinking water, loss of visual and verbal memory, typical for Mn-induced brain damage, was described¹⁷. The neurotoxic spectrum of Mn is variable and goes beyond the classical manganism. In shipyard workers, EEG and visual evoked potential alterations were observed and elevated blood Mn levels were measured¹⁸.

The aim of this work was to model the complex (occupational and environmental) human exposure to Mn and Pb in rats as a model, with combined – oral and intratracheal – administration using dissolved and nanoparticulate form of the metals.

Methods

Animals and treatment

Young adult male Wistar rats (initial body weight 280–350 g) obtained from the Breeding Centre of the University, were used for the experiments.

The animals were housed under standard conditions (22–24°C, 12 h light/dark cycle with light on at 6:00 a.m., up to four rats in one cage) with free access to conventional pelleted feed and drinking water

Aqueous solution of Mn and Pb was given to the rats orally by gavage (per os, po.), while the suspension of the metals in NP form was instilled in the trachea (intratracheally, it.; for details see⁶).

Table 1 The substances used for treatment and the doses applied

Group code	Substance and dose (mg kg ⁻¹ b.w.)	Treatment time
MnC3	untreated	3 weeks
MnVC3	distilled water, per os	3 weeks
MnL3	MnCl ₂ ·4H ₂ O 15 mg kg ⁻¹ b.w. po.	3 weeks
MnH3	MnCl ₂ 60 mg kg ⁻¹ b.w. po.	3 weeks
MnC33	untreated*	6 weeks
MnVC33	distilled water, po. + HEC (hydroxyethyl cellulose) it.	3 weeks + 3 weeks
MnL33	MnCl ₂ 15 mg kg ⁻¹ b.w. po. + MnO ₂ NPs 2.63 mg kg ⁻¹ b.w. it.	3 weeks + 3 weeks
MnH33	MnCl ₂ , 60 mg kg ⁻¹ b.w. po. + MnO ₂ NPs 2.63 mg kg ⁻¹ b.w. it.	3 weeks + 3 weeks
MnC6	untreated*	6 weeks
MnVC6	distilled water, po.	6 weeks
MnL6	MnCl ₂ 15 mg kg ⁻¹ b.w. po.	6 weeks
MnH6	MnCl ₂ 60 mg kg ⁻¹ b.w. po.	6 weeks
MnC66	untreated	12 weeks
MnVC66	distilled water, po. + HEC it.	6 weeks + 6 weeks
MnL66	MnCl ₂ , 15 mg kg ⁻¹ b.w. po. + MnO ₂ NPs 2.63 mg kg ⁻¹ b.w. it.	6 weeks + 6 weeks
MnH66	MnCl ₂ , 60 mg kg ⁻¹ b.w. po. + MnO ₂ NPs 2.63 mg kg ⁻¹ b.w. it.	6 weeks + 6 weeks
Group code	Substance and dose (mg/kg b.w.)	Treatment time
PbC3	untreated	3 weeks
PbVC3	distilled water, po.	3 weeks
PbL3	Pb(CH ₃ COO) ₂ , 80 mg kg ⁻¹ b.w. po.	3 weeks
PbH3	Pb(CH ₃ COO) ₂ , 320 mg kg ⁻¹ b.w. po.	3 weeks
PbC33	untreated*	6 weeks
PbVC33	distilled water, po. + HEC it.	3 weeks + 3 weeks
PbL33	Pb(CH ₃ COO) ₂ , 80 mg kg ⁻¹ b.w. po. + PbO NPs 2 mg kg ⁻¹ b.w. it.	3 weeks + 3 weeks
PbH33	Pb(CH ₃ COO) ₂ , 320 mg kg ⁻¹ b.w. po. + +PbO NPs 2 mg/kg b.w. it.	3 weeks + 3 weeks
PbC6	untreated*	6 weeks
PBVC6	distilled water, po.	6 weeks
PbL6	Pb(CH ₃ COO) ₂ , 80 mg kg ⁻¹ b.w. po.	6 weeks
PbH6	Pb(CH ₃ COO) ₂ , 320 mg kg ⁻¹ b.w. po.	6 weeks
PbC66	untreated	12 weeks
PbVC66	distilled water, per os + HEC it.	6 weeks + 6 weeks
PbL66	Pb(CH ₃ COO) ₂ , 80 mg kg ⁻¹ b.w. po. + PbO NPs 2 mg kg ⁻¹ b.w. it.	6 weeks + 6 weeks
PbH66	Pb(CH ₃ COO) ₂ , 320 mg kg ⁻¹ b.w. po. + +PbO NPs, 2 mg kg ⁻¹ b.w. it.	6 weeks + 6 weeks

* C33 and C6 were always two different groups of rats.

Chemical identity and dose of the substances applied to the rats, along with treatment times, are given in Table 1. For intratracheal administration, the NPs were suspended in 1% hydroxyethyl cellulose dissolved in PBS (pH 7.4). This vehicle was physiologically neutral and slowed the aggregation of the NPs. There was one administration every workday (that is, 5 times a week); body weight was measured before every administration to determine the exact daily doses and to follow weight gain.

Behavioral investigation by the open field method

At the end of the treatment periods, open field (OF) test was done, in one 10-min session per rat, to assess their spontaneous locomotor activity. The test was performed between 8 and 11 hours in the morning, after 30 min adaptation to the dimly lighted test room. The instrument recorded the animal's horizontal and vertical motor activity, from which counts, time and run length of the activity forms (ambulation, local activity, immobility, rearing) were automatically calculated (for technical details and suitability, see⁷).

Electrophysiological investigation

The electrophysiological recording was done on the same day after the OF test or on the following day. The animals were anaesthetized by intraperitoneal injection of 1000 mg/kg b.w. urethane, and the left hemisphere was exposed by opening the bony skull. For recording, the rat was placed into the stereotaxic frame of the electrophysiological setup. Body temperature was maintained by the thermostated (+36.5°C) support plate. To record spontaneous and evoked cortical activity, a ball-tipped silver recording electrode was positioned on the dura over the primary somatosensory (SS) area. SS stimulation was done by a pair of needles inserted into the whiskery part of the nasal skin, delivering square electric pulses. The recording session started with six minutes recording of spontaneous activity (electrocorticogram, ECoG) first. From the ECoG records, the relative spectral power of the frequency bands. Then evoked potentials (EPs) from the same cortical site were recorded. Electrical stimulation of the whiskers was done by delivering rectangular electric stimuli (3-4 V, 0.05 ms). Trains of 50 stimuli were applied, one each with 1, 2 and 10 Hz frequency. Individual EPs were automatically averaged, and their latency and duration was measured manually.

From the general toxicological, behavioral and electrophysiological data, group mean values (\pm SD) were calculated. All results were checked for normality by means of the Kolmogorov-Smirnov test, then were tested for significance using one-way ANOVA with post hoc LSD test by the SPSS 15.0 for Windows software package. Significance was accepted at $p < 0.05$. During the whole study, the principles of the Ethical Committee for the Protection of Animals in Research of the University were strictly followed. The authority competent in animal welfare issues licensed the methods used in the experiments under No. XXI./02039/001/2006.

Results

Body weight gain

Oral Mn treatment had minimal effect on body weight; but as soon as it, administration of Mn NPs started, the weight gain in the treated groups got substantially slower than either in the vehicle-treated (MnVC; Fig. 1) or untreated (MnC, not shown) control. Oral Pb had visible effect on body weight gain from the 4th week on (Fig. 1) but switching to it, administration on the 6th week caused also here a marked drop.

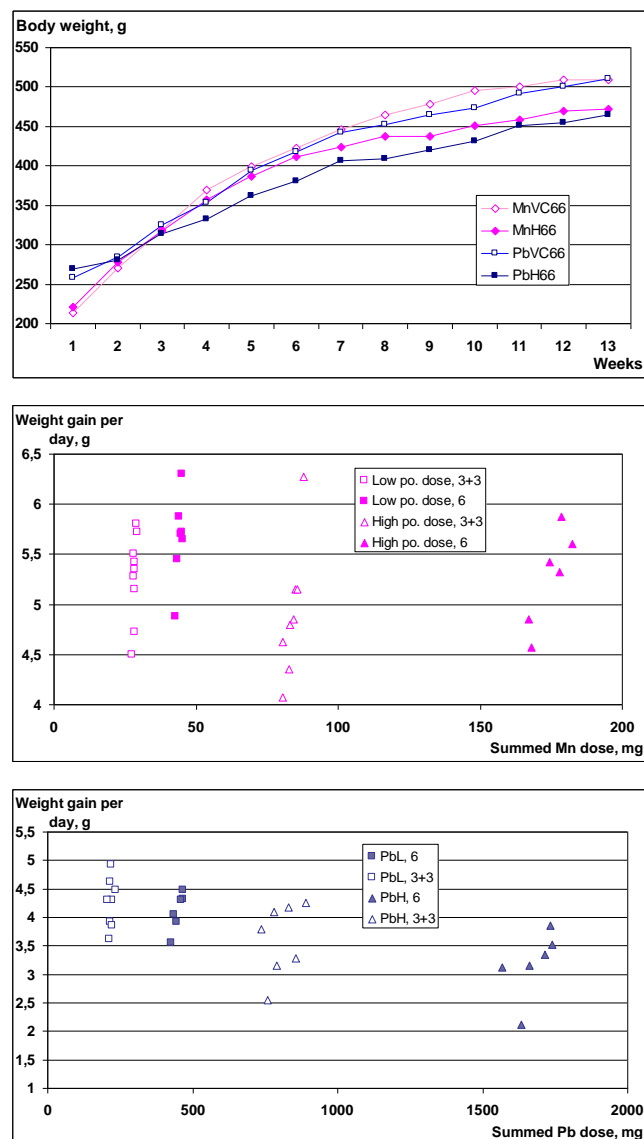


Figure 1. Top: body weight curves of high dose Mn and Pb treated rats and the corresponding controls. Middle and bottom: relationship of metal dose and weight gain. See Table 1 for group coding and doses.

The relationship between weight gain and summed dose was dissimilar: for Mn it was more influenced by the form (NP vs. dissolved) but for Pb, more by the summed dose.

Open field motility

Noteworthy changes in OF motility were seen only after 6 and 6+6 weeks of metal exposure (Fig. 2). Mn decreased ambulation and rearing (the latter, only after 6+6 weeks) and increased local activity and immobility. Pb caused increased ambulation but decreased rearing.

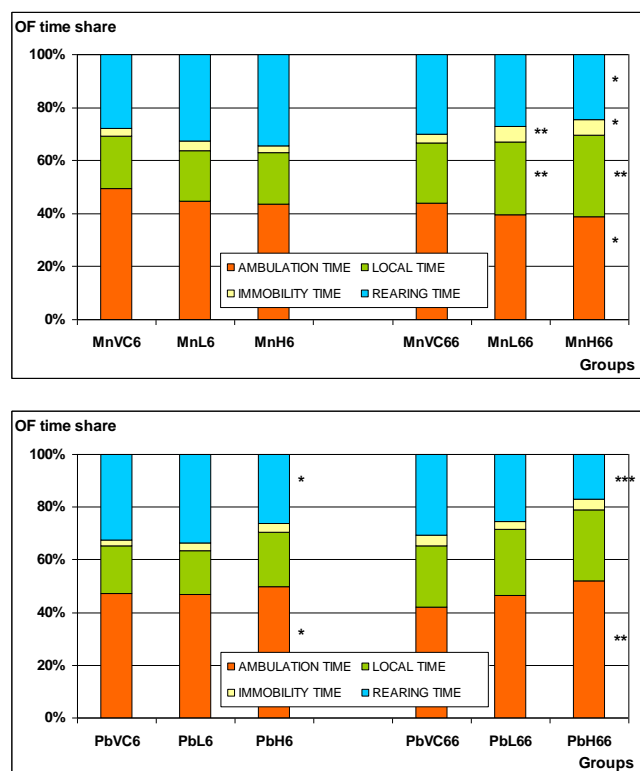


Figure 2. Time share of the four open field activity forms in the total session time (top, Mn treated; bottom, Pb treated rats). *, **: $p < 0.05$, 0.01 vs. VC.

Cortical electrical activity

The general trend in the electrocorticogram (ECoG) band spectra on Mn effect was decrease in the delta, and increase in the theta and in the fast (beta, gamma) bands. Similarly to the OF effects, these changes were relatively more pronounced only after 6 and 6+6 weeks Mn treatment (Fig. 3). After 6 weeks oral Pb treatment, increased slow and decreased fast ECoG activity was seen, compared to the control **PbVC6**. However, in the rats receiving 6+6 weeks Pb exposure, this frequency shift disappeared.

Latency of the SS EP was increased by Mn (Fig. 4). This increase was seen at all stimulation frequencies but the slope of frequency dependence of the latency (a possible indicator of metal-induced cortical fatigability) was not much altered.

Latency lengthening was of similar magnitude in **MnL33** and **MnL6** (and was only slightly more different in **MnH33** vs. **MnH6**) in spite of the dissimilar summed dose, in accordance with the relationship of summed Mn dose and body weight (Fig. 1).

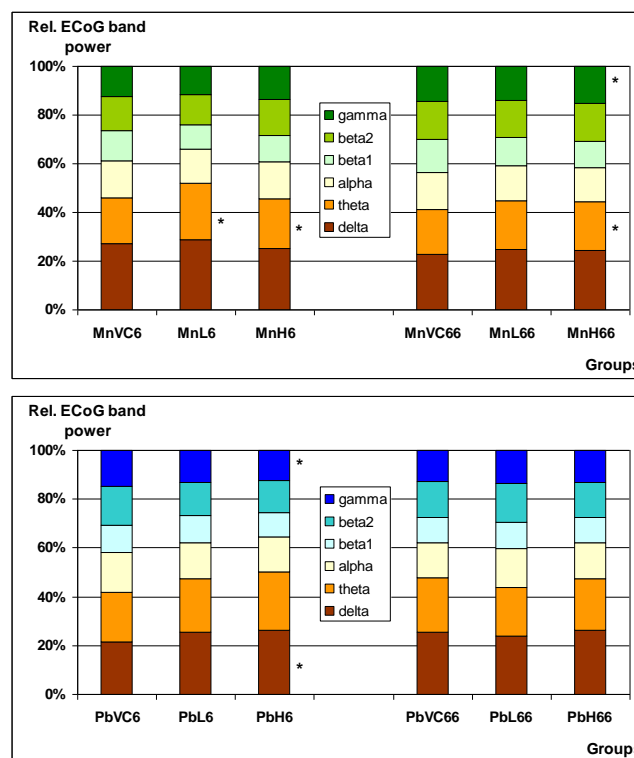


Figure 3. Band spectrum of the spontaneous activity recorded from the somatosensory cortex of rats after 6 and 6+6 weeks of Mn (top) and Pb (bottom) exposure. *: $p < 0.051$ vs. VC

Latency of the SS EP was increased in the Pb-treated rats (Fig. 5). The change was significant vs. vehicle control in rats with 3+3, 6 and 6+6 weeks treatment. The change in **PbH33** and **PbH6** was nearly equal, and in **PbL33** somewhat bigger than in **PbL6**; indicating that the NP form could have disproportionately strong effect on the nervous system (but not on body weight, see Fig. 1) also in case of Pb. In **PbH33** and **PbH66**, the frequency dependent lengthening of latency became also more intense.

Discussion

General and neuro-functional parameters indicated repeatedly that there could be a non-additive interaction between the amounts of heavy metals given by po. and it, application.

In Mn exposure, the disproportionately strong effect of NPs was seen on the body weight gain, a general toxic parameter. Metal level data from previous comparable experiments^{6,7} suggest that inhaled NPs cause internal exposure more efficiently than ingested, dissolved metals. Pb is known to affect BBB¹⁹, which may explain that, among the Pb-treated rats, lengthening of SS EP latency was nearly equal in **PbH33** and **PbH6**, despite the ca. twice higher summed dose in the 6 weeks po. Pb administration.

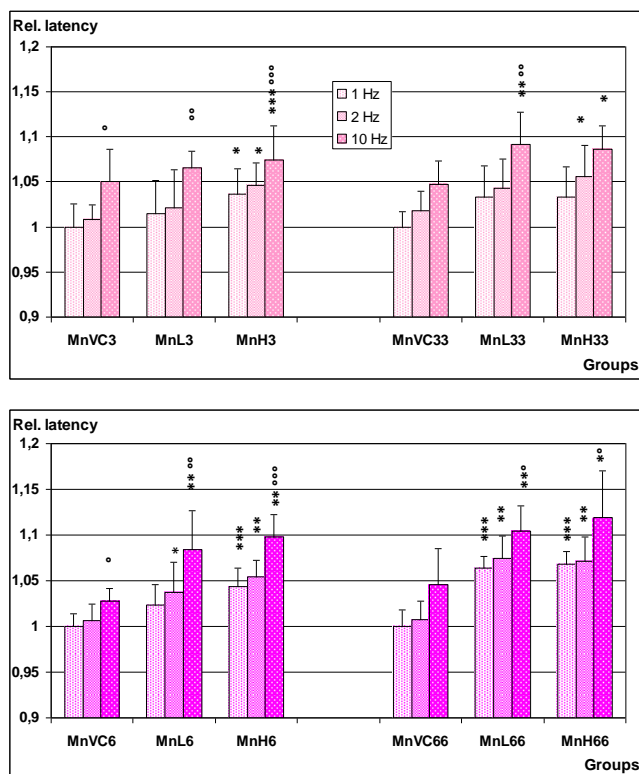


Figure 4. Latency of the somatosensory evoked potential in Mn treated rats (relative values normalized to VC, 1 Hz).
 *, **, ***: $p < 0.05, 0.01, 0.001$ vs. VC
 °, °°, °°°: $p < 0.05, 0.01, 0.001$ vs. 1 Hz stimulation within the same group.

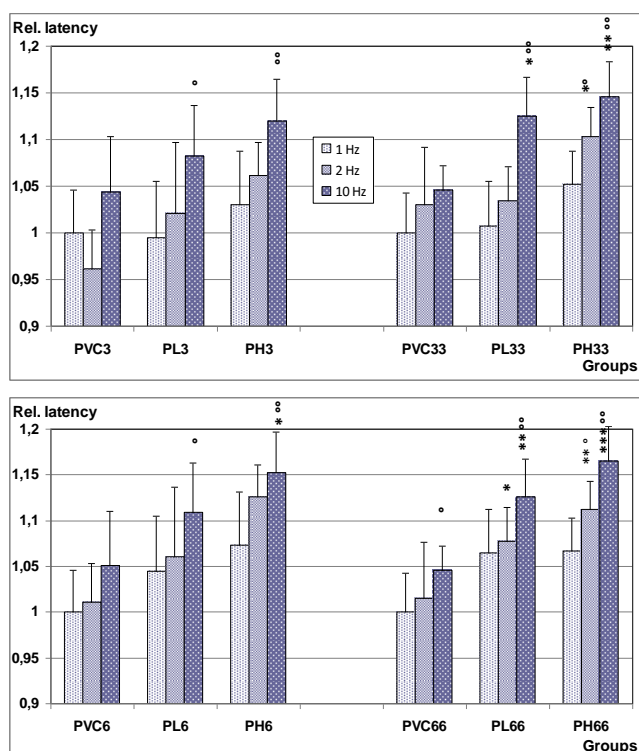


Figure 5. Latency of the somatosensory evoked potential in Pb treated rats (relative values normalized to VC, 1 Hz).
 *, **, ***: $p < 0.05, 0.01, 0.001$ vs. VC
 °, °°: $p < 0.05, 0.01$ vs. 1 Hz stimulation within the same group.

Metal NPs are always likely to cause oxidative stress. Metabolites indicating oxidative damage upon Pb exposure were detected in humans²⁰. Generation of reactive oxygen species was detected in the brain in case of both Mn and Pb, resulting in membrane lipid peroxidation^{20,21}, leading to changes of membrane functions, such as synaptic transmission, which may be reflected in various forms of cortical activity.

Increased latency in the rats treated with both metals might be, at least partly, due to decreased synaptic efficiency. Pb^{2+} and Mn^{2+} ions block the voltage-gated Ca-channels in presynaptic endings, impeding this way intracellular Ca^{2+} rise and depolarization on arrival of an axonal discharge, and preventing synchronous emptying of vesicles. Inside, however, both ions can activate a number of Ca-dependent processes including those involved in exocytosis, so the spontaneous release of the transmitter will be more likely^{22,23}.

Glutamate, the main excitatory transmitter in the CNS, is neutralized by uptake in astrocytes and conversion to glutamine; and this uptake is decreased by Mn²⁴ and Pb²⁵. Excess glutamate may desensitize the postsynaptic receptors leading finally to smaller/slower cortical evoked responses. Altered glutamatergic excitation, and energetic shortage from mitochondrial effect of the metals, might have opposite effect on the ECoG spectrum. The resulting net change was in fact different depending on the relative strength of the two opposite influences.

The changes in open field motor behavior may result from the general CNS effects, but even more from the dopaminergic effects, of the metals or NPs. Motivation, determining OF activity, is regulated by mesolimbic/mesocortical dopaminergic structures. Dopaminergic neurons are especially vulnerable to oxidative stress, due to the auto-oxidizing tendency of dopamine and to the presence of monoamine oxidase producing hydrogen peroxide²⁶ and the metals investigated are known to cause oxidative stress as mentioned above. Decreased horizontal movements in-group **MnH66** is a feature of general hypomotility, possibly analogous to the Mn-exposed welders' syndrome²⁷. Increased locomotion of the Pb-treated rats may be analogous to the human "attention deficit hyperactivity disease" found more frequently among children with elevated blood Pb²⁸.

Conclusion

The attempt to model a complex metal exposure, coming both from environmental (food/waterborne) and occupational (inhalational) sources, was apparently successful. With respect to the general use and ubiquitous presence of metals, their health effects in general, and in particular the nervous system and other sensitive systems, are of primary concern. Occurrence of metals in nanoparticulate form, let it be nanotechnological materials or unwanted pollutants, adds a new feature to the old problem.

References

- ¹Antonini, J.M., Lewis, A.B., Roberts, J.R. and Whaley, D.A. *Am. J. Ind. Med.*, **2003**, *43*, 350.
- ²Oberdörster, G., Oberdörster, E., Oberdörster, J., *Environ. Health Persp.*, **2005**, *7*, 829.
- ³ICRP, *Publication 66*, Pergamon Press, **1994**
- ⁴Szabó, P., *Agrokémia és Talajtan*, **1991**, *40*, 297. [in Hungarian]
- ⁵Nagymajtényi, L., Schulz, H., Papp, A., Dési, I., *Centr. Eur. J. Occup. Environ. Med.* **1997**, *3*, 195.
- ⁶Oszlanczi, G., Horváth, E., Szabó, A., Horváth, E., Sági, A., Kozma, G., Kónya, Z., Paulik, E., Nagymajtényi, L., Papp, A., *Acta Biol. Szeged.*, **2010**, *54*, 165.
- ⁷Vezér, T., Papp, A., Hoyk, Z., Varga, C., Náray, M., Nagymajtényi, L., *Environ. Toxicol. Pharmacol.*, **2005**, *19*, 797.
- ⁸ATSDR, Toxicological profile for lead. *Agency for Toxic Substances and Disease Registry, U.S. Department of Health and Human Services*, **1999**.
- ⁹Araki, S., Sato, H., Yokoyama, K., Murata, K., *Am. J. Ind. Med.* **2000**, *37*, 193.
- ¹⁰Gerhardsson, L., Englyst, V., Lundstrom, N.G., Nordberg, G., Sandberg, S., Steinvall, F., *J. Trace Elem. Med. Biol.*, **1995**, *9*, 136.
- ¹¹Ruff, H.A., Markowitz, M.E., Bijur, P.E., Rosen, J.F. *Environ. Health Persp.* **1996**, *104*, 180.
- ¹²Goyer, R.A., *Environ. Health Persp.*, **1996**, *104*, 1050.
- ¹³Füzesi, Zs., Levy, B.S., Levenstein, C., *From science to action: the lead hazard in Hungary - a fact report. Fact Foundation, Pécs*, **1997**
- ¹⁴ATSDR, Draft toxicological profile for manganese. *Agency for Toxic Substances and Disease Registry, U.S. Department of Health and Human Services*. **2008**.
- ¹⁵Saric, M., Markicevic, A., Hrustic, O., *Br. J. Ind. Med.*, **1977**, *34*, 114.
- ¹⁶Ohtake, T., Negishi, K., Okamoto, K., Oka, M., Maesato, K., Moriya, H., Kobayashi, S., *Amer. J. Kidney Dis.*, **2005**, *46*, 749.
- ¹⁷Woolf, A., Wright, R., Amarasiriwardena, C., Bellinger, D. *Environ. Health Persp.*, **2002**, *110*, 613-616
- ¹⁸Halatek, T., Sinczuk-Walczak, H., Szymcsak, M., Rydzynski, K., *Int. J. Occup. Med. Environ. Health.*, **2005**, *18*, 265.
- ¹⁹Goldstein, G.W., Asbury, A.K., Diamond, I., *Arch. Neurol.* **1974**, *1*, 382.
- ²⁰Ahamed, M., Siddiqui, M.K.J., *Clin. Chim. Acta*, **2007**, *383*, 57.
- ²¹Avila, D.S., Gubert, P., Fachineto, R., Wagner, C., Aschner, M., Rocha, J.B., Soares, F.A., *NeuroToxicol.*, **2008**, *29*, 1062.
- ²²Kita, H., Narita, K., Van der Kloot, W., *Brain Res.*, **1981**, *205*, 111.
- ²³Suszkiv, J., Toth, G., Murawsky, M., Cooper, G.P., *Brain Res.*, **1984**, *323*, 31.
- ²⁴Erikson, K.M., Aschner, M., *Neurochem. Int.*, **2003**, *43*, 475.
- ²⁵Struzynska, L., Chalimoniuk, M., Sulkowski, G., *Toxicology*, **2005**, *212*, 185.
- ²⁶Alexi, T., Borlongan, C.V., Faull, R.L.M., Williams, C.E., Clark, R.G., Gluckmann, P.D., Hughes, P.E. *Prog. Neurobiol.*, **2000**, *60*, 409.
- ²⁷Bowler, R., Koller, W., Schultz, P.E., *NeuroToxicol.*, **2006**, *27*, 327.
- ²⁸Needleman, H.L., Gatsonis, C.A., *J.A.M.A.* **1990**, *263*, 673.

Received: 15.10.2012.

Accepted: 01.11.2012.



HEAVY METAL DISTRIBUTION OF FLOODPLAIN SOILS AND PASTURES OF THE TISZA RIVER

Zoltán Gyóri^[a,b], Norbert Boros^[c], Emese Bertáné Szabó^{[a]*}, Péter Sipos^[a]

Paper was presented at the 4th International Symposium on Trace Elements in the Food Chain, Friends or Foes, 15-17 November, 2012, Visegrád, Hungary

Keywords: Tisza River, heavy metal pollution, Lakanen-Erviö extraction

In January and March 2000 two tailings dam failed in Baia Mare (Nagybánya) and Baia Borsa (Borsabánya) which resulted cyanide and metal pollution in the Lápos - Szamos - Tisza and metal pollution in the Visó - Tisza rivers, respectively. The main aim of this study was to evaluate the long term effects of pollution on environment. Samples of easily available metal contents were collected in year 2011 from these floodplains and pastures along the Tisza (Tivadar, Vásárosnamény, Rakamaz, Tiszacsege) and were investigated and compared with our earlier results. It was noticed that during an 11 year span the easily available Cd, Cu, Zn and Pb contents of the floodplain soils have increased. This may be due to the periodical floods and the mobilization of the pollutants. Furthermore, high concentration of Zn and Pb contents – crossing the natural background values of available metal content – were also observed in the soils studied.

* Corresponding Authors

Tel.: +(36).(52).417572

Fax: +(36).(52).417572

E-mail address: szaboemese@agr.unideb.hu (E. Bertáné Szabó).

[a] Institute of Food Science, Quality Assurance and Microbiology, University of Debrecen, Debrecen, H-4032, Hungary

[b] Institute of Regional Economics and Rural Development, Szent István University, Gödöllő, H-2100, Hungary

[c] Department of Chemical Engineering, University of Debrecen, Debrecen, H-4032, Hungary

In January and March 2000 two tailings dam failed in Baia Mare (Nagybánya) and Baia Borsa (Borsabánya) and resulted cyanide and metal pollution in the Lápos - Szamos - Tisza and metal pollution in the Visó - Tisza river systems, respectively.³

The short term effects of the pollution events were studied by many of researchers, and the Lápos-Szamos-Tisza and Visó-Tisza river systems were found to be contaminated by Cu, Zn, Pb and Cd.^{2,4-8}

Introduction

The Hungarian part of the Tisza River is highly contaminated by metals from mining activities in Romania. Mining in Maramures County (former Máramaros) traditionally exploits host ores of base metals (Cu, Zn and Pb) and precious metals (Au and Ag). Besides mining, metal pollution in upper Tisza catchment has also a long history.¹ Nowadays the processing of old tailings pond material by using cyanide in the recovery of Ag and Au is spread over this region. Mining activities use dangerous and toxic chemicals like cyanide which is prime source of contamination. Besides this, wastewater may contain some other heavy metals associated with fine-grained sediments. However, metal concentration of river water is not remarkable 30 km downstream from the point sources,² sediment-associated metals are dispersed at much greater distances.

The mining accidents were followed by floods; therefore the metal pollution of the floodplains were also observed.^{9,10} Deposition of contaminated sediment on floodplains during flood events and the mobilization of the pollutants may increase the plant available metal content of the upper soil layer.

The mobility and phyto- availability of metals depend on their chemical compositions.¹¹ Hence, the floodplain soils and river sediment were measured by sequential extraction procedures (SEP)^{4,10} and Lakanen-Erviö extraction.⁶ A remarkable rate of Cd and Zn contents of polluted sediments (Lápos, Szamos and Tisza Rivers) were in exchangeable form.⁴ Besides this, the Cd and Zn contents of the floodplain soils (Szamos and upper Tisza) could be found in an easily available form.¹⁰

Table 1. Sampling sites

Sampling sites	Geographical coordinates	River km	Type of samples	Additional information
Tivadar	N 48° 04' 00.6" E 22° 31' 04.8"	709	active floodplain	affected by the 2 nd pollution event
Vásárosnamény	N 48° 07' 46.5" E 22° 19' 39.5"	683	pasture	affected by the 1 st and 2 nd pollution events
Rakamaz	N 48° 07' 43.8" E 21° 26' 28.7"	543	pasture	affected by the 1 st and 2 nd pollution events
Tiszacsege	N 47° 42' 59.9" E 20° 57' 08.7"	455	active floodplain	affected by the 1 st and 2 nd pollution events 8 years ago the area was refilled with soil

The aim of this study was to evaluate the phyto-available metal content of soils by Lakanen-Erviö extraction, and comparing these results to our earlier results.

Experimental

Soil samples were collected in April 2011 by deep drilling with a Nordmeyer drill (Nordmeyer Holland, Overveen, The Netherlands). We collected samples from the 300 cm deep soil layer in three replications. Sampling sites are represented in Table 1.

The control area was an arboretum in Tiszakürt. The metal content of the soils originated from Tiszakürt could be considered as natural background levels, because the only source of pollution was atmospheric deposition in this site.

Soil samples were air dried, grinded and sieved (<2mm) for further analysis. The extraction of the easily available metal content was conducted according to Lakanen and Erviö.¹⁴ Cu, Zn contents were determined by an Optima 3300 DV ICP-OES (Perkin-Elmer). The measurement of Pb and Cd was conducted by a QZ 939 GF-AAS (Unicam) in 2000 and by an X7 ICP-MS (Thermo Fisher) in 2011.

All statistical analyses were performed with SPSS (version 13). Significant differences between the metal contents of the soils in the year 2000 and 2011 were examined by nonparametric, two related samples test (Wilcoxon test).

Results and discussion

Lakanen-Erviö extractable Zn, Pb and Cu contents of the studied soils (average element content of the 100 cm deep soil profile) and the background values are presented in Figure 1. Tivadar floodplain is considered to be unpolluted, because its metal content did not exceed background values. Our finding is in accordance with the results of other researches.¹² The easily available metal contents of Vásárosnamény, Rakamaz and Tiszacsege were remarkable compared to the background levels.

Cadmium contents of Vásárosnamény, Rakamaz and Tiszacsege (Figure 2) were found in remarkable amount comparing them to the average Cd content of the unpolluted reference soil. The Cd content of Vásárosnamény was higher by two orders of magnitude than that of unpolluted soil.

Sharma et al.¹⁵ studied the easily mobilizable (Lakanen-Erviö extraction) Cd, Cu, Pb and Zn contents of high, medium and low contamination areas (due to mining activities). Comparing our observations to these results it is concluded that the Cd, Cu and Zn contents of the studied soils in Vásárosnamény, Rakamaz and Tiszacsege exceed the average Cd, Cu and Zn contents (0.87, 12 and 26 mg kg⁻¹, respectively) of the low contamination area.

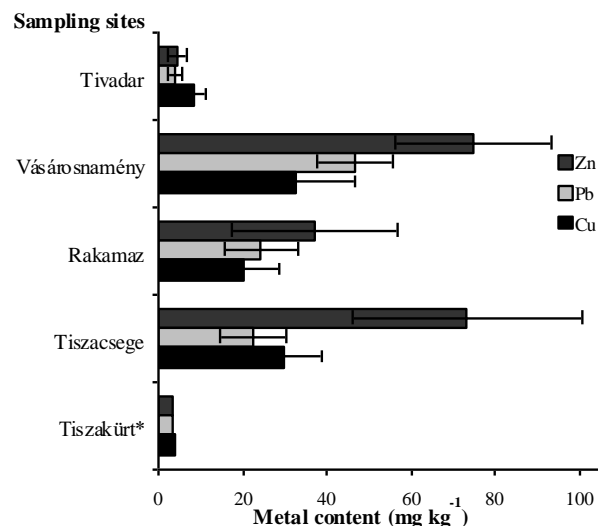


Figure 1. Available Zn, Pb and Cu contents (mg kg⁻¹) of the 1 m deep soil profile (2011) (*Natural background value for the measured river section; Remark: Error bars represent the 95% confidence interval)

Farsang et al.¹³ studied the health risk of metals in the topsoil of a Fluvisol soil (pH_{H2O} 7.7, loamy texture) located near the River Tisza. They found moderate risk (if the proportion of vegetables grown in the studied soil is extremely increased in the consumption) when the Lakanen-Erviö extractable Cd, Cu and Zn contents were 0.41, 27.1 and 53.1, respectively. Cadmium contents in Vásárosnamény, Rakamaz and Tiszacsege, and Zn contents in Vásárosnamény and Tiszacsege exceed these values, which refers to the hazard of the agricultural use of these soils.

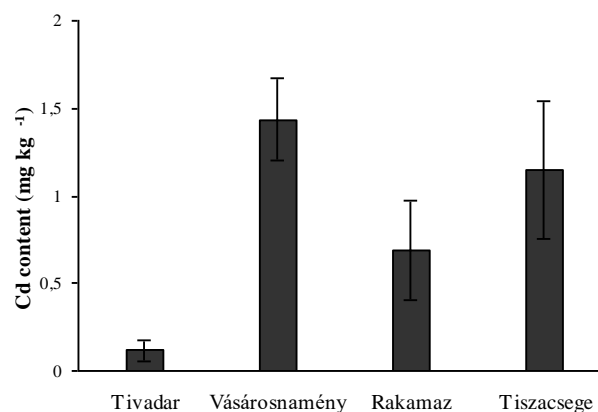


Figure 2. Cadmium contents (mg kg⁻¹) of the 1 m deep soil profile. Cadmium level of the unpolluted reference soil (Tiszakürt) was <0.02 mg kg⁻¹; Remark: Error bars represent the 95% confidence interval).

We compared the metal contents of the 300 cm deep soil profile with our earlier results [9]. Significant increases were observable ($P \leq 0.05$) in the case of Zn, Cd and Pb contents (data not shown). The increase was remarkable in the upper soil layers of the pasture near Vásárosnamény (Figure 3).

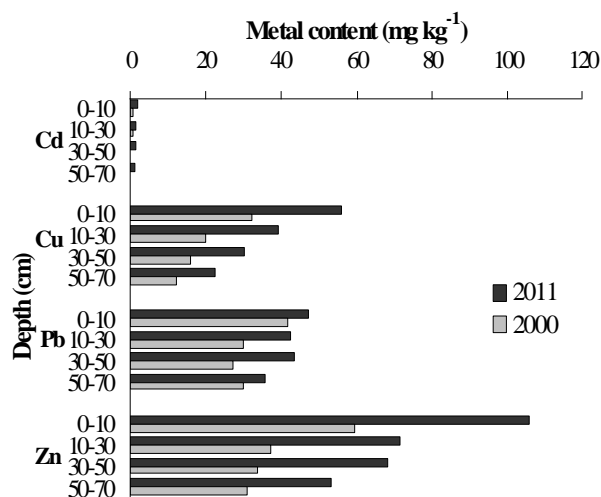


Figure 3. The Lakanen-Erviö extractable metal content of the 0-70 cm deep soil layer of a pasture near Vásárosnamény in 2000 and 2011

Conclusion

Our results proved that the sampling sites affected by the first pollution event (Baia Mare, January 2000) are significantly contaminated. Zinc, Pb and Cd contents of Vásárosnamény, Rakamaz and Tiszacsege were remarkably high. The effect of the second pollution (Baia Borsa, March 2000) on the available metal contents of the Tivadar floodplain was not detectable.

We found that during the 11 year period the easily available Cd, Zn and Pb contents of Vásárosnamény floodplain increased significantly. This may be due to by the periodical flood events and the mobilization of the pollutants.

Acknowledgements

The work is supported by the TÁMOP 4.2.1/B-09/1/KONV-2010-0007 project. The project is implemented through the New Hungary Development Plan, co-financed by the European Social Fund and the European Regional Development Fund.

This research was supported by the Environmental Remediation Sciences Division of the Office of Biological and Environmental Research, U.S. Department of Energy, through Financial Assistance Award No. DE-FC09-96-SR18546 to the University of Georgia Research Foundation.

References

- ¹Nguyen, H. L., Braun, M., Szaloki, I., Baeyens, W., Grieken, R., Van Leermakers, M., *Water Air Soil Pollut.* **2009**, *200*, 119-132.
- ²Macklin, M. G., Brewer, P. A., Balteanu, D., Coulthard, T. J., Driga, B., Howard, A. J., Zaharia, S., *Appl. Geochem.* **2003**, *18*, 241-257.
- ³UNEP/OCHA. *Assessment Mission Report*, **2000**, Geneva.
- ⁴Bird, G., Brewer, P. A., Macklin, M. G., Balteanu, D., Driga, B., Serban, M., Zaharia, S. *Appl. Geochem.* **2003**, *18*, 1583-1595.
- ⁵Brewer, P. A., Macklin, M. G., Balteanu, D., Coulthard, T. J., Driga, B., Howard, A. J., Bird, G., Zaharia, S., Serban, M. *NATO Science Series: IV: Earth and Environmental Sciences*, **2003**, *20*, 73-83.
- ⁶Györi, Z., Alapi, K., Sipos, P., Zubor, Á. In: *Natural Attenuation of Metals Along the Tisza River-Floodplain-Wetlands Continuum*, Debreceni Egyetem, **2003**, Debrecen, pp. 161-163.
- ⁷Osán, J., Kurunczi, S., Török, S., Van Grieken, R., *Spectrochim. Acta* **2002**, *57*, 413-422.
- ⁸Wehland, F., Panaiotu, C., Appel, E., Hoffmann, V., Jordanova, D., Jordanova, N., Denut, I. *Phys. Chem. Earth*, **2002**, *27*, 1371-1376.
- ⁹Györi, Z., Alapi, K., Szilágyi, Sz. In: *Natural Attenuation of Metals Along the Tisza River-Floodplain-Wetlands Continuum*, Debreceni Egyetem, **2003**, Debrecen, pp. 146-160.
- ¹⁰Kraft, C., von Tümpling J. W., Zachmann, D. W. *Acta Hydrochim. Hydrobiol.*, **2006**, *34*(3), 257-264.
- ¹¹Kabata-Pendias, A.; Pendias, H. *Trace Elements in Soils and Plants*, CRC Press, Ltd. Boca Raton, **2001** (3rd ed.), Florida.
- ¹²Szabó, Sz., Posta, J., Gosztonyi, Gy., Mészáros, I., Prokisch, J. *AGD Landscape & Environ.*, **2008**, *2*(2), 120-131.
- ¹³Farsang A.,; Puskás I., Szolnoki Zs., *AGD Landscape and Environ.*, **2009**, *3*(1), 11-27.
- ¹⁴Lakanen, E., Erviö, R., *Acta Agr. Fenn.* **1971**, *123*, 223-232.
- ¹⁵Sharma, P., Steckel, H., Koschinsky, A., Schnug E. *Landbauforschung – VTI Agricult. Forestry Res.*, **2009**, *59*/1, 11-18.

Received: 24.10.2012.

Accepted: 07.11.2012



DEPOSITION OF ORGANIC TRACE METAL COMPLEXES AS FEED ADDITIVES IN FARM ANIMALS

Miklós Mézes^[a], Márta Erdélyi^[a], Krisztián Balogh^[a]

Paper was presented at the 4th International Symposium on Trace Elements in the Food Chain, Friends or Foes, 15-17 November, 2012, Visegrád, Hungary

Keywords: Copper, zinc, iron, manganese; metal complexes, feed additives, deposition

Trace elements are essential for maintenance and production of farm animals, but most of the feeding stuffs do not contain adequate amount of most of them, therefore to supplement them in complete feed with trace elements is necessary. However, the rate of absorption and tissue deposition of trace elements from different complexes is also different which may have food safety aspects because of the maximum level of some trace minerals. The present review, based on scientifically proved results, discussions about the rate of absorption and deposition of different metal (Cu, Zn, Fe and Mn) proteinates, amino acid chelates (e.g. lysine, methionine, methyl-hydroxy-methionine) and humic acid complexes of trace elements. The results showed that metal proteinates have higher rate of tissue accumulation as compared to inorganic salts, and additionally some metal-proteinates (e.g. copper-proteinate) also improves the tissue deposition of manganese. Metal propionates, as possible new trace element supplements have positive effects on the rate of absorption which was proved by the higher blood serum levels. In the case of humic acid chelates there are some results about their positive effects on bioavailability of trace minerals but those were not scientifically proved. In conclusion it can be stated that organic metal complexes have better bioavailability than their inorganic counterparts, in particular modern farm animal genotypes with higher requirement level and also in stress conditions.

* Corresponding Authors

Fax: +36-38410804

E-Mail: Mezes.Miklos@mkk.szie.hu

[a] Department of Nutrition, Szent István University H-2103 Gödöllő, Páter Károly u. 1., Hungary

iron may be deposited in the heart and kidneys.⁶ Generally, livestock do not accumulate extremely high levels of manganese in their tissues when excess manganese is fed.⁶ Manganese concentrations in edible tissues linked with the dietary manganese intake.

Introduction

Trace elements are essential elements for maintenance and production of farm animals, because they are constituents of hundreds of proteins involved in intermediary metabolism, hormone secretion pathways, and immune defense systems.¹ However, most of the feeding stuffs do not contain adequate amount of most of the trace minerals,^{2,3,4} therefore supplementation of complete feeds with trace elements is necessary. However, the bioavailability and tissue deposition of trace elements is different from different sources, which may have food safety aspects because of the maximum level of some trace minerals. Knowledge on typical concentrations and accumulation in edible tissues and products of the element is an important tool for risk assessment and consumer protection.

For instance copper concentrations are highest in most of farm animals in the liver, and are related to the dietary intake, whereas muscle concentrations are more conserved.⁵ Normal liver copper concentrations are higher in ruminants than in pigs and chickens, and also found that relatively small amounts of dietary copper greatly increase liver copper concentrations in ruminants. Excess intake of zinc leads to an higher deposition in the liver, pancreas, kidney, and bone. Concentrations in milk and skeletal muscle of various species are more conserved.⁶ Zinc concentrations in edible tissues linked with dietary intake of various zinc compounds and doses.⁷ When animals are exposed to excessive amounts of iron, it is preferentially deposited in the liver, spleen, and bone marrow. With very high doses,

Inorganic trace mineral supplementation of the diets of farm animals result in a high level of mineral excretion. Obviously, this is not only wasteful but also harmful to the environment. For example, poultry manure, applied on a nitrogen basis, contains Zn and Cu approximately 66 and 56%, respectively, above the level of crop requirements.⁸ As compared to Cu, Mn, and Zn, Fe increased linearly with increasing intakes of these trace minerals, as was found in a poultry experiments.⁹ However, a noticeable reduction in Zn and Cu (but not Mn or Fe), excretion could only be achieved by dietary manipulation.^{10,11} There are contradictory results in respect of trace mineral excretion, as in a trial with broiler chicken the replacement of inorganic copper or iron with amino acid chelates decreased by 34% and 5-21% of Cu and Fe respectively, in the excreta,¹² but in another one a partial or complete replacement of inorganic with amino acid chelates of iron, copper, zinc and manganese at the rate of 25, 50, 75 and 100% in the diets but did not find consistency in decreasing values of the above mentioned trace element content of the excreta. However, the reduction was significant in laying hens.¹³

Inorganic salts of trace elements usually have poor bioavailability, primarily because of the numerous nutrient and ingredient antagonisms that impair absorption.¹⁴ In contrary organic metal complexes with small peptides (refer as proteinates), lysine, methionine or methyl-hydroxy-methionine chelates,¹⁵ propionates¹⁶ and humic acid chelates¹⁷ have higher bioavailability.¹⁸ The higher bioavailability in the case of chelates probably based on the ring structure of such chelates which protects trace minerals from chemical reactions in the gastrointestinal tract, and

keeps its stability even at low pH. Additionally, chelates carry negative charge therefore they are more effectively pass through the intestinal wall, and by different other routes, mainly by the amino acid transport system than inorganic compounds. The rate of passive diffusion is higher because of the less interaction between the mineral and other nutrients. This alternative pathway for absorption is leading to a reduction in the excretion. However, in the case of propionates two postulations are available about their absorption. The first is that metal-propionates absorb as complex, and the other one is that before absorption the complex hydrolyse and absorb independently the metal ion and propionate.¹⁸ Higher rate of relative bioavailability of the so-called organic forms of trace minerals has been proven, among others, in the case of copper, zinc, manganese and iron.¹⁷ Chelated zinc increased by 35% more broiler chicken tibia mineral content, manganese chelate bioavailability is about 1.2 times of its sulphate; iron has a bioavailability of 1.3-1.85 times of its inorganic form.²¹

Copper complexes

Relative bioavailability of different copper compounds in poultry as compared to CuSO₄ in poultry was Cu-Lys: 114%; Cu-Met: 92%; Cu-proteinates: 108%,¹⁹ in piglets CuCl₂ : 118%; Cu-Met: 85% and Cu-Lys: 105%²⁰ and in ruminants (sheep and cattle) Cu-Lys: 104%.¹⁹

In a mineral balance study with pigs²³ the diet was supplemented with 0, 50, or 100 mg kg⁻¹ copper as Cu-proteinates, or 250 mg kg⁻¹ as CuSO₄. There were linear increases ($P < 0.001$) in Cu absorption, retention, and excretion with increasing Cu-proteinates. Pigs fed 100 mg kg⁻¹ copper as Cu-proteinates absorbed and retained more and excreted less Cu than pigs fed 250 mg kg⁻¹ copper as CuSO₄. Blood plasma copper concentrations increased linearly with increasing Cu-proteinates. However, 50 or 100 mg kg⁻¹ copper as Cu-proteinates increased Cu absorption and retention, and decreased Cu excretion with 77 and 61%, respectively, as compared to 250 mg kg⁻¹ copper as CuSO₄.

In broiler chicken the most sensitive indicator is the tibia which is showed a linear increase of its copper content with the dose, but the rate of increase depends on the Cu salt or complex. Organic complexes, such as Cu-proteinates showed higher rate of accumulation as compared to inorganic salt (CuSO₄). The results also indicated that organically-complexed copper demand the actual requirement at lower dose than inorganic salt²⁴. However, in other trial¹³ partial or complete replacement of inorganic Cu with amino acid chelate at the rate of 25, 50, 75 and 100% in the diets did not increase significantly the tibia copper content.

Zinc complexes

Relative bioavailability of different zinc compounds in poultry as compared to ZnSO₄ and based on the tibia Zn content was ZnO: 85 %; Zn-Met: 133 %; Zn-proteinates: 120 % and Zn-propionate: 126 %, ^{19,25,28} in piglets ZnO: 55-87 %; Zn-Lys: 83%; Zn-Met: 99 % and Zn-proteinates: 100 %^{19,26} and in ruminants (sheep and cattle) Zn-Lys:102 %; Zn-Met: 109 % and Zn-proteinates: 112%.¹⁹

The bioavailability of zinc from different sources also depends on the composition of the diet. For instance higher phytate and fibre content reduce the bioavailability of zinc from sulfate, whereas zinc in the form of Zn-Met was protected from their negative effect²⁸.

Humic acid complexes of zinc did not increase the zinc accumulation in muscle, kidney, liver and blood plasma, which means that humic acid do not have positive effect on bioavailability of zinc as compared to ZnSO₄.²⁹ That negative result is contrary to a few previous findings where it was found that humic acid has high bivalent cation binding capacity in the order of Cu²⁺>Fe²⁺>Mn²⁺>Zn²⁺ and improves their absorption. However, it also has been found that the interaction of humic acid with metal ions in solution increases with pH and humic acid concentration³⁰ whereas decreases with metal ion concentration.

In weaned piglet nutrition zinc-oxide used as antibacterial compound against gastrointestinal diseases at high dose (2000 mg kg⁻¹ feed as zinc)³¹ but it resulted high rate of zinc excretion through feces, while zinc-methionine at the dose of 200 mg kg⁻¹ feed as zinc reduce the occurrence of diarrhea at the same rate.³²

In broiler chicken the Zn content of tibia showed a linear increase with the dose of Zn-proteinates but even at the highest dose did not lead to a higher concentration as in the case of inorganic salt. However, zinc concentration reached a plateau at a lower concentration level. This probably due to a smaller exchangeable pool of zinc from organic complexes, which mobilize more efficiently during the high growth phase of fattening period than from inorganic source.²⁵ In contrary another trial¹⁴ partial or complete replacement of inorganic Zn with amino acid chelate at the rate of 25, 50, 75 and 100 % in the diet did not increase significantly the tibia zinc content.

Zinc as zinc propionate was more effective than inorganic zinc salts or zinc-acetate, for the induction of moulting. Additionally zinc propionate resulted quick recovery, and more yields after the moulting period. It suggested that zinc propionate is more effective, and less toxic, zinc source for moulting induction than inorganic or even some organic compounds.³³

There are few reports available about the effect of different zinc complexes in ruminants. Zinc-methionine chelate increased significantly the activity of Cu/Zn superoxide-dismutase activity in dairy cows as compared to the same dose of ZnSO₄. Higher rates of incorporation of zinc to metallo-enzymes, such as superoxide-dismutase, probably due to the higher by-pass rate of Zn-Met through rumen passage.³⁴ This higher rate of incorporation of Zn-Met into zinc metallo-enzymes would be the cause, that this Zn-chelate improves the reproductive traits (fewer days to conception after calving) of high lactating dairy cows.³³ Zinc propionate also recommended using as zinc complex for dairy cows because of its significantly higher rate of absorption, as determined by blood plasma zinc level after bolus intake, than other zinc sources.³⁴

Iron complexes

Relative bioavailabilities of different iron compounds in piglets, as compared to ZnSO₄, are as follows: Fe-fumarate: 95-100 %; Fe-proteinate: 110-122 % and Fe-Met: 177-184%.²²

In broiler chicken the Fe content of tibia did not show increase with the dose of Fe-proteinate, and iron excretion increased with the dose, but it was lower, but not dose-dependent manner and significantly than using inorganic salt. Which means iron has no exchangeable pool of iron in tibia, or that iron content of the basal diet was higher than the actual requirement which resulted dose-dependent rate of excretion.^{13,25}

In laying hens replacement of inorganic iron with 75 or 100 % iron amino acid chelate in the diet significantly decreased the iron content of the liver.¹³

Manganese complexes

Relative bioavailability of different manganese compounds in broiler chickens based on tibia deposition as compared to MnSO₄ as follows: MnO: 127 %; Mn-Met: 110 %; Mn-Met-hydroxy analogue: 114 %.³⁵ Similar tendency was found based on an ileal absorption study with broiler chicken³⁶ and on the basis of tibia manganese content in piglets MnO: 85 % and Mn-Met: 120 %, respectively.²² However, it should be noted that in the above mentioned studies the Mn content of the diets was higher than the maximum permitted level in the EU countries legislation.

Bioavailability of Mn from Mn-proteinate seems to affect by, among other factor, some adverse situations, such as; it was found that the bioavailability of Mn-proteinate showed much higher values (125-140%) as compared to MnSO₄ in heat-stressed broiler chickens.²²

Tibia content is generally accepted as a suitable indicator of manganese levels of animals. In contrary to that some trials showed that partial or complete replacement of inorganic Mn with amino acid chelates at the rate of 25, 50, 75 and 100% in the diets did not increase the tibia manganese content¹³. Additionally a novel manganese chelate, Mn-methionine hydroxyl analogue also did not result in significant higher tissue concentration than MnSO₄ at the same dietary levels³⁶. The same tendency was found using tibia manganese content in laying hens and piglets and excretion in milk as indicator³⁷.

Conclusions

In conclusion, based on scientifically proved data, it may be assumed that organic metal complexes usually have better bioavailability than their inorganic counterparts in most of farm animal species. This is important for better demand for the requirement of trace minerals of modern farm animal genotypes in particular in adverse conditions, and also important for decreasing the environmental load with manure.

Acknowledgements:

The publication is supported by the TÁMOP-4.2.2.B-10/1-2010-0011 and TÁMOP-4.2.1.B-11/2/KMR-2011-0003 projects. The projects are co-financed by the European Union and the European Social Fund.

References

- Dieck, H.T., Doring, F., Roth, H.P., Pand, H., Daniel, H., *J. Nutr.* **2003**, *133*,1004–1010
- CVB, *Feed Table. Productschap Diervoeder, the Netherlands*, 2007
- INRA, *Tables of composition and nutritional value of feed materials*. Wageningen Academic Publishers, & INRA, Paris, **2004**
- Batal, A.B., Dale, N.M.. *Feedstuffs* **2008**, *80* (37), 16
- Jongbloed, A.W., Kemme, P.A., De Groot, G., Lippens, M., Meschy, F., *Bioavailability of major and trace minerals. International Association of the European Manufacturers of Major, Trace and Specific Feed Mineral Materials; Brussels*, **2002**
- SCAN *Opinion of the Scientific Committee for Animal Nutrition on the use of copper in feedingsuffs*. **2003**
- NRC, *Mineral Tolerance of Animals, 2nd Revised Edition*. National Academy Press, **2005**
- Cao, J., Henry, P.R., Guo, R., Holwerda, R.K., Toth, J.P., Littell, R.C., Miles, R.D., Ammerman, C.B., *J. Anim. Sci.* **2000**, *78*, 2039-2054
- Dozier, W.A., Davis, A.J., Freeman, M.E., Ward, T.L.. *Br. Poult. Sci.* **2003**, *44*, 726–731
- Bao, Y.M., Choct, M., Iji, P.A., Bruerton, K., *J. Appl. Poult. Res.* **2007**, *16*, 448-455
- Dozier, W. A., Davis, A.J., Freeman, M.E., Ward, T.L.. *Br. Poult. Sci.* **2003**, *44*,726–731
- Mohanna, C., Nys, Y., *Br. Poult. Sci.* **1999**, *40*, 108–114
- Untea, A.E.; Olteanu, M.; Maros, I.; Criste, R.D.. *Biotechnol. Anim. Husbandry (Serbia)*, **2011**, *27*, 759-768
- Mapesos-De Vera, M.B. *Efficacy of amino acid chelates of iron, copper, manganese and zinc in broilers and layer diets. College, Laguna (Philippines)*. **2010**
- Underwood, E., Suttle, N.. *The mineral nutrition of livestock*. CABI Publishing, **2001**
- EFSA.. *The EFSA Journal* **2008**, *692*,1-17
- Nelson, C.E.. *United States Patent* 5,707,679 ,**1998**
- EFSA , *The EFSA Journal* , **2009**, *1147*, 1-36
- Dubey, D.K.. *Metal propionates: A boon for today's dairy animal*. Download at: <http://www.engormix.com/MA-dairy-cattle/nutrition/articles/metal-propionates-boon-today-12212/141-p0.htm>, **2012**
- Ammerman, C. B., Baker, D. H., Lewis A. J. (eds).. *Bioavailability of Nutrients for Animals*. Academic Press, **1995**
- Miles, R.D., Henry, P.R. *Proc. California Animal Nutrition Conference, Fresno, CA*, **1999**, 1-24
- Ammerman, C.B., Henry, P.R., Miles, R.D.. *In: Recent Advances in Animal Nutrition*. Garnsworthy, P.C-. Wiseman, J. (eds.) Nottingham University Press, **1998**, 123-147
- Bruerton, K.I.. *In: Redefining mineral nutrition*. Taylor-Pickard, J.A., Tucker, L.A. eds. Nottingham University Press, Nottingham, **2005**, 179-186

- ²³Veum, T.L., Carlson, M.S., Wu, C.W., Bollinger, D.W., Ellersieck, M.R., *J. Anim. Sci.* **2004**, *82*, 1062-1070
- ²⁴Revy, P.S., Jondreville, C., Dourmad, J.Y., Nys, Y., *Anim. Feed Sci. Technol.* **2004**, *116*, 143-155
- ²⁵Bao, Y.M., Choct, M., Iji, P.A., Bruerton, K., *Austr. Poult. Sci. Symp.* **2006**, *18*, 222-225
- ²⁶Bao, Y., Choct, M., Iji, P., Bruerton, K., *Br. Poult. Sci.* **2009**, *50*, 95-102
- ²⁷Kemin B.V. *Bioavailability of zinc from organic and inorganic sources using the chick bioassay technique. Internal publication, BB-03-00234, 1995.*
- ²⁸Wedekind, K.J., Horan, A.E., Baker, D.H., *J. Anim. Sci.* **1992**, *70*, 178-185
- ²⁹Herzig, I., Navratilova, M., Totušek, J., Suchy, P., Večerek, V., Bláhova, J., Zrally, Z. *Czech J. Anim. Sci.*, **2009**, *54*, 121-127
- ³⁰Erdogan, S., Baysal, A., Akba, O., Hamamci, C., *Polish J. Environ. Stud.* **2007**, *16*, 671-675
- ³¹Marianne, J.W., Melin, L., Lindberg, R., Johannisson, A., Petersson, L., Wallgren, P., *Res. Vet. Sci.* **1998**, *64*, 225-231.
- ³²Wang, J.H., Wu, C.C., Feng, J., *Czech J. Anim. Sci.*, **2011**, *56*, 30-36
- ³³Park, S.Y., Birkhold, S.G., Kubena, L.F., Nisbet, D.J., Ricke, S.C. *Poult. Sci.* **2004**, *83*, 24-33
- ³⁴Sobhanirad, S., Valizadeh, R., Moghimi, A., Naserian, A., *EAAP 60th Annual Meeting, Barcelona, 2009*, 517
- ³⁵Uchida, J., Mandevu, P., Ballard, C.S., Sniffen, C.J., Carter, M.P., *Anim. Feed Sci. Technol.* **2001**, *93*.193-.200
- ³⁶EFSA, *The EFSA Journal* **2008**, *692*, 1-17
- ³⁷Yan, F., Waldroup, P.W., *Int. J. Poultry Sci.* **2006**, *5*, 708-713
- ³⁸EFSA, *The EFSA Journal*, **2010**, *8*(1):1424

Received: 29.10.2012.

Accepted: 07.11.2012



ADVANTAGES AND DISADVANTAGES OF ARSENAZO III AND CHLOROPHOSPONAZO III UTILIZATION FOR SPECTROPHOTOMETRIC THORIUM DETERMINATION

Jozef Uhrovčík*, Maroš Juraška, Juraj Lesný

Paper was presented at the 4th International Symposium on Trace Elements in the Food Chain, Friends or Foes, 15-17 November, 2012, Visegrád, Hungary.

Keywords: thorium, Arsenazo III, Chlorophosponazo III, spectrophotometry, limit of detection (LOD).

The presented work is devoted to the evaluation of important validation descriptors concerning the spectrophotometric determination of thorium using Arsenazo III and Chlorophosponazo III. In diluted hydrochloric acid the complex between Th(IV) and Arsenazo III is formed instantly and remains stable for 25 minutes with constant absorbance. Beer's law is obeyed in the range from 0.70 to 11.64 $\mu\text{mol} \cdot \text{L}^{-1}$. The molar absorptivity at 660 nm is equal to $9.74(\pm 0.09) \cdot 10^4 \text{ cm}^{-1} \text{ mol}^{-1} \text{ L}$ (data in parentheses stands for standard deviation). The relevant relative standard deviations (RSD) reached $\pm 1.48 \%$, $\pm 4.34 \%$ and $\pm 3.07 \%$, respectively. Thorium concentration can be quantified using Chlorophosponazo III in media of diluted nitric acid. The linear range of the proposed method was from 1.59 to 18.10 $\mu\text{mol L}^{-1}$ of thorium(IV). The experimentally determined values of molar absorptivity reached $\epsilon_{691} = 3.76(\pm 0.05) \cdot 10^4 \text{ cm}^{-1} \text{ mol}^{-1} \text{ L}$. The repeatability and trueness of determination in the linear range did not exceed $\pm 2.2\%$ and 3.3% , respectively. Color stability of the Th(IV)-Chlorophosponazo III complex maintained a constant value for at least two hours. LOD and LOQ values for both methods were established applying three approaches – the 3- σ , the ULA2 and the Hubaux-Vos ones.

* Corresponding Authors

Fax: +421335921403

E-Mail: j.uhrovcik@gmail.com

[a] Department of Ecochemistry and Radioecology, University of SS. Cyril and Methodius in Trnava, Nám. J. Herdu 2, SK-917 01 Trnava, Slovak Republic

of partial hydrolysis of metal ions to be determined. They are complexing reagents suggested primarily for spectrophotometric determination of lanthanides, actinides and alkaline earth metals.²⁷

Introduction

Thorium is a naturally occurring radioactive element of extraordinary long lifetime. The most reliable sources of elemental concentrations in earth crust report values representing approx. 6 ppm of thorium in average. Thorium is first of all a worthwhile potential raw material for fissile nuclear fuel production. Taking in account chemical and geochemical determinateness of thorium, the quantification of its concentration in different matrices requires in addition to high accuracy also satisfactory detection limits. The mentioned element can be determined by many instrumental techniques based on different principles including mass spectrometry with inductively coupled plasma¹⁻², electrochemical methods³⁻⁶, atomic emission spectrometry with inductively coupled plasma,⁷⁻⁸ atomic absorption spectrometry⁹, chromatography¹⁰⁻¹³ and others. A necessary part of most analytical determinations of elements in real matrices is separation and preconcentration. To achieve this goal a number of effective procedures have been developed¹⁴⁻¹⁸. There are many spectrophotometric methods for thorium determination in environmental samples.¹⁹⁻²⁶

The application of organic reagents for spectrophotometric determination of thorium is well known and continues to be interesting. Chlorophosponazo III and Arsenazo III belong to azo-dyes based on chromotropic acids. The reagents have ability to form stable chelates and can work in strongly acidic medium eliminating the chances

Russian scientists Fadeeva and Alimarin²⁸ have published the first use of complexing agent Chlorophosponazo III for spectrophotometric determination of thorium(IV) in diluted hydrochloric acid media. Extraction of Th(IV)-Chlorophosponazo III complex into organic solvent led to an increase of selectivity and sensitivity of the relevant determination.²⁹⁻³⁰ In monazite sand samples, the spectrophotometric determination of thorium using Chlorophosponazo III in presence of diluted phosphoric acid was carried out as well. The relative error of the determination did not exceed 1%.³¹ While the successful applicability of Chlorophosponazo III for spectrophotometric quantification of thorium(IV) in different matrices is indisputable, the number of works dealing with detailed evaluation of particular determinations is surprisingly limited. The use of Arsenazo III for spectrophotometric determination of thorium(IV) was described in work of soviet scientist Savvin. Measurements were carried out in presence of diluted hydrochloric acid at the 665 nm. Molar absorptivity reached the value $1.3 \cdot 10^5 \text{ L mol}^{-1} \text{ cm}^{-1}$. This method proved to be suitable for the determination of microgram amounts of Th in minerals and natural waters. The relative error of the determination does not exceed 4%.³² A rapid and sensitive spectrophotometric method has been developed for the determination of thorium(IV) using 0.04% Arsenazo-III in a 2M perchloric acid solution.³³ The complex is formed instantly in perchloric acid and remains stable for 45 minutes with constant absorbance. Beer's law is obeyed in the range 1 – 60 $\mu\text{g g}^{-1}$ of thorium(IV) concentration with a molar absorptivity at 654 nm = $3.07 \cdot 10^5 \text{ M}^{-1} \cdot \text{cm}^{-1}$. The foreign ions interference in thorium determination have been

checked. The cations were tested at > 60-fold excess of thorium(IV), Mn(II), Fe(III), Co(II) and Ni(II) interfere negatively, whereas only Ce(III) has increased the absorbance. Among the anions, cyanide, phosphate, thiocyanate and acetate at 150-fold excess of thorium(IV) cause significant interference. However, thorium can be determined in the presence of nitrate, chloride, oxalate, tartrate, ascorbate, thiosulphate and citrate. The method has been applied on certified reference material for thorium determination after extractive separation and the result was found in good agreement with the certified value.³³

The utilization of mentioned complexing agents in question has valuable advantages such as an excellent time stability of the absorbance and a relatively wide linear range, etc. Chlorophosphonazo III and Arsenazo III still have a justified place among the complexing agents utilized in trace analysis and the interest in their analytical applications significantly grows in recent years.

The presented study is focused on the evaluation and comparison of important validation parameters for spectrophotometric determination of thorium in $\mu\text{mol L}^{-1}$ concentration range using abovementioned reagents.

Material and methods

We performed all measurements using the Cary WinUV 50 (Varian Inc.) spectrophotometer. We used three replicate samples for each absorbance determination and we utilized the average value of the signal versus blank in next computations. The value of the specific conductivity of the deionized water used in experiments was $0.054 \mu\text{S cm}^{-1}$. All reagents used were of analytical grade and all the solutions were prepared in deionized water. Thorium(IV) stock solution (Fluka Analytical) containing $43.1 \mu\text{mol L}^{-1}$ was used. The concentration of solution of the Chlorophosphonazo III (Dojindo Laboratories) was 0.04% (w./v.) and Arsenazo III (Fluka Analytical) was 0.02% (w./v.). The medium of measured solutions has been adjusted by addition of diluted nitric acid or hydrochloric acid (Mikrochem) with concentration 10 mol L^{-1} . The foreign ions stock solutions were prepared by dilution of standard solutions (Fluka Analytical, Merck).

Results and discussion

Arsenazo III method

Thorium stock solution containing up to $11.64 \mu\text{mol L}^{-1}$ of Th (IV) was transferred into 10 mL volumetric flask, then 2.3 mL of diluted hydrochloric acid and 2 mL of Arsenazo III solution have been added. The mixture was filled up to the mark with distilled water. After thorough mixing the absorbance at 660 nm against a reagent blank was measured. The upper limit of the linear range was established by application of QC parameter³⁴ and application of F-test of significance of quadratic parameter.³⁵ The Beer's law was obeyed from 0.7 to $11.64 \mu\text{mol L}^{-1}$ (Figure 1). Beyond this value, a significant deviation from the linearity was observed. The molar absorptivity reached value $\varepsilon_{660} = 9.74(\pm 0.09) \cdot 10^4 \text{ cm}^{-1} \text{ mol}^{-1} \text{ L}$ (data in parentheses represents standard deviation).

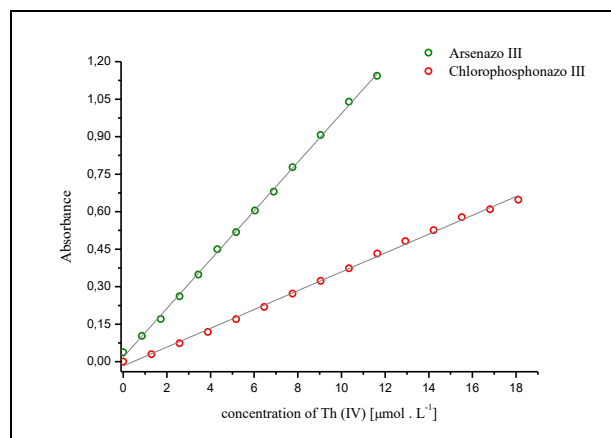


Figure 1 Absorbance of thorium(IV)-Arsenazo III (Chlorophosphonazo III) complex as a function of thorium concentration against a reagent blank.

The optical density was found constant only 25 minutes under normal laboratory conditions. A significant decrease in the absorbance was observed only for thorium(IV) concentration exceeding $6.90 \mu\text{mol L}^{-1}$ (data not shown). The values of limit of detection (LOD) and limit of quantification (LOQ) were calculated by $3\text{-}\sigma$,³⁶ ULA2³⁷ and Hubaux-Vos³⁸ approaches as well. In the case of computation by $3\text{-}\sigma$ approach residual standard deviation ($s_{y/x}$), standard deviation of y-intercept (s_b) and standard deviation of blank (s_{blank}) were applied. Results of these theoretical computations are summarized in Table 1.

Table 1 LOD and LOQ computed by using three different approaches. †10 replicate determinations of blank.

3- σ		
s_{blank}^\dagger	LOD [$\mu\text{mol L}^{-1}$]	0.63
	LOQ [$\mu\text{mol L}^{-1}$]	2.07
$s_{y/x}$	LOD [$\mu\text{mol L}^{-1}$]	0.34
	LOQ [$\mu\text{mol L}^{-1}$]	1.12
s_b	LOD [$\mu\text{mol L}^{-1}$]	0.17
	LOQ [$\mu\text{mol L}^{-1}$]	0.57
ULA2		
	LOD ($\alpha = 0.05$) [$\mu\text{mol L}^{-1}$]	0.23
	LOQ ($\alpha = 0.05$) [$\mu\text{mol L}^{-1}$]	0.68
	LOD ($\alpha = 0.01$) [$\mu\text{mol L}^{-1}$]	0.34
	LOQ ($\alpha = 0.01$) [$\mu\text{mol L}^{-1}$]	1.03
Hubaux-Vos		
	LOD ($\alpha = 0.05$) [$\mu\text{mol L}^{-1}$]	0.22
	LOQ ($\alpha = 0.05$) [$\mu\text{mol L}^{-1}$]	0.65
	LOD ($\alpha = 0.01$) [$\mu\text{mol L}^{-1}$]	0.31
	LOQ ($\alpha = 0.01$) [$\mu\text{mol L}^{-1}$]	0.93

The experimentally verified limit of detection and limit of quantification reached the following values: LOD = $0.22 \mu\text{mol L}^{-1}$ and LOQ = $0.70 \mu\text{mol L}^{-1}$. The best agreement between theoretically computed and practically verified values of LOD and LOQ was observed using ULA2 and Hubaux-Vos approaches namely at significance level $\alpha = 0.05$. The results were satisfactory even in the case of $3\text{-}\sigma$ approach application, where s_b was implemented into the calculation. The precision and trueness of the method was examined using 7 replicate solutions and conclusions are in Table 2.

Table 2 Obtained data for precision and trueness appraisal concerning the studied method.

Th (IV) concentration [$\mu\text{mol L}^{-1}$]	Relative error [%]	RSD [%]
1.30	-3.09	± 4.34
3.88	-0.72	± 1.48
7.76	-2.11	± 3.07

Influence of potentially interfering ions has been checked. The impact of 60-fold foreign ions excess (Th(IV) concentration $4.31 \mu\text{mol L}^{-1}$) is summarized in Table 3. Our results indicated that U(VI), Co(II) and Ce(IV) caused significant interference.

Table 3 Effect of chosen ions on thorium(IV) determination with Arsenazo III in hydrochloric acid.

Foreign ion	Relative error [%]	Foreign ion	Relative error [%]
Cu(II) ^a	+3.74	La(III) ^b	+13.25
Zn(II) ^a	+0.37	U(VI) ^a	+57.50
Co(II) ^a	+49.63	Eu(III) ^a	+7.37
Mn(II) ^a	+5.03	Ce(IV) ^a	+36.99

(a) as nitrate (b) as chloride

Chlorophosphonazo III method

Thorium stock solution containing up to $18.10 \mu\text{mol L}^{-1}$ of Th(IV) was transferred into 10 mL volumetric flask, then we added 1.5 mL of diluted nitric acid and 0.7 mL of Chlorophosphonazo III solution. The mixture was filled up to the mark with deionized water. After thorough mixing, the absorbance at 691 nm against a reagent blank was measured. The upper limit of the linear range was established by application of QC parameter and application of F-test of significance of quadratic parameter as in previous method. The Beer's law was obeyed from 1.59 to $18.10 \mu\text{mol L}^{-1}$ (Figure 1). Beyond this value, a significant deviation from the linearity was observed. The molar absorptivity was established to be $\varepsilon_{691} = 3.76(\pm 0.05) \cdot 10^4 \text{ cm}^{-1} \text{ mol}^{-1} \text{ L}$ (data in parentheses represents standard deviation). The optical density was found constant at least for 2 hours under normal laboratory conditions within the linear range.

The values of LOD and of LOQ were calculated by $3\text{-}\sigma$, ULA2 and Hubaux-Vos approaches as well. Results of these theoretical computations are summarized in Table 4. The experimentally verified limit of detection and limit of quantification reached the following values: $\text{LOD} = 0.55 \mu\text{mol L}^{-1}$ and $\text{LOQ} = 1.59 \mu\text{mol L}^{-1}$. The best agreement between theoretically computed and practically verified values of LOD and LOQ was observed using ULA2 and Hubaux-Vos approaches namely at significance level $\alpha = 0.05$. This is due to the fact that the mentioned statistical models take into account the uncertainty of the regression line and multiplying factors are not fixed (as in $3\text{-}\sigma$ approach), but their values depend on the design of the experiment.

Table 4. LOD and LOQ computed by using three different approaches. [†]10 replicate determinations of blank.

3- σ		
<i>S</i> _{blank} [†]	LOD [$\mu\text{mol} \cdot \text{L}^{-1}$]	0.12
	LOQ [$\mu\text{mol} \cdot \text{L}^{-1}$]	0.40
<i>S</i> _{y/x}	LOD [$\mu\text{mol} \cdot \text{L}^{-1}$]	0.71
	LOQ [$\mu\text{mol} \cdot \text{L}^{-1}$]	0.37
<i>S</i> _b	LOD [$\mu\text{mol} \cdot \text{L}^{-1}$]	0.40
	LOQ [$\mu\text{mol} \cdot \text{L}^{-1}$]	1.34
ULA2		
	LOD ($\alpha = 0.05$) [$\mu\text{mol} \cdot \text{L}^{-1}$]	0.53
	LOQ ($\alpha = 0.05$) [$\mu\text{mol} \cdot \text{L}^{-1}$]	1.61
	LOD ($\alpha = 0.01$) [$\mu\text{mol} \cdot \text{L}^{-1}$]	0.80
	LOQ ($\alpha = 0.01$) [$\mu\text{mol} \cdot \text{L}^{-1}$]	2.41
Hubaux-Vos		
	LOD ($\alpha = 0.05$) [$\mu\text{mol} \cdot \text{L}^{-1}$]	0.52
	LOQ ($\alpha = 0.05$) [$\mu\text{mol} \cdot \text{L}^{-1}$]	1.57
	LOD ($\alpha = 0.01$) [$\mu\text{mol} \cdot \text{L}^{-1}$]	0.75
	LOQ ($\alpha = 0.01$) [$\mu\text{mol} \cdot \text{L}^{-1}$]	2.25

The precision and trueness of the method was examined by 7 replicate solutions. The relevant conclusions are shown in Table 5.

Table 5 Obtained data for precision and trueness appraisal for the studied method.

Th (IV) concentration, $\mu\text{mol L}^{-1}$	Relative error [%]	RSD [%]
6.03	+0.11	± 2.15
10.78	+3.32	± 1.14
16.38	-2.27	± 0.95

The influence of potentially interfering ions was checked. The impact of 50-fold foreign ions excess (Th(IV) concentration $6.47 \mu\text{mol} \cdot \text{L}^{-1}$) is summarized in Table 6.

It was carried out five replicate determinations for each interfering ion. The average value of three replicate Th-Chlorophosphonazo III absorbances (not containing foreign ions) was taken into account as a reference value. Results indicated that all the studied cations except of Ca(II) caused significant interferences.

Table 6 Effect of chosen ions on thorium determination with Chlorophosphonazo III in nitric acid.

Foreign ion	Relative error [%]
Cerium(IV) ^a	+26.6(± 1.8)
Lanthanum(III) ^b	+78.1(± 3.8)
Europium(III) ^a	+22.2(± 1.6)
Calcium(II) ^b	-0.4(± 1.2)
Uranium(VI) ^a	+38.8(± 2.9)

(a) as nitrate (b) as chloride

Conclusions

The studied spectrophotometric methods for determination of Th (IV) in water solutions using Arsenazo III or Chlorophosphonazo III in hydrochloric (nitric) acid enable the quantification of the analyte in wide concentration range.

Both reagents are characterized by excellent repeatability of the results expressed by the relative standard deviation, whose value does not exceed the limit of $\pm 4.4\%$ and also favorable value relative errors ($<3\%$). Some differences between these two methods can be observed in the time stability of absorbance. Using Arsenazo III method the time stability of absorbance is limited to 25 minutes and the concentration limits $6.90 \mu\text{mol L}^{-1}$ Th(IV), in contrast use of Chlorophosphonazo III method extended stability up to two hours within whole linear range. Influence of selected foreign ions for accuracy determination of thorium is not negligible, but after their removal, or masking it would be possible to obtain relevant information about the concentration of Th in some types of real samples. As mentioned before - these complexing agents react with many other elements, and because the content of thorium in environmental samples is very low, it is not possible to use the method described for the direct determination of this element without appropriate separation and preconcentration procedures.

References

- ¹Zheng, Y., Weinman, B., Croninc, T., Fleisher, M. Q., Anderson, R. F., *Appl. Geochem.*, **2003**, 18, 539.
- ²Grinberg, P., Willie, S., Sturgeon, R., *Anal. Chem.*, **2005**, 77, 2432.
- ³Hassan, S. S. M., Elnemm, M. E., Attawiya, M. A. Y., *Electroanalysis*. **2008**, 20, 2063.
- ⁴Chandra, S., Agarwal, H., Singh, CH. K., *Anal. Sci.*, **2007**, 23, 469.
- ⁵Ju-Nan, L., Fe-Yun, Y., Zhong-Min, J., Jun-Jie, F., *Microchim. Acta.*, **2007**, 143, 287.
- ⁶Liu, S., Li, J., Xun, M., Gao, P., *Anal. Lett.*, **2003**, 36, 1381.
- ⁷Ujino, O., Umetani, S., *Anal. Chim. Acta*, **2000**, 420, 65.
- ⁸Thangavel, S., Dhavile, S. M., Dash, K., Chaurasia, S. C., *Atom. Spectrosc.*, **2010**, 31, 92.
- ⁹Castro, M. A., Aller, J. A., McCabe, A., Smith, W. E., Littlejohn, D., *J. Anal. At. Spectrom.*, **2007**, 22, 310.
- ¹⁰Al-Shawi, W. A., Dahl, R., *J. Chromatogr. A*, **1995**, 706, 175.
- ¹¹El-Dessouky, S. I., Borai, E. H., *J. Radioanal. Nucl. Chem.*, **2006**, 268, 247.
- ¹²Jackson, P. A., Carnevale, J., Fuping, H., Haddad, P. R., *J. Chromatogr. A*, **1994**, 671, 181.
- ¹³Jaison, P. G., Raut, N. M., Aqqarwal, S. K., *J. Chromatogr. A*, **2006**, 1122, 47.
- ¹⁴Aydin, F. A., Soylak, M., *Talanta*. **2007**, 72, 187.
- ¹⁵Büyüktiryaki, S., Say, R., Ersöz, A., Birlik, E., Denizli, A., *Talanta*. **2005**, 67, 640.
- ¹⁶De Carvalho, M. S., De Domingues, M. L. F., Mantovano, J. L., Da Cunha, J. W. S. D., *J. Radioanal. Nucl. Chem.*, **2002**, 253, 253.
- ¹⁷Maierov, V. G., Nikolaev, A. I., Adkina, O. P., Mazunina, G. B., *Radiochemistry*. **2006**, 48, 576.
- ¹⁸Patkar, N. S., Burungale, A. S., Patil, R. J., *RASAYAN J. Chem.*, **2009**, 2, 825.
- ¹⁹Shiri, S., Delpisheh, A., Haeri, A., Poornajah, A., Khezeli, T., Badkiu, N., *Anal. Chem. Insights*. **2011**, 6, 1.
- ²⁰Chalapathi, P. V., Subba Rao, Y., Jagadeesh, M., Prathima, B., Reddy, A. S., Reddy, K. J., Varadareddy, A., *J. Chem. Pharm. Res.*, **2011**, 3, 223.
- ²¹Chalapathi, P. V., Subba Rao, Y., Jagadeesh, M., Prathima, B., Reddy, A. S., Reddy, K. J., Varadareddy, A., Ramesh, G. N., *Res. J. Chem. Environ.*, **2011**, 15, 579.
- ²²Zhai, Q. Z., Zhang, X. X., Chen, L., *Asian J. Chem.*, **2008**, 20, 5187.
- ²³Garg, A., Kakkar, L. R., *Proc. Indian Nat. Sci. Acad. Part A*. **2007**, 77, 27.
- ²⁴Ghasemi, J. B., Zolfonoun, E., *Talanta*. **2010**, 80, 1191.
- ²⁵Pouretedal, H. R., Shafiee, B., Keshavarz, M. H., *Bulg. Chem. Commun.*, **2009**, 41, 230.
- ²⁶Kandil, A. T., Faramawy, H. F., Amin, R. M., *Egypt. J. Chem.*, **2007**, 50, 709.
- ²⁷Marczenko, Z., Balcerzak, M., *Separation, Preconcentration and Spectrophotometry in Inorganic Analysis (Analytical Spectroscopy Library)*, 1st Edition, Elsevier, **2000**.
- ²⁸Fadeeva, V. I., Alimarin, I. P., *Zh. Anal. Khim.*, **1962**, 17, 1020.
- ²⁹Chen, J. F., Khalilli, F. I., Mohammed, A. K., Chopin, G. R., *Anal. Chim. Acta*. **1994**, 284, 593.
- ³⁰Yamamoto, T., *Anal. Chim. Acta*. **1973**, 63, 65.
- ³¹Lukin, A. M., Titov, V. I., Chernyshova, T. V., Evdokimova, N. N., *Zavod. Lab.*, **1973**, 39, 1174.
- ³²Savvin, S., *Talanta*. **1961**, 8, 673.
- ³³Khan, M. H., Ali, A., Khan, N. N., *J. Radioanal. Nucl. Chem.*, **2001**, 250, 353.
- ³⁴Van Loco, J., Elskens, M., Croux, C., Beernaert, H., *Accredit. Qual. Assur.*, **2002**, 7, 281.
- ³⁵Araujo, P., *J. Chromatogr. B.*, **2009**, 877, 2224.
- ³⁶Long, G. L., Winefordner, J. D., *Anal. Chem.*, **1983**, 55, 712A.
- ³⁷Mocák, J., Bond, A. M., Mitchell, S., Scollary, G., *Pure Appl. Chem.*, **1997**, 69, 297.
- ³⁸Hubaux, A., Vos, G., *Anal. Chem.*, **1970**, 42, 849.

Received: 15.10.2012.

Accepted: 07.11.2012.



METHODOLOGICAL DEVELOPMENT IN DETERMINATION OF COPPER CONTENT IN THE ROOT ZONE OF HUNGARIAN SOIL TYPES: PRELIMINARY RESULTS

Edit Sárközi^a, Levente Kardos^a, Panna Sepsi^a, Márta Ladányi^b, László Tókei^a

Paper was presented at the 4th International Symposium on Trace Elements in the Food Chain, Friends or Foes, 15-17 November, 2012, Visegrád, Hungary.

Keywords: copper, root zone, soil, adsorption, pollution

History reveals that heavy metals have been used since ancient times. The human body contains about 80 mg copper, which can be present mostly in eyes, brain, liver, heart, kidneys and musculature. In our study we determine the adsorption capacity of copper in five different concentrations and in four different soil types: brown forest soil, chernozem, meadow and sand with humus. In our method we prepared soil columns, in which we put 50 g experimental soil samples and poured on copper solutions of known concentrations. The concentrations of runoff filtrates were determined by titration methods. The adsorption capacity of soil samples were calculated from the two different concentration values.

* Corresponding Authors

Tel.: (+36) 1 482 6466

E-Mail: edit.sarkozi@uni-corvinus.hu

- [a] Corvinus University of Budapest, Faculty of Horticultural Science, Department of Soil Science and Water Management, H-1118 Budapest Villányi út 29-43., Hungary
- [b] Corvinus University of Budapest, Faculty of Horticultural Science, Department of Mathematics and Informatics, H-1118 Budapest Villányi út 29-43., Hungary

Introduction

Heavy metals have been used in the history since ancient times.¹ Copper was the first heavy metal in the history, which was used in large quantities. There was the Copper Age in Europe between 3500 2500 B.C.² Shortly copper turned out to be easily mixable. It was used for various castings and in bronze also. An important feature of copper is the resistance to corrosion that makes it a functional and decorative material in construction since the Middle to present ages of the history.³

The chemical, physical and biological reactions between the soil components and the pollution affect the form of pollutions conditions of heavy metal. Considering the adsorption, it is important that the humus is generally negatively charged in 4.5 – 9.0 pH range. In aqueous phase the interaction can be physical, physico-chemical or chemical bond between the solutes and solid surface. In the physical adsorption (physisorption) the molecules bind to surface with long-range, low bonds or electrostatic attraction. The chemisorption (chemical adsorption) results stronger interactions than physisorption, in which small-range chemical bonds are formed.^{4,5,6}

Earth crust contains 10-50 mg kg⁻¹ copper, especially in the form of copper sulphides. The copper content of uncontaminated soil is 1-140 mg kg⁻¹ in global average - it strongly depends upon the soil's clay fraction content.^{7,8} Most of the copper is in divalent form bonded to organic or inorganic adsorption surface in soil. Because of strong

tendency of complex formation it develops complex formation with varied biological molecules. The copper binds strongly to these complexes, where as other cations can only displace them with difficulty, except the hydrogen ion. Consequently, the soluble copper content increases in acidic medium. Mobility of copper is very low in soils. In humus soil its deficiency has been observed. It was found, that the humus complex forms have high stability, which is typical in low pH^{9,10}.

Materials and methods

In this study our aim was to determine the adsorption capacity of copper as laboratory method in root zone of Hungarian soil types.

Four different soil types were examined: brown forest soil, meadow soil, chernozem and sand with humus. Each soil type came from two sampling sites, so eight soil samples were processed. The sampling sites and the soil types are given in Table 1.

Table 1. Sampling sites and soil types

Sampling site	Soil type
Tiszavasvári	sand with humus
	meadow soil
Gödöllő	chernozem
	brown forest soil
Budapest - Soroksár	sand with humus
	meadow soil
Dunaújváros	brown forest soil
	chernozem

The soil samples were collected from 0-30 cm depth, in the month of March 2012. After sampling, exhaustive soil analysis were done, e.g. pH (distilled water (DW) and KCl), conductivity, total salt content, N-P-K-content, humus content and quality, CaCO₃% content were determined.

One can observe the chemical properties of soil types from different sampling sites in Table 2.

Table 2. Soil chemical analysis results of brown forest soil samples

Sampling site	pH		Content		
	DW	KCl	Total salt, mg L ⁻¹	CaCO ₃ , %	Humus, H %
Gödöllő	6,72	5,92	29,9	0,21	2,98
Budapest - Soroksár	6,36	5,63	45,4	0,47	1,77

The brown forest soil came from Gödöllő and the Experimental and Research Farm of Corvinus University of Budapest, Soroksár. The chemical properties (pH, total salt and carbonate content) of both soil showed similarity. In humus content a small difference was noticeable, but copper is expected to behave similarly in case of both soil samples.

Table 3. Soil chemical analysis results of chernozem soil samples

Sampling site	pH		Content		
	DW	KCl	Total salt, mg L ⁻¹	CaCO ₃ , %	Humus, %
Dunaújváros	7,94	7,35	100,8	11,65	5,37
Tiszavasvári	5,83	4,49	38,5	0,84	3,29

The chernozem samples came from an oil trap from Dunaújváros and from a cultivated area from Tiszavasvári. The effect of cultivation shows clearly in soil test results. The acidifying effect of fertilizer resulted lower pH. Plants detracted Ca ions and various ion forms, so the salt and carbonate content were less in soil sample from Tiszavasvári. There is a difference in humus content, because the effect of cultivation and ventilation starts mineralization in humus. A Difference is expected in copper adsorption capacity in case of the two soil samples.

Table 4. Soil chemical analysis results of sand with humus samples

Sampling site	pH		Content		
	DW	KCl	Total salt, mg L ⁻¹	CaCO ₃ , %	Humus, H%
Budapest – Soroksár	7,78	7,31	69,3	4,2	1,42
Tiszavasvári	8,15	7,37	57,0	3,19	0,53

The humus with sand samples came from Soroksár and Tiszavasvári. The sample from Tiszavasvári is also cultivated (as the previous chernozem) which is reflected in the analysis values: a CaCO₃ % smaller, because the plants are utilized the Ca ions, besides the humus content is lower because of the cultivation. A difference is expected in case of these two soil samples after copper pollution.

Table 5. Soil chemical analysis results of meadow soil samples

Sampling site	pH		Content		
	DW	KCl	Total salt mg L ⁻¹	CaCO ₃ , %	Humus, H%
Budapest - Soroksár	7,63	7,34	115,7	13,28	4,15
Tiszavasvári	5,56	4,59	39,2	0,26	6,12

The meadow soil samples came from Soroksár and Tiszavasvári. The effect of agricultural cultivation is noticeable in pH, total salt content and carbonate content. A difference was found in humus content. The meadow soil sample from Tiszavasvári was after ploughing – the crop residues have begun to humificate, therefore higher humus content was measured. Differences are expected in copper adsorption capacity from these meadow soil samples.

The copper pollution in laboratory was carried out with soil column experiments. The soil columns are shown in Figure 1 a and b.

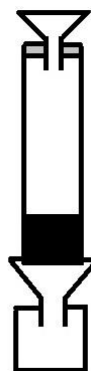


Figure 1. Soil column.



Figure 2. Copper pollution in laboratory

The soil column was prepared as follows: a cork was placed on top of a glass tube; a funnel was put in the middle of the cork. The bottom of the glass tube was tied up with mesh. 50 g pre-treated, air-dried soil samples were poured into the top of the funnel. There was also a funnel at the bottom of the soil column to guide the filtrate to the glass cup directly.

The copper pollution was carried out with CuSO₄ aqueous solution. 50 g L⁻¹ concentrated copper solution was made, which was extenuated to 25, 10, 5 and 1 g L⁻¹ concentrated solutions. 200-200 cm³ copper solution were poured from each concentration to each prepared soil columns, and then the copper content of filtrate were determined by complexometric titration method.

Before titration, 10 cm³ filtrates were pipette out into titration flask, pH 9.0 – 10.0 was adjusted by concentrated ammonia. Samples were titrated with murexid indicator, 0.05 mol L⁻¹ EDTA from red to violet.

The adsorption capacity of the soil samples were calculated from the two different concentration values.

$$C_{\text{adsorbed}} = C_{\text{pollution}} - C_{\text{filtrate}}$$

Statistical analysis was carried out by two-factor ANOVA (soil type and contamination concentration) for copper adsorption of soil using SPSS 20 software (<http://www.spss.com>). In order to normalize the data, after a shift of +0.3, Box-Cox transformation was executed with $\lambda = 0.2$.¹¹ We also considered the effect size measure (denoted by partial η^2) which gives the variance explained

by a given independent factor of the variance remaining after excluding variance explained by the other independent factors as well as the observed power of the test. Normality of residuals was proved using the Kolmogorov-Smirnov's test ($p = 0.2$). Homogeneity of variances was tested by Levene's test ($p = 0.19$) and it was followed by Tukey's post hoc test for the contamination concentration.

Results and Discussion

The adsorption results of the brown forest soil are shown on Figure 3 and Figure 4.

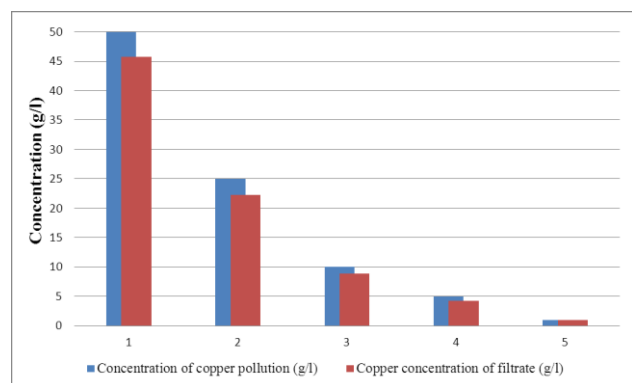


Figure 3. The copper adsorption results of brown forest soil from Gödöllő

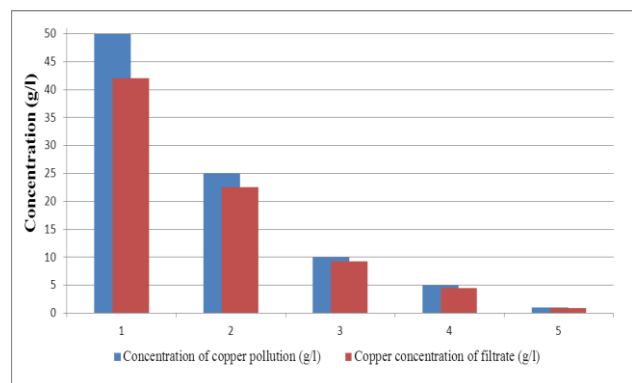


Figure 4. The copper adsorption results of brown forest soil from Soroksár

Analysis results of these two soil samples showed similarity. The same was expected by contamination. Adsorption was observed in case of both soil samples by each concentrations, so these two samples behave similarly after copper pollution.

Figure 5 and 6 show the results of copper pollution in chernozem samples.

The results of soil analysis showed difference in humus content, which may result difference in copper adsorption. It was confirmed by the laboratory analysis, because copper adsorption capacity was higher in sample from Dunaujváros (expect 1 g L^{-1} concentrated pollution), as more humus were in the soil. According to the literature, the soluble copper content increases in acidic medium, which is demonstrated well in case of the sample from Tiszavasvári.

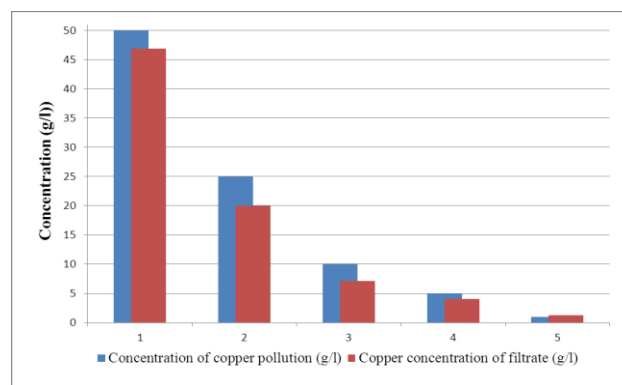


Figure 5. The copper adsorption results of chernozem from Dunaujváros

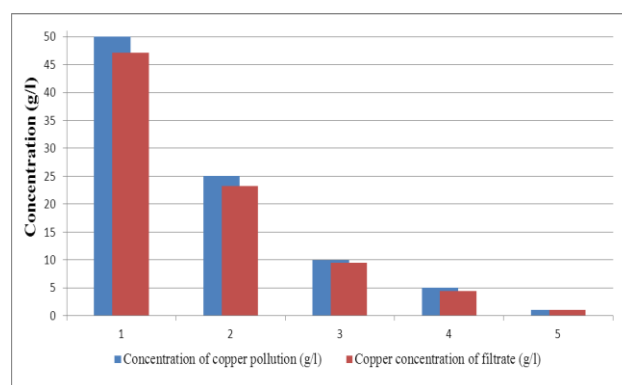


Figure 6. The copper adsorption results of chernozem from Tiszavasvári

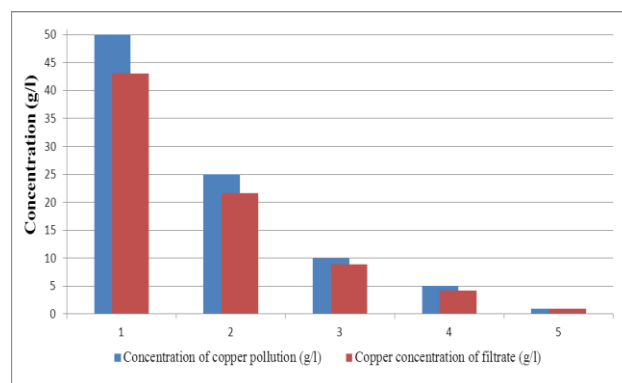


Figure 7. The copper adsorption results of sand with humus from Soroksár

Figure 7 and 8 show the results of sand with humus samples. A difference was measured in humus content as in the previous sample, which also resulted different copper adsorption. The humus-rich sample from Soroksár adsorbed more copper, than sample from Tiszavasvári in case of every concentration.

Figure 9 and 10 show the results of copper adsorption capacity in meadow soil samples from Soroksár and Tiszavasvári. Although the sample from Soroksár has less humus content, than sample from Tiszavasvári, the pH was having more important role in this soil type. During pollution demonstration very fast flow was observed, it was a very short time to complex formation, but the small pH resulted increasing soluble copper content, so the larger concentrations were measured by sample from Tiszavasvári.

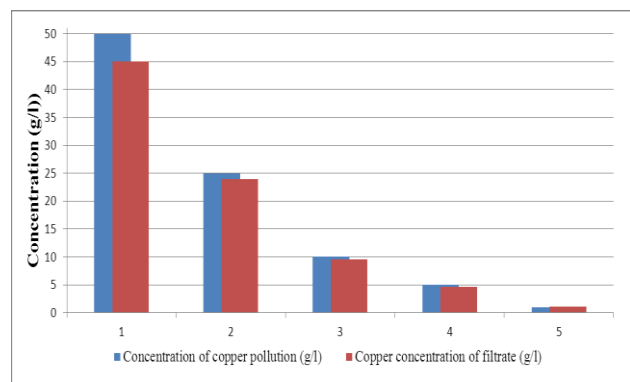


Figure 8. The copper adsorption results of sand with humus from Tiszavasvári

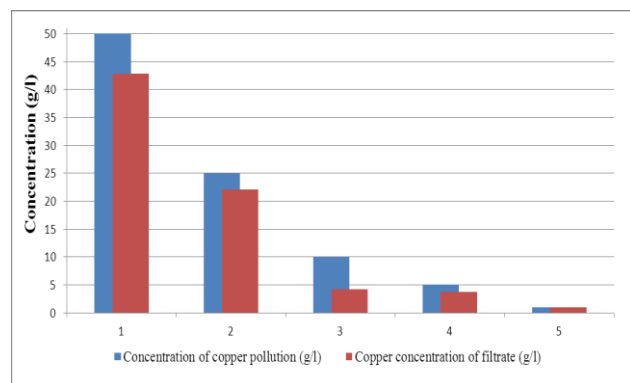


Figure 9. The copper adsorption results of meadow soil from Soroksár

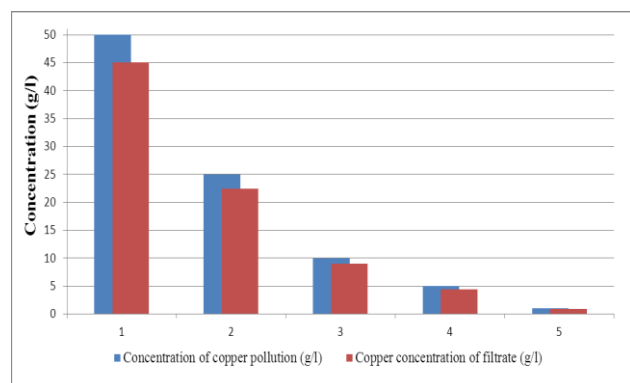


Figure 10. The copper adsorption results of meadow soil from Tiszavasvári

Our results showed that the copper adsorption of soil is significantly varied at different contamination concentration ($F(4; 20) = 11.81$; $p < 0.001$) with high effect size (partial $\eta^2 = 0.88$) and observed power (> 0.99). However, the difference is insignificant in case of the four soil types ($F(3; 20) = 1.45$; $p = 0.26$). The results of the Tukey's post hoc test for the contamination concentration for each soil type can be found in Table 6.

Table 6. The results of the Tukey's post hoc test for the contamination concentration for each soil type

Concentration	Soil type			
	brown forest	Cherno-zem	sand with humus	meadow soil
1 g L ⁻¹	0,036 a	-0,138 a	-0,058 a	0,061 a
5 g L ⁻¹	0,630 ab	0,765 ab	0,596 ab	0,945 ab
10 g L ⁻¹	0,937 bc	1,691 ab	0,742 ab	3,418 ab
25 g L ⁻¹	2,625 cd	3,399 b	2,171 bc	2,710 ab
50 g L ⁻¹	6,084 d	3,034 b	5,950 c	6,049 b

Conclusion

Overall, it was observed that the copper adsorption capacity of soils depends on pH and humus content. At higher humus content, the copper adsorbs better in form of chelate complex, so the copper adsorption increasing. At lower pH level, more copper could be stationary, because the soluble copper content of soil increases in acidic medium.

References

- ¹Dudka, S., Piotrowska, M., Terelak, H., *Environmental Pollution*, **1996**, *94*(2), 181-188.
- ²Accampo, N., Roberts, S., Cohen, O., Neuschel. *Western Civilization Beyond Boundaries*. Fifth Edition. USA. **2008**. 9.
- ³<http://www.copper.org/education/history/60centuries/introduction/index.html> (Copper Development Association Inc.)
- ⁴Ford, R. G., *Chemisorption and precipitation reactions*. In: Huang, P.M., Hi, Y., Summer, M.E. *Handbook of soil sciences. Properties and processes*. 2nd Ed., USA. **2012**.
- ⁵Yong, R.N., Nakano, M., Pusch, R., *Environmental soil properties and behaviour*. USA. **2012**. 298-305.
- ⁶Fülek, Gy., (ed.) *Talajvédelem, talajtan*. 2. bővített kiadás. Veszprém. **2011**. 175-178.
- ⁷Neubauer, U., Nowack, B., Furrer, G., Schulin R., *Environ. Sci. Technol.*, **2000**, *34*, 2749-2755.
- ⁸Wilson, M.J., Maliszewska-Kordybach, B., *NATO Sci. Ser.*, **1997**, *69*, 40.
- ⁹Loch, J., Réz a talajban. In: Fülek, Gy. (ed.) *Tápanyag-gazdálkodás*. Budapest. **1999**. 255.
- ¹⁰Fülek, Gy., Réz. In: Stefanovits, P., Filep, Gy., Fülek, Gy. *Talajtan*. Budapest. **2010**. 217.
- ¹¹Box, G. E. P., Cox, D. R., *J. Royal Statistical Soc.*, **1964**. Ser. B *26*(2), 211-252.

Received: 15.10.2012.
Accepted: 08.11.2012.



ANODIC AND CATHODIC PROCESSES IN PIPERIDINIUM-BASED IONIC LIQUID MIXTURES WITH AlCl_3

Mandar S. Risbud^{[a],[b]}, Ring Kononov^[a], Martin Bucknall^[c], Barry J. Welch^[a], John F. McCann^[a], and Maria Skyllas-Kazacos^{[a]*}

Keywords: aluminium chloride, cyclic voltammetry, ionic liquids, Al electro-deposition.

Low temperature molten salts based on ionic liquids have received considerable attention over the last 3 decades as potential alternative solvents for aluminium reduction. Recent reports in the literature have identified 1-propyl-1-methylpiperidinium bis(trifluoromethylsulfonyl) amide ($[\text{C}_3\text{mpip}][\text{NTf}_2]$) as a promising candidate for low temperature aluminium reduction processes. The formation of aluminium metal deposition was confirmed in these studies by both visual inspection and SEM-EDX analysis in the selected mixtures with AlCl_3 , but little is known about the anodic processes occurring in the cell. This work presents the results of a preliminary electrochemical study of the anodic and cathodic reactions occurring in the ionic liquid mixtures 1-propyl-1-methylpiperidinium bis(trifluoromethylsulfonyl)amide ($[\text{C}_3\text{mpip}][\text{NTf}_2]$) with AlCl_3 at different temperatures, concentrations and electrode materials. Analysis of voltammetric responses of $[\text{C}_3\text{mpip}][\text{NTf}_2]-[\text{AlCl}_3]_x$ for $x=0.3$ indicated that the anodic process is limited by mass transport for this particular electrolyte composition. In addition, the formation of Cl_2 was confirmed to take place at a dimensionally stable anode. Aluminium deposition experiments gave inconsistent results however and gas analysis indicated that the $[\text{C}_3\text{mpip}][\text{NTf}_2]-[\text{AlCl}_3]_x$ mixture at a prolonged elevated temperature at least partially decomposes into fluoro-carbons and chloro-compounds.

* Corresponding Author

Phone: +61 2 9385 4335

Fax: +61 2 9385 5966

E-Mail: m.kazacos@unsw.edu.au

- [a] School of Chemical Engineering and Industrial Chemistry, University of New South Wales, Sydney, NSW 2052, Australia;
- [b] Present address: Corrosion Centre for Education, Research and Technology, School of Chemical and Petroleum Engineering, Curtin University, Technology Park, GPO Box U1987, Perth, WA 6845, Australia;
- [c] Bioanalytical Mass Spectrometry Facility, University of New South Wales, Sydney, NSW 2052, Australia.

1. Introduction

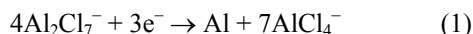
Aluminium is the most abundant element found in nature and has wide range of applications in automotive, aviation, ships and food packaging industries. Its corrosion resistance and light weight makes it one of the most widely used metals around the world. However due to its reactivity it does not occur in the free elemental state in nature and has to be extracted from bauxite using a very high energy intensive process. The electro-deposition of aluminium from aqueous solution is not feasible as the reduction of water to hydrogen occurs before the negative potential required for the reduction of aluminium ions can be reached. Therefore the potential electrolytes used for aluminium deposition are molten salts or non-aqueous organic solvents. The conventional Hall-Heroult process originally developed in 1886¹ is still the primary process used for aluminium production worldwide. This involves electrolysis at a very high temperature (950-1000 °C), of calcined alumina obtained from refined bauxite from the Bayer process. This process has very high energy consumption, complicated

operation and also produces emissions of gaseous hydrofluoric acid (HF) and other vapourised fluorides formed by hydrolysis during the electro-winning process. A further drawback of the Hall-Heroult process is the use of a consumable anode that gives rise to the formation of CO_2 as a by-product of the electrowinning process². Incremental improvements to the Hall-Heroult process have occurred over the last decade, especially in the area of process control where major reductions have been made in anode effects and accompanying CFC emissions. Despite these improvements, however, no major breakthroughs which would ameliorate the main disadvantages of the current Hall-Heroult process are likely to occur³. In recent years with growing awareness about global warming, cleaner and greener alternatives are being sought to make the process more environment friendly. Over the last few decades the development of ionic liquids has provided an alternative approach for a cleaner and less energy-intensive process for low temperature aluminium electro-deposition.

Ionic liquids generally have melting points below 100 °C, with high conductivity, high solubility of metal salts and a wide electrochemical window that allows the reduction of highly electro-active ions, making them an attractive alternative to high temperature molten salts with additional benefits such as low operational cost, low energy consumption⁴⁻⁷. Aluminium electro-deposition from aromatic hydrocarbons and ether has had limited success due to factors such as low electrical conductivity, narrow electrochemical windows and the pyrophoric nature of the materials involved^{8,9}. Extensive work has been done for aluminium electro-deposition using chloroaluminate ionic liquids showing successful electro-deposition^{4,9-29}. These studies indicate that the aluminium electro-deposition occurs only from Lewis acid melts where the molar ratio of

AlCl_3/IL is greater than 1. At lower molar ratios (Lewis base), the prominent aluminium species in the electrolyte is AlCl_4^- and in this case the organic cations undergo reduction at lower negative potentials than the dominant AlCl_4^- anion³⁰.

In the case of Lewis acid melts, the AlCl_4^- forms a further complex with AlCl_3 leading to formation of the Al_2Cl_7^- ion which is the electro-active species responsible for Al electro-deposition. The reaction can be represented as follows^{30,31}.



Despite success in laboratory studies, aluminium electro-deposition using chloroaluminate ionic liquids has thus far been not commercially attractive due to their moisture sensitivity and air instability. Recent reports in the literature have identified 1-propyl-1-methylpiperidinium bis(trifluoromethylsulfonyl) amide ($[\text{C}_3\text{mpip}][\text{NTf}_2]$) as a promising candidate for low temperature aluminium reduction processes^{25-28,32}, however, little is known about the electrochemical reactions occurring in the cell. In the present work, we have conducted a preliminary investigation of the anodic reaction taking place in $[\text{C}_3\text{mpip}][\text{NTf}_2]-[\text{AlCl}_3]_x$ mixtures using glassy carbon electrodes and dimensionally stable anodes (DSA) (Ir_2O_3 on Ti) at various compositions and temperatures. The cathodic reactions have also been the subject of a preliminary investigation at a range of temperatures, as has the stability of the ionic liquid under anticipated likely operating conditions for metal deposition.

2. Experimental section

2.1. Synthesis of ionic liquid

N-Methylpiperidine (99 wt%), 1-iodopropane (99 wt%), acetonitrile (99.8 wt%) and acetone (99.9 wt%) were used as received from Aldrich.

Bis(trifluoromethane)sulfonimide lithium salt (LiNTf_2) (99.95 wt%) was purchased from Iolitec (Germany). The

white hygroscopic powder was kept in a glove box with moisture and oxygen levels ~ 5 ppm. Milli-Q deionized water was used for the final liquid product rinsing. The theoretical yield of $[\text{C}_3\text{mpip}][\text{NTf}_2]$ for the first batch was 75 ml (108.8 g) whereas the theoretical yield for the second and third batches was 250 ml (362.5 g), assuming a $[\text{C}_3\text{mpip}][\text{NTf}_2]$ density of 1.45 g/ml.

The $\text{C}_3\text{mpip-I}$ solid precursor was synthesized by mixing N-Methylpiperidine and 1-iodopropane for 24 hours in a nitrogen atmosphere resulting in the following reaction:



The reaction was performed with 5 wt% excess of 1-iodopropane with addition some acetone. An ice bath was used in the first 3-4 hours to prevent the overheating of the mixture (although no significant heat effects were observed). The resultant yellow solid agglomerate was crushed into powder and repeatedly washed with acetone and collected with a Buchner funnel. The white powder was collected and dried under vacuum at room temperature for at least 48 h. The dried solid was recrystallised using acetonitrile. The $\text{C}_3\text{mpip-I}$ saturation concentration level was approximately 36 g/100 ml of acetonitrile at temperature close to boiling temperature of 82 °C. The hot saturated solution was either left on the bench top to cool down to room temperature for 1-2 h or placed in a freezer overnight. The crystalline product was collected and washed with cold acetonitrile on the Buchner funnel. The use of a freezer in the batch-3 recrystallisation was an attempt to achieve better final yield. The white crystalline product from each batch was dried in a desiccator under vacuum for at least 48 h. In all drying and mixing steps described above aluminium foil was used to cover flasks and desiccators to minimise the $\text{C}_3\text{mpip-I}$ exposure to light and prevent oxidation of iodide (I^-) to iodine (I_2).

The ionic liquid $[\text{C}_3\text{mpip}][\text{NTf}_2]$ was synthesised via an ion exchange reaction between the $\text{C}_3\text{mpip-I}$ precursor and bis(trifluoromethane)sulfonimide lithium salt:



Table 1. Phase behavior of $[\text{C}_3\text{mpip}][\text{NTf}_2]-[\text{AlCl}_3]_x$ sample mixtures at different IL: AlCl_3 molar ratios and temperatures

x (AlCl_3)	0.30	0.50	0.70
22 °C	yellowish white solid paste	grey-brownish gel-like solid	brownish gel-like solid
50 °C	clear, light yellowish monophasic solution	grey-brownish gel-like solid	brownish gel-like solid
60 °C	monophasic yellowish solution	biphasic layers (almost equal quantity), upper layer brownish, lower turbid white	brownish gel-like solid
70 °C	monophasic yellowish solution	biphasic layers (almost equal quantity), upper layer brownish, lower turbid white	biphasic layers (lower layer ~ 33 % of total volume). Upper layer dark brown colour, lower layer is clear colourless solution.
80 °C	monophasic yellowish solution	biphasic layers (almost equal quantity), upper layer brownish, lower turbid white	biphasic layers (lower layer ~ 33 % of total volume). Upper layer dark brown colour, lower layer is clear colourless solution.
90 °C	monophasic yellowish solution	biphasic layers (almost equal quantity), upper layer brownish, lower turbid white	biphasic layers (lower layer ~ 33 % of total volume). Upper layer dark brown colour, lower layer is clear colourless solution.

Equimolar amounts of $[\text{C}_3\text{mpip}][\text{NTf}_2]$ and LiNTf_2 were dissolved in Milli-Q water and then mixed together. The resultant biphasic mixture which had a slightly brown or yellow colour was stirred for 24 h under a nitrogen atmosphere. The lower phase of the biphasic mixture containing the crude $[\text{C}_3\text{mpip}][\text{NTf}_2]$ product was repeatedly washed with Milli-Q water using a separating funnel. Batches 1 and 2 were each rinsed 10 times although 6-7 times was enough to get rid of colouration and achieve a negative iodide test by AgNO_3 . Batch 3 was washed 20 times and a negative silver test was confirmed after 8 times rinsing. The final ionic liquid product retained a very faint yellow tone. The residual water was removed in vacuo on a rotary evaporator. The products were stored in a flask inside a desiccator. We chose not to take any additional precautions in terms of lowering moisture content of the ionic liquid, since we wanted to evaluate the commercial viability of these ionic liquids for aluminium deposition when the moisture content in the liquids was at the upper end of the spectrum.

2.2. IL- AlCl_3 mixtures preparations

AlCl_3 (99.99%, Sigma) was dissolved slowly in $[\text{C}_3\text{mpip}][\text{NTf}_2]$ with stirring at room temperature in a glove box under nitrogen atmosphere and heated to complete dissolution. Table 1 shows the phase behavior of these mixtures at various temperatures and compositions.

2.3. Electrochemical cell and instrumentation

A three-electrode cell consisting of a Pyrex glass cylindrical vessel with a flat-flange joint at the top was used for cyclic voltammetry tests of $[\text{C}_3\text{mpip}][\text{NTf}_2]$ - $[\text{AlCl}_3]_x$ mixtures. The Pyrex top, which was connected to the cell, had another glass flange joint with three standard glass sockets for the working, counter and reference electrodes. The electrochemical cell assembly was carried out in a nitrogen atmosphere environment of a glove box with oxygen and moisture level less than 5 ppm. After filling the cell with electrolyte components and inserting the electrodes into the sockets, the air-tight cell assembly was removed from the glove box to carry out the electrochemical studies.

A computer programmable Solartron SI 1287 potentiostat was used to study the electrochemical behavior of $[\text{C}_3\text{mpip}][\text{NTf}_2]$ - $[\text{AlCl}_3]_x$ mixtures. The working electrodes were a Metrohm Teflon sheathed glassy carbon (D= 2 mm), and a dimensionally stable anode (DSA) (Ir_2O_3 on Ti). The glassy carbon electrodes were polished to a mirror-like finish, sonicated, washed with acetone and dried in an oven at 60 °C for 3-5 hours prior to the cyclic voltammetry tests. The glassy carbon rod had a diameter of 2 mm while the dimensionally stable anode was a 1 cm wide plate that was dipped into the melt to a fixed immersion depth. The counter electrode used for all the experiments was a graphite rod and the reference electrode consisted of silver wire dipped into a solution of silver triflate in the ionic liquid under investigation²⁶.

3. Results and discussion

3.1. Electrochemical study

Cyclic voltammetry was used to investigate both the cathodic and anodic processes in pure $[\text{C}_3\text{mpip}][\text{NTf}_2]$ and $[\text{C}_3\text{mpip}][\text{NTf}_2]$ - $[\text{AlCl}_3]_x$ mixtures. Figure 1 depicts the voltammetric responses obtained for a glassy carbon working electrode in pure $[\text{C}_3\text{mpip}][\text{NTf}_2]$ at various temperatures (60, 70, 80, 90 °C) at a scanning rate of 100 mV s^{-1} . A representative voltammetric response from Figure 1 for pure $[\text{C}_3\text{mpip}][\text{NTf}_2]$ at glassy carbon electrode at 80 °C, 100 mV s^{-1} is depicted in Figure 2.

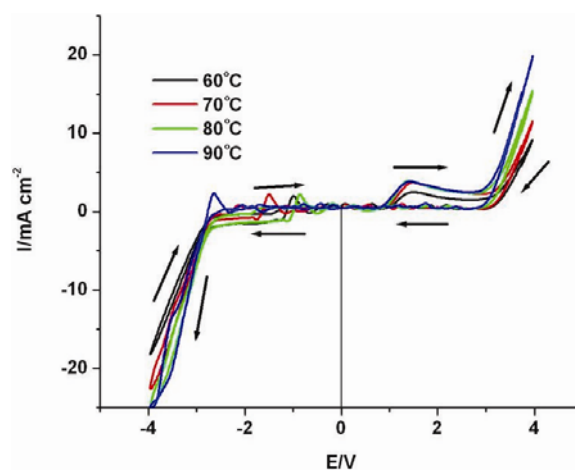


Figure 1. Voltammetric responses for glassy carbon working electrode in pure $[\text{C}_3\text{mpip}][\text{NTf}_2]$ at various temperatures (60, 70, 80, 90 °C), 100 mV s^{-1} .

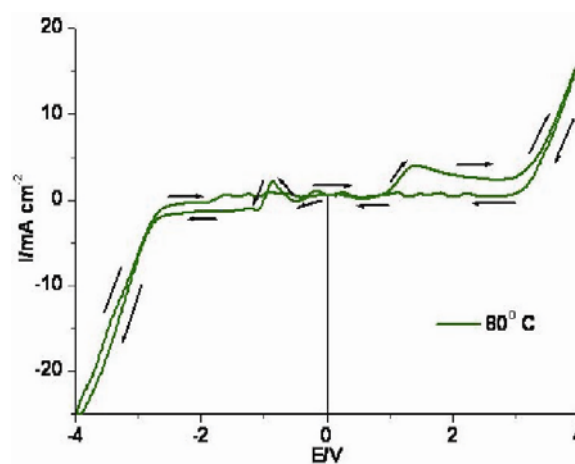


Figure 2. Representative voltammetric response from Figure 1 for pure $[\text{C}_3\text{mpip}][\text{NTf}_2]$ at glassy carbon electrode at 80 °C, 100 mV s^{-1} .

During cyclic voltammetry, the potential was swept from 0 V vs the reference electrode to -4V, then to +4V and then back to 0 V. The wide scanning range as opposed to the much narrower scanning range of about 1.8 to -1.1V (vs $\text{Fc}|\text{Fc}^+$) reported by earlier workers²⁶ was chosen so as to provide an indication of what was occurring over a broader voltage range. As seen from the

Figure 1, the decomposition of the pure ionic liquid would appear to start at around -2.8 V and $+3$ V on the cathodic and anodic sides respectively. Figure 3 depicts the voltammetric response for $[\text{C}_3\text{mpip}][\text{NTf}_2]-[\text{AlCl}_3]_x$ mixtures at 80°C at various AlCl_3 mole fractions ($x = 0.3, 0.5, 0.7$).

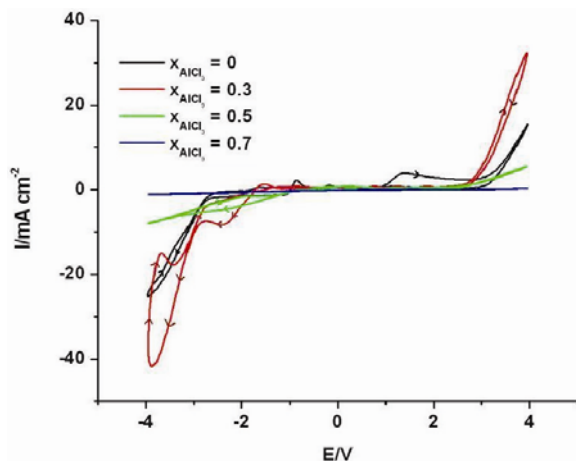


Figure 3. Voltammetric response for glassy carbon working electrode in pure $[\text{C}_3\text{mpip}][\text{NTf}_2]-[\text{AlCl}_3]_x$ mixtures with increasing AlCl_3 ($x = 0, 0.3, 0.5, 0.7$) at 80°C , 100 mV s^{-1} .

A cathodic reduction wave which is apparently due to the reduction of an aluminium species in the ionic liquid electrolyte (given that it is not present when Al is not present in the electrolyte – see Figure 1) starts in the $x = 0.3$ mixture at around -1.7 V (see Figure 3). Figures 4 and 5 depict the voltammetric response for a $[\text{C}_3\text{mpip}][\text{NTf}_2]-[\text{AlCl}_3]_x$ mixture ($x = 0.3$) at various temperatures ($50, 60, 70, 80$ and 90°C) from -4 V to $+4$ V. Figure 6 shows the cyclic voltammetric responses at various scan rates for $x=0.3$ at 50°C .

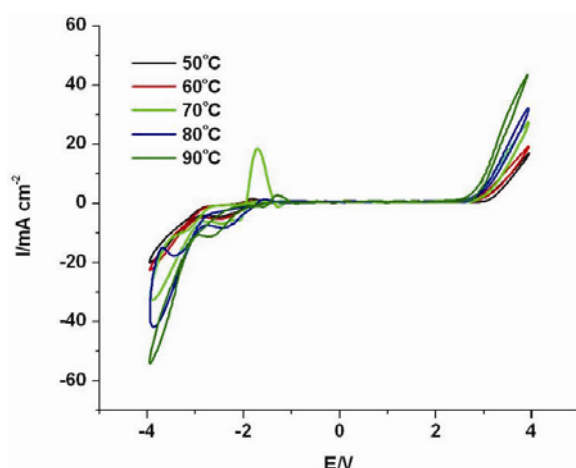


Figure 4. Voltammetric response for glassy carbon working electrode in a $[\text{C}_3\text{mpip}][\text{NTf}_2]-[\text{AlCl}_3]_x$ mixture ($x = 0.3$) at various temperatures ($50, 60, 70, 80$ and 90°C), 100 mV s^{-1} .

As per Figure 3 in Figure 4 the cathodic reduction wave which is apparently due to the reduction of an aluminium species in the ionic liquid electrolyte (given that it is not present when Al is not present in the electrolyte – see

Figure 1) generally starts in the $x = 0.3$ mixture at around -1.7 V apparently regardless of the temperature of the electrolyte although unlike Figure 3 the onset of the cathodic wave is masked somewhat by a large anodic peak that appears in the cyclic voltammogram scan at 70°C as shown in Figures 4 and 5.

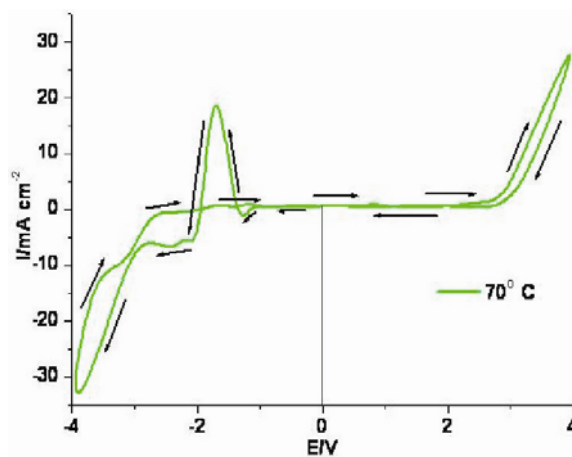


Figure 5. Representative voltammetric response from figure 4 for $[\text{C}_3\text{mpip}][\text{NTf}_2]-[\text{AlCl}_3]_x$ mixture ($x = 0.3$) at glassy carbon electrode at 70°C , 100 mV s^{-1} .

As can be seen from Figs. 3 and 4 the aluminium cathodic reduction peak seems to be present for $x=0.3$ at temperatures $50-90^\circ\text{C}$ whereas according to the literature temperatures greater than 80°C were required to achieve Al deposition²⁶. Surprisingly, however, the voltammetric results presented in Figure 3 indicate that increasing the AlCl_3 molar ratio does not produce an increase in the reduction peak height as would be expected if the concentration of the electro-active aluminium species had increased. This suggests a complex equilibrium associa-

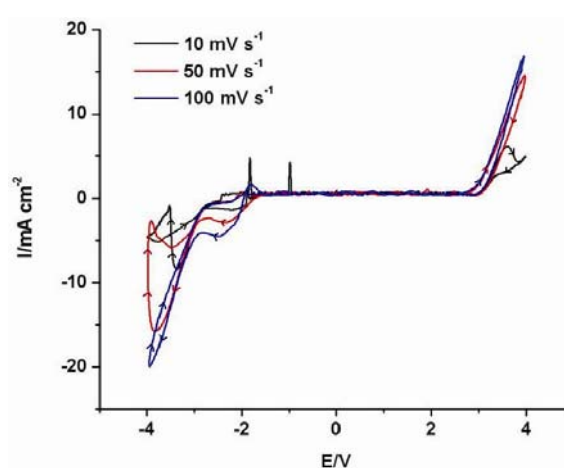


Figure 6. Voltammetric response for glassy carbon working electrode in a $[\text{C}_3\text{mpip}][\text{NTf}_2]-[\text{AlCl}_3]_x$ mixture ($x = 0.3$) at various scan rates ($100, 50, 10\text{ mV/s}$), 50°C .

ted with the formation of the electro-active species produced as a result of a reaction between $[\text{NTf}_2]^-$ and AlCl_3 . Earlier workers have attributed this electro-active species to be $[\text{AlCl}_3(\text{NTf}_2)]^-$ ²⁶.

A positive current peak is seen in each of the voltammograms of Figures 1 to 6 for scans in the cathodic direction of a glassy carbon working electrode in the voltage range -0.5 to -3 V vs Ag triflate electrode. The magnitudes and positions of the positive current peaks at different temperatures were inconsistent with one another as is especially apparent in the voltammograms of Figures 4, 5 and 6 which utilized a $[\text{C}_3\text{mpip}][\text{NTf}_2]-[\text{AlCl}_3]_x$ ($x=0.3$) mixture. The magnitude of the positive current peak appearing at about -1.75 V vs Ag triflate in the cathodic scan at 70 °C is much greater than the positive current peaks occurring in the same regions of the scans at 50 °C, 60 °C, 80 °C and 90 °C. Whilst it is not clear as to what caused this variation it is noted that the anodic peaks of variable magnitude and position which appear to be at least partially temperature dependent are clearly present in the region of about -0.9 to -2.8 V vs Ag triflate in voltammetric scans of pure $[\text{C}_3\text{mpip}][\text{NTf}_2]$ when scanning in the cathodic direction (see e.g. Figure 1) and in the region of about -0.9 to -2.9 V vs Ag triflate in voltammetric scans of $[\text{C}_3\text{mpip}][\text{NTf}_2]-[\text{AlCl}_3]_x$ mixtures when scanning in the cathodic direction (see e.g. Figures 3 to 6). It is noted from the observations described in Table 1 that the appearance of a $[\text{C}_3\text{mpip}][\text{NTf}_2]-[\text{AlCl}_3]_x$ mixture for $x=0.3$ did not visibly change from the appearance of a monophasic yellowish solution in the temperature range 60 °C to 90 °C when it had not been subjected to voltammetric scanning. However, if each of these large magnitude anodic current peaks is due to the dissolution of a film formed on the electrode during forward scanning in the anodic voltage range of 0 to 4 V vs Ag triflate then variations in the nature of the film might be a possible cause of these variations in peak magnitude and position.

In most of the voltammetric scans of Figures 1 to 6 covering both pure $[\text{C}_3\text{mpip}][\text{NTf}_2]$ and $[\text{C}_3\text{mpip}][\text{NTf}_2]-[\text{AlCl}_3]_x$ mixtures, the anodic peak in the region -0.5 to -2.75 V vs Ag triflate is followed by a cathodic wave before a sharp cathodic drop-off starts in the region -2.75 to -2.9 V vs Ag triflate as the scanning progresses in the cathodic direction. Comparing the CVs in both the $[\text{C}_3\text{mpip}][\text{NTf}_2]$ and $[\text{C}_3\text{mpip}][\text{NTf}_2]-[\text{AlCl}_3]_x$ mixtures, it would appear from Figures 3 to 6 that aluminium reduction occurs in the potential range -1.8 to about -3.8 V vs Ag triflate, while at cathodic potentials more negative than about -2.8 V vs Ag triflate, decomposition of the $[\text{C}_3\text{mpip}][\text{NTf}_2]$ is occurring simultaneously.

3.2. Deposition of Al and cathodic other reactions

To confirm the aluminium reduction process at -3.7 V, galvanostatic experiments were conducted in which aluminium was electrodeposited at 90 °C onto graphite and copper electrode substrates from $[\text{C}_3\text{mpip}][\text{NTf}_2]-[\text{AlCl}_3]_x$ ($x=0.5$) at potential -3.7 V for 10 min. The presence of aluminium deposits were confirmed firstly by visual inspection. Both substrates showed white metallic coatings when taken out from the cell. The deposits were then washed thoroughly with acetone and dried. Not surprisingly, given the relatively negative deposition potential of -3.7 V, the subsequent SEM-EDS analyses of the deposits showed the presence of residual ionic liquid and/or ionic liquid decomposition products on the surfaces of the electrode substrates. This was particularly

evident for the graphite substrate which analysis showed the existence of isolated Al. It was found to be very hard to clean the coated graphite as the ionic liquid and/or ionic liquid decomposition products were well adhered and penetrated into the porous substrate surface.

The quality of the aluminium deposits can be seen from BSE micrographs in Figs. 7, 8, 9, 10(a) and 10(b).

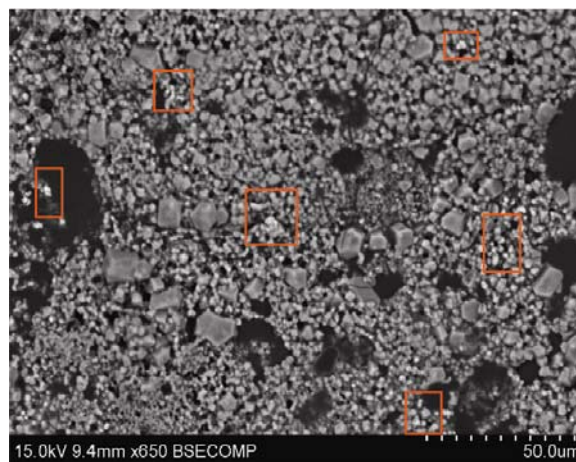


Figure 7. BSE image of aluminium electrodeposited at 90 °C from $[\text{C}_3\text{mpip}][\text{NTf}_2]-[\text{AlCl}_3]_x$ ($x=0.5$) onto graphite.

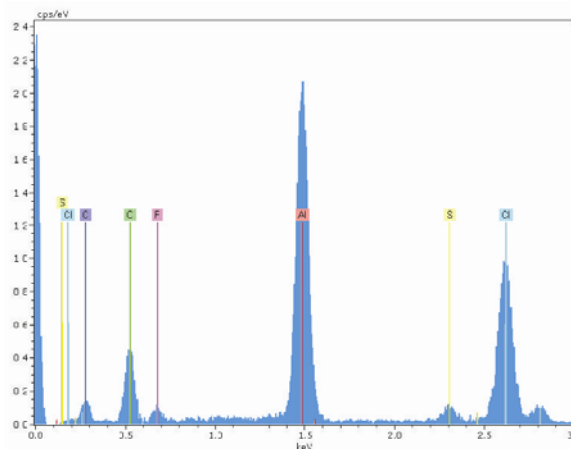


Figure 8. Energy spectra of aluminium deposits (whole area of the Figure 7 scan).

As is apparent from the highlighted regions in Figure 7 the aluminium deposits on the graphite electrode substrate appear to be in the form of crystals of up to 10 μm in size. The aluminium deposits on copper (Figures 9, 10(a) and (b)) have a fractured surface comprising large and bulky aluminium clusters with irregular shapes. The fractured clusters are thought to have been induced by mechanical stresses which occurred during the cleaning process.

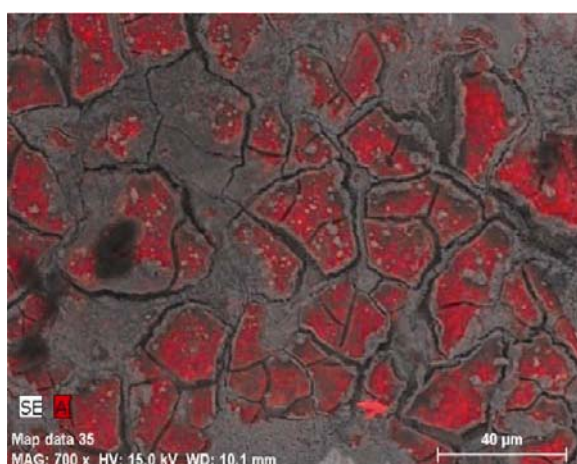
From the BSE images it is evident that the nature of the electrode substrate has a great influence on the quality of the aluminium deposits.

Further Al deposition experiments were conducted with a copper electrode. There was visible Al deposition on a

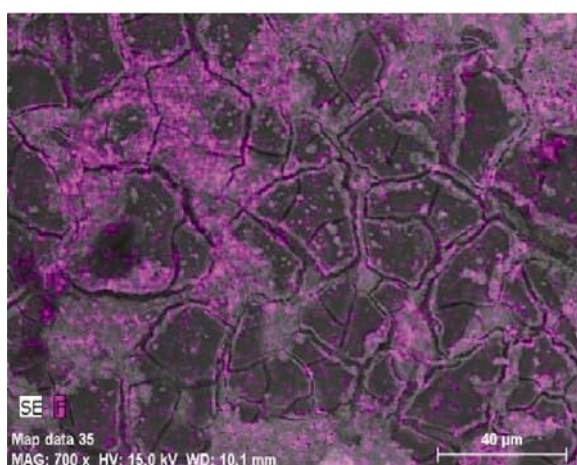
copper electrode after 5 minutes at -1.0 V at 60 °C, however at higher potentials a black deposit was observed on the electrode which may have been due to the decomposition of ionic liquid leading to poisoning of the electrode surface. The products of the electrolyte decom-



Figure 9. BSE image of Al film electrodeposited at 90 °C from $[\text{C}_3\text{mpip}][\text{NTf}_2]-[\text{AlCl}_3]_x$ ($x=0.5$) onto Cu foil.



(a)



(b)

Figure 10. (a) aluminium, and (b) fluorine mapping of aluminium deposits for the image in Figure 9.

position may also have been passivating any aluminium deposited during the cathodic scan and preventing the appearance of the anodic re-oxidation peak on scan reversal, as would normally be expected during any metal deposition process. This might explain the absence of the expected metal re-oxidation peaks in most of the cyclic voltammograms presented above.

Additional cathodic potentiostatic experiments were carried out to study the deposition of Al from $[\text{C}_3\text{mpip}][\text{NTf}_2]-[\text{AlCl}_3]_x$ mixtures at copper electrodes as well as graphite and stainless steel electrodes. The constant potential values were chosen from previous studies and electrolysis was carried out at 90 °C for 2 hours. The chosen test potentials of -1 , -1.5 , -2 , -2.5 and -3 V yielded no aluminium deposits however, unlike results reported previously in literature²⁶. One likely reason for the failure to produce aluminium deposits in these latter experiments is thought to be at least partially due to the level of the moisture content in the ionic liquid electrolytes used in these experiments since after drying in a rotary evaporator they were not further subjected to drying in vacuo at elevated temperatures for an extended period in attempt to simulate extreme conditions that one might encounter in an industrial scenario. This view is consistent with the observations of earlier workers, albeit for a different type of ionic liquid, who have reported that even if only a small amount of water remained in the ionic liquid they were using, namely an aliphatic quaternary ammonium imide-type ionic liquid containing metal ions, even after dehydration in vacuo, it can cause some problems in metal deposition from the ionic liquid³³. Another reason for the lack of Al deposition is probably due to the formation of a passivating film on the electrode surface caused either by the presence of a small amount of water in the ionic liquid electrolyte or by decomposition of the ionic liquid or a combination of both (see for example the BSE image of the film on the graphite electrode substrate shown in Figure 7 surrounding the isolated Al deposits). This finding suggests that if Al was to be deposited from a $[\text{C}_3\text{mpip}][\text{NTf}_2]-[\text{AlCl}_3]_x$ mixture on a commercial scale that the water content and the deposition potential would need to be carefully controlled for Al deposition and minimal electrolyte decomposition as was apparently done by earlier workers²⁶ who used thoroughly dried $[\text{C}_3\text{mpip}][\text{NTf}_2]-[\text{AlCl}_3]_x$ electrolytes²⁶ and a narrow potential range for Al deposition in order to achieve good quality deposits of Al. In addition, those earlier workers²⁶ indicated that $[\text{C}_3\text{mpip}][\text{NTf}_2]$ is “air- and water-stable”, however, this statement should perhaps be a more qualified one that warns of the potential risks of too high a level of water in the electrolyte and of exposing the electrode on which Al is to be deposited to too negative or too positive a potential on either side of the optimum Al deposition potential range. Otherwise, a film detrimental to Al deposition may be formed on the electrode.

3.3. Anodic reactions

Linear sweep voltammograms obtained at the DSA electrode in the mixture $[\text{C}_3\text{mpip}][\text{NTf}_2]-[\text{AlCl}_3]_x$ ($x = 0.3$) are shown in Figure 11 at various temperatures and at a scan rate of 10 mV/s.

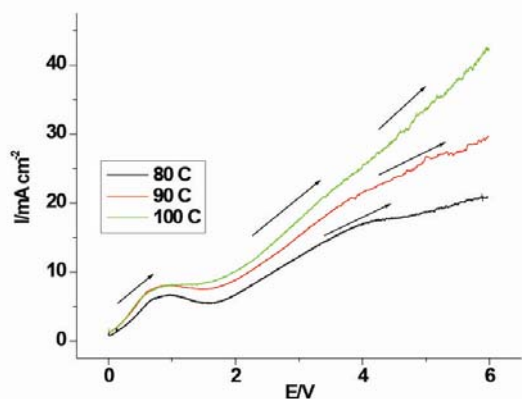


Figure 11. Linear sweep voltammograms obtained at DSA electrode for $[\text{C}_3\text{mpip}][\text{NTf}_2]-[\text{AlCl}_3]_x$ ($x = 0.3$) at various temperatures, 10 mV/s.

A small anodic peak is seen at around 1V beyond which the current increases before reaching a limiting current at about 4 V. The initial anodic peak in the 0 - 2 V range is assumed to be at least partly associated with an anodic reaction occurring prior to chlorine evolution. This peak is also present in the absence of AlCl_3 (see Figs. 1 and 2) and consequently it is thought to be associated with the oxidation of $[\text{C}_3\text{mpip}][\text{NTf}_2]$.

As expected, the limiting current increases with increasing temperature due to the higher diffusion rates of the reacting ions. The slope of the voltammograms is indicative of a high cell resistance. This is again expected given the low conductivity of these ionic liquids^{34, 35}.

Galvanostatic experiments were also carried out to confirm evolution of chlorine. After completion of the electrochemical studies the visible appearances of the mixtures changed markedly and the initial colourless appearance had changed to a light to dark yellow colour with a Cl_2 like odour. Another indication of gas formation was the presence of bubbles around the electrode. To identify the possible reaction products, further potentiostatic tests were carried out and the collected gases were analyzed using GC-MS. Scanning electron microscopy and XPS techniques were also used to investigate the nature of deposits on the electrode surfaces.

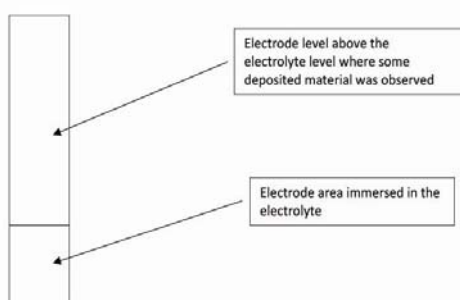
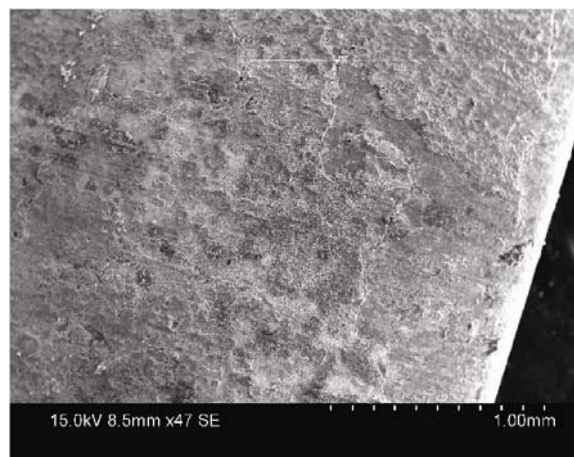


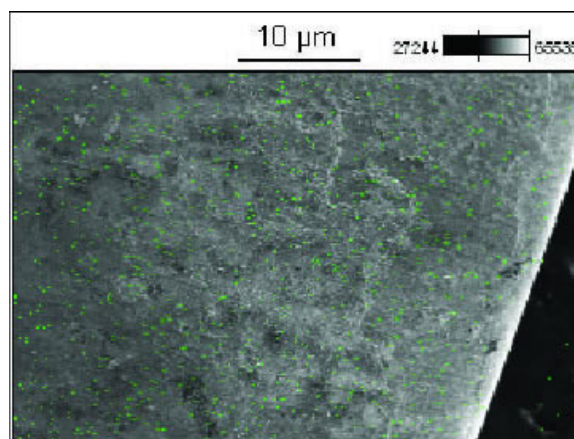
Figure 12. Schematic diagram of a DSA electrode subjected to the electrolysis tests of Figures 13 - 19.

For these studies, $[\text{C}_3\text{mpip}][\text{NTf}_2]-[\text{AlCl}_3]_x$ mixtures ($x = 0.24, 0.35$) were used as electrolytes with a DSA (Ir_2O_3 on Ti) working electrode (see Figure 12). All tests were carried out in a single compartment cell.

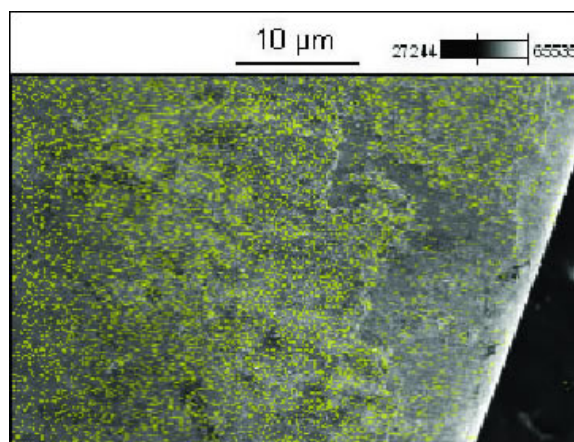
3.3.1. SEM and XPS analysis



(a)



(b)(i)

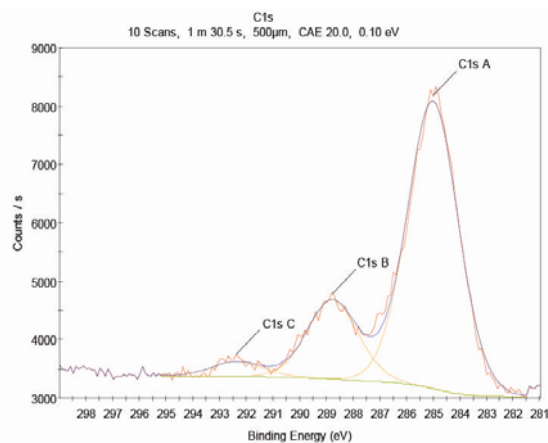


(b)(ii)

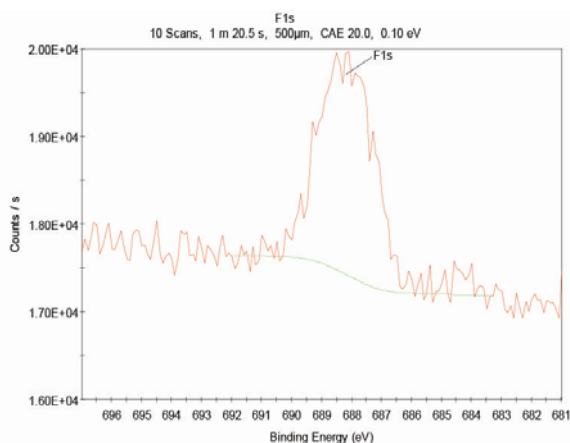
Figure 13. (a) SEM image and elemental mapping results for (b)(i) Al, and (b)(ii) Cl for a DSA anode after a potentiostatic test (2 V vs Ag/Ag triflate for 2 hours) for $[\text{C}_3\text{mpip}][\text{NTf}_2]-[\text{AlCl}_3]_x$ mixture ($x=0.24$).

Potentiostatic experiments were performed on a DSA working electrode at an anodic potential of 2 V vs Ag triflate reference electrode for 2 hours in a $[\text{C}_3\text{mpip}][\text{NTf}_2]-[\text{AlCl}_3]_x$ mixture ($x = 0.24$). The morphology of the DSA electrode was then examined for any deposits using scanning electron microscopy and elemental mapping was used to identify the deposits. Figure 13 (a) shows the SEM image of the electrode while Figures 13(b)(i) and (ii) show the corresponding mapping results for Al and Cl respectively.

The presence of aluminium and chlorine is believed to be due to physical adsorption of the ionic liquid mixture on the electrode surface as when the electrode was completely washed with acetone, these materials were not detected. To understand the exact nature of the deposits on the DSA electrode, XPS was used and binding energy value comparisons were done for better understanding of bonding involved. The corresponding XPS data are shown in Figures 14(a) and 14(b).



(a)

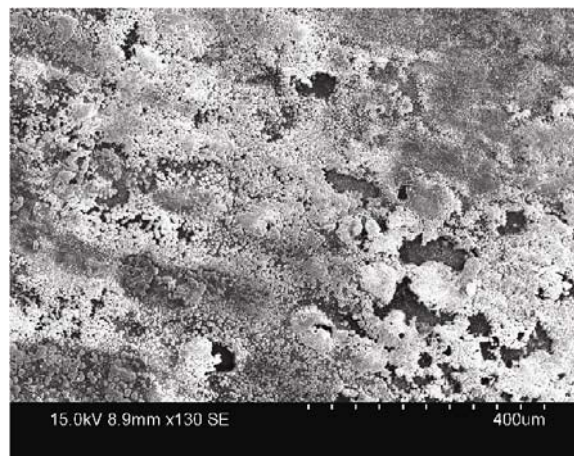


(b)

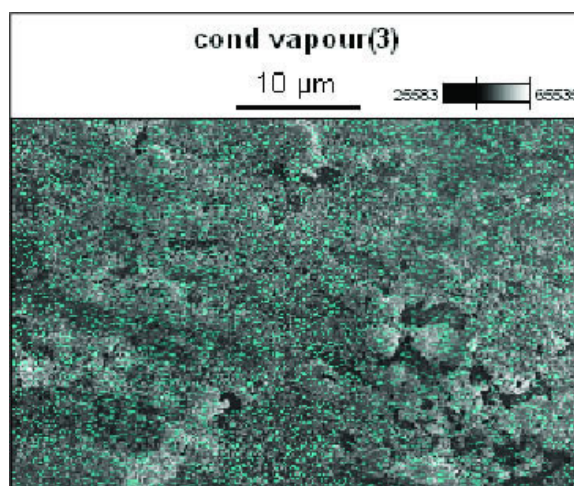
Figure 14. Binding energy spectra obtained at the DSA working electrode after a potentiostatic test in a $[\text{C}_3\text{mpip}][\text{NTf}_2]-[\text{AlCl}_3]_x$ mixture ($x = 0.24$): (a) C, and (b) F.

The spectral lines (peaks) in Figure 14(a) corresponding to binding energies 285, 289 and 291 eV values correspond to carbon (1s states) in fluorocarbon compounds²⁷ [e.g. CF_4 , $(-\text{CF}_2-\text{CF}_2)_n$]. This is in complete agreement with the binding energy values obtained for

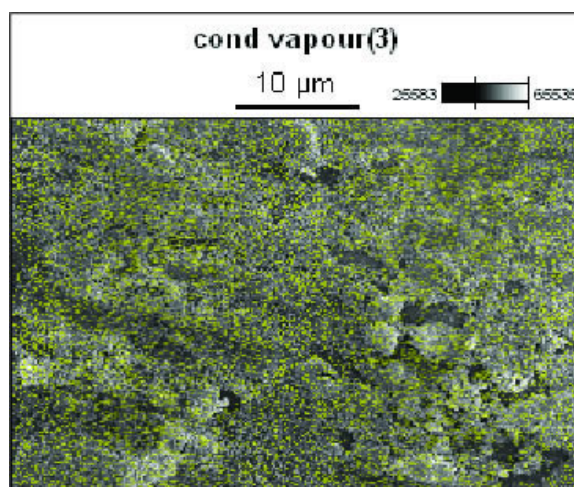
fluorine shown in Fig. 14(b). The peak corresponding to a binding energy of 689 is due to F(1s) state [e.g. CF_2 etc] which indicates the presence of fluorocarbons. The gas analysis for the DSA electrode is discussed later.



(a)



(b)(i)

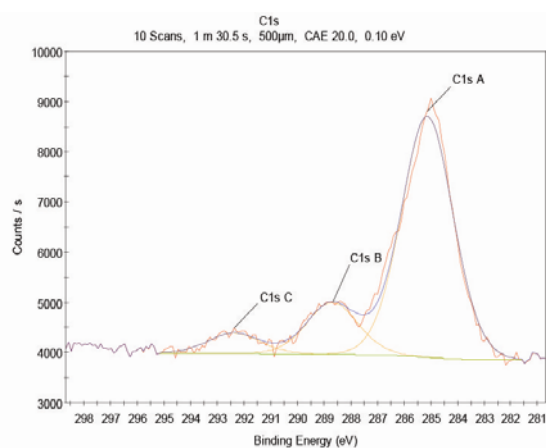


(b)(ii)

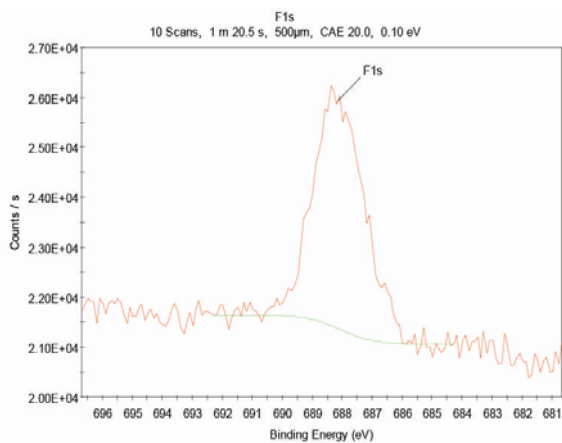
Figure 15. (a) SEM image of condensed vapours deposited on DSA electrode after a potentiostatic test (2 V for 2 hrs, 90 °C) in a $[\text{C}_3\text{mpip}][\text{NTf}_2]-[\text{AlCl}_3]_x$ mixture ($x = 0.24$) and corresponding elemental mapping for (b)(i) Al and (b)(ii) Cl.

Another interesting observation was the presence of some condensed material on the DSA working electrode that was not in contact with the electrolyte directly (see schematic in Figure 12). This deposited material was analyzed using SEM and XPS techniques. Figure 15 (a) shows the SEM image of condensed vapours on part of the electrode and Figures 15 (b)(i) and (b)(ii) show the corresponding elemental mapping for Al and Cl respectively.

These results possibly indicate the sublimation and condensation of AlCl_3 from the mixture. This electrode structure was also investigated using the XPS technique. XPS line spectra for the condensed vapour region using the DSA electrode are shown in Figures 16(a) and (b).



(a)



(b)

Figure 16. XPS spectra of the DSA electrode surface with deposited condensed vapours for a $[\text{C}_3\text{mpip}][\text{NTf}_2]-[\text{AlCl}_3]_x$ ($x = 0.24$) mixture at 90°C : (a) C, and (b) F.

The peaks in Figure 16(a) corresponding to 285, 289 and 292 eV values represent C (1s spectral lines)²⁷. This is characteristic for fluorocarbon compounds. Also a spectral line for F (1s spectral line) shows a peak at around 689 eV which confirms the presence of fluorocarbon based compounds $(-\text{CF}_2-\text{CF}_2-)_n$. To confirm if these compounds were actually formed as a result of an anodic reaction or decomposition of the ionic liquid due to heating (without any electrolysis), an experiment was carried out where the mixture was heated for 3-4 hrs at 90°C

and electrodes immersed in the mixture in a sealed cell. The XPS analysis of these samples confirmed the presence of fluorocarbons on the electrodes, indicating that these compounds were formed as a result of decomposition of the ionic liquid itself at higher temperatures.

3.3.2. GC-MS analysis

For identification of gaseous reaction products, mass spectral data was acquired in positive ion electron impact (EI^+) mode using a Thermo Trace DSQ II GC-MS (Thermo Scientific). Gaseous samples (100 μL) were injected onto a 30 m x 0.25 mm J&W DB5-MS capillary column (Agilent Technologies), at an initial temperature of 35°C with helium carrier gas set to a constant flow rate of 1 mL/min. The GC temperature was ramped to 260°C . The spectral matches were obtained using Xcalibur library associated with the instrument.

Separate experiments were carried out for a $[\text{C}_3\text{mpip}][\text{NTf}_2]-[\text{AlCl}_3]_x$ mixture ($x = 0.35$). In a first experiment the mixture was simply heated at 90°C for 3 hours (without any electrolysis test). The GC-MS analyses qualitatively determined the presence of (a) Methanamine N,N -bis(trifluoromethoxysulfinyl); (b) Chlorotrimethyl silane; and (c) Dichloro dimethyl silane. A second mixture was subjected to electrolysis at constant potential of 3 V vs Ag triflate for 3 hrs, the gas samples were analysed using GC-MS and the analyses qualitatively determined the presence of (a) Methanamine N,N -bis(trifluoromethoxysulfinyl); (b) Ether, bis(chloromethyl); (c) Tromethamine; (d) Chlorotrimethyl silane; and (e) Dichloro dimethyl silane. Also a fused silica column was used instead of DB5-MS capillary column and the analysis with this arrangement confirmed qualitatively that chlorine gas was being formed in the second mixture.

The GC-MS results confirm the formation of various decomposition products of the ionic liquid electrolyte even without any electrolysis tests. Cl_2 is also seen to be present since it reacts with the column to form chlorosilanes. Further, the formation of fluorocarbons found in the XPS spectra may be difficult to avoid due to the operating conditions required for Al electro-deposition. The occurrence of fluorocarbons thus suggests that on a commercial scale the process is unlikely to be environmentally friendly. Other products like trimethanamine and chloro-ethers are also formed during the electrolysis. Due to formation of these decomposition products, the ionic liquids are unlikely to be reusable in an Al deposition process. This conclusion is supported by Roudopoulos et al.²⁶

3.3.3. ^{27}Al NMR spectroscopy

Aluminium speciation change during the electrolysis was investigated by ^{27}Al NMR spectroscopy using a double compartment H shaped cell. Electrolysis was conducted in a potentiostatic mode at 2.0 V vs Ag triflate at 90°C for 20 hours in $[\text{C}_3\text{mpip}][\text{NTf}_2]-[\text{AlCl}_3]_x$ mixtures where $x = 0.24, 0.35$ and 0.45 . The counter electrode was a graphite rod with a diameter of 15 mm,

the working electrode was a stainless steel wire (L= 25 mm and D= 0.8 mm) and a 0.5 mm silver wire dipped in silver triflate was used as reference electrode. The ^{27}Al NMR of electrolyte samples before the tests and samples from the cathodic and anodic compartments after tests were recorded at a temperature of 90 °C. The ^{27}Al chemical shift values were measured relative to an aqueous solution of $\text{Al}(\text{NO}_3)_3 \cdot 9\text{H}_2\text{O}$ as an external reference. The interpretation of ^{27}Al NMR spectra in connection with speciation in these mixtures is well presented by T. Rodopoulos et al.²⁶ and was adopted in the following analysis. The ^{27}Al NMR shifts (δ) of the resonances obtained in the experiments are shown in Figures 17 to 19.

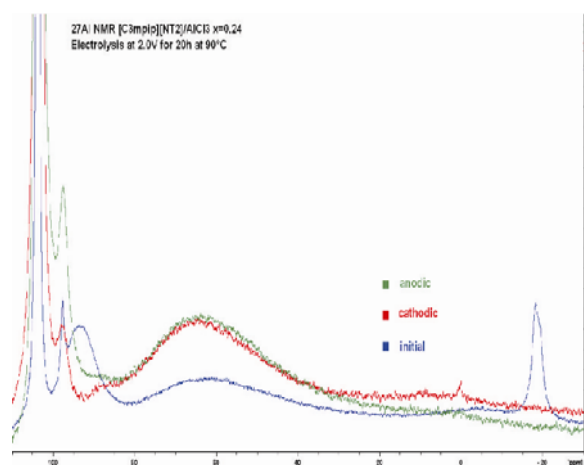


Figure 17. The ^{27}Al NMR spectra of $[\text{C}_3\text{mpip}][\text{NTf}_2]-[\text{AlCl}_3]_x$ mixture at $x=0.24$ taken at 90 °C before and after electrolysis test. Cell voltage kept 2.0 V for 20 h at 90 °C.

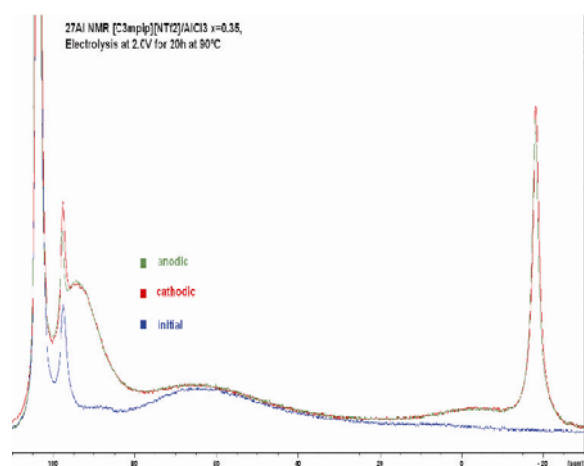
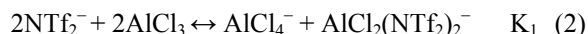


Figure 18. The ^{27}Al NMR spectra of $[\text{C}_3\text{mpip}][\text{NTf}_2]-[\text{AlCl}_3]_x$ mixture at $x=0.35$ taken at 90 °C before and after electrolysis test. Cell voltage kept 2.0 V for 20 h at 90 °C.

The ^{27}Al NMR shifts (δ) of the resonances obtained in the experiments are summarized in Table 2. All samples showed the dominant strong resonance at $\delta=104$ ppm (Figs. 17-19) which has been assigned previously to the presence of a 4-coordinated AlCl_4^- ion²⁶. The following equilibrium has been suggested in $[\text{C}_3\text{mpip}][\text{NTf}_2]-[\text{AlCl}_3]_x$ mixtures:



A large equilibrium constant K_1 for reaction (2) would account for the strong resonance observed.

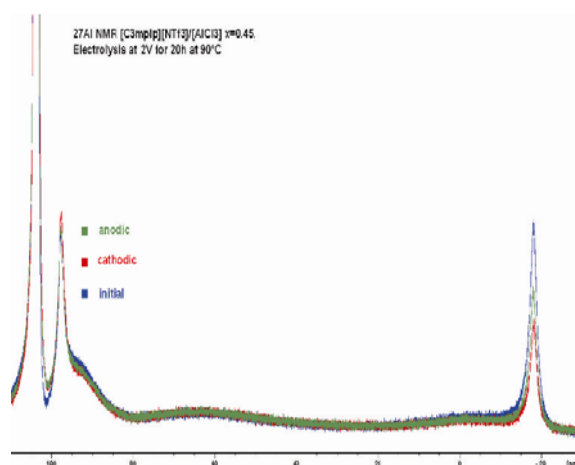


Figure 19. The ^{27}Al NMR spectra of $[\text{C}_3\text{mpip}][\text{NTf}_2]-[\text{AlCl}_3]_x$ mixture at $x=0.45$ taken at 90 °C before and after electrolysis test. Cell voltage kept 2.0 V for 20 h at 90 °C.

Table 2. ^{27}Al NMR shifts (δ) of the resonances in the spectra of $[\text{C}_3\text{mpip}][\text{NTf}_2]-[\text{AlCl}_3]_x$ mixtures for $x=0.24, 0.35$ and 0.45 initially and mixtures in the anodic and cathodic chambers after being held at 2 V at 90 °C for 20 h.

x	Sample	δ [ppm] for $[\text{C}_3\text{mpip}][\text{NTf}_2]-[\text{AlCl}_3]_x$
0.24	Initial mixture	104 s, 98m, 94m, -5vw, -18m
	Anodic chamber mixture	104 s, 98m
	Cathodic chamber mixture	104 s, 98m, -1w
0.35	Initial mixture	104 s, 98m, 90w
	Anodic chamber mixture	104 s, 98m, 94m, -3vw, -18m
	Cathodic chamber mixture	104 s, 98m, 94m, -3vw, -18m
0.45	Initial mixture	104 s, 98m, 94mw, -3vw, -18m
	Anodic chamber mixture	104 s, 98m, 94mw, -3vw, -18m
	Cathodic chamber mixture	104 s, 98m, 94mw, -3vw, -18m

A peak similar to the medium resonance at $\delta=98$ ppm found in all test samples has been assigned in previous studies to being due to a hydrolysis product^{26,36}. Analogously, we suggest the medium resonance at $\delta=98$ ppm found in the present study is likely to be due to a hydrolysis product resulting from the reaction of residual water with the $[\text{C}_3\text{mpip}][\text{NTf}_2]-[\text{AlCl}_3]_x$ mixtures. Franzen et al.³⁷ identified hydrolysis products as $\text{Al}_2\text{Cl}_6\text{OH}$ and Al_2OCl_5 using secondary ion mass spectrometry. Other reaction products were determined by passing nitrogen gas over a $[\text{C}_3\text{mpip}][\text{NTf}_2]-[\text{AlCl}_3]_x$ mixture and bubbling the off-gas in a silver nitrate solution for 2 hours. The silver nitrate solution showed a transparent to milky appearance transition which is indicative of the presence of chlorine ions (Cl^-). The absence of aluminium ions in the silver nitrate solution

was verified by an alizarin test. These tests suggest that another by-product was hydrogen chloride (HCl). The magnitude of the peak at $\delta=98$ ppm is consistent with the electrolytes containing more hydrolysis products than has been reported in an earlier study²⁶ in which the magnitude of the peak at $\delta=98$ ppm was weak. This would at least partly explain the poor Al deposition outcomes obtained in the present study compared with those reported earlier²⁶, but once again casts doubt on the industrial viability of these apparently moisture sensitive ionic liquids.

The tetrahedral $[\text{AlCl}_3\text{-(NTf}_2\text{)}]^-$ electro-active ion resonance at $\delta=94$ ppm (assigned previously by T. Rodopoulos et al.²⁶ and thought to be the 4-coordinate Al species from which Al can be electrodeposited) is evident in the initial mixtures with $x=0.24$ and 0.45 (Figs. 13 and 15) and is not present in the initial mixture with $x=0.35$ (Fig. 14) although both cathodic and anodic samples with $x=0.35$ showed the resonance at $\delta=94$ ppm in the form of a broad shoulder adjacent to a hydrolysis resonance at $\delta=98$ ppm. The aluminium electro-active ion resonance at $\delta=94$ ppm correlates with the presence of an octahedral $\text{Al(NTf}_2\text{)}_3$ complex at $\delta=-18$ ppm (see Figs. 17-19) (assigned previously by T. Rodopoulos et al.²⁶ and thought to be due to a number of isomers of $\text{Al(NTf}_2\text{)}_3$). In addition to this, it can be noted that cathodic and anodic $x=0.24$ sample mixtures showed neither $\delta=94$ nor $\delta=-18$ ppm resonances at a given temperature. These correlations suggest that both the $\text{Al(NTf}_2\text{)}_3$ complex and the $[\text{AlCl}_3\text{-(NTf}_2\text{)}]^-$ electro-active ion could be the equilibrium products of some reaction. These results support the following equilibrium reaction:



It should be noted that this correlation is only valid at temperatures above 55 °C. At temperatures below 55 °C the electro-active ion $[\text{AlCl}_3\text{-(NTf}_2\text{)}]^-$ becomes unstable, while the $\text{Al(NTf}_2\text{)}_3$ complex is well manifested in ²⁷Al NMR spectrum²⁶.

The lack of an $\text{Al(NTf}_2\text{)}_3$ complex resonance in the initial sample mixture with $x=0.35$ could be due to slow kinetics of reaction (2) during AlCl_3 dissolution although this would need to be confirmed by further experiments.

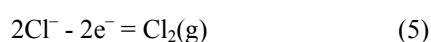
The presence of the octahedral ion $\text{AlCl}_2(\text{NTf}_2)_2^-$ resonance at $\delta=-3$ ppm is clearly visible in the cathodic sample spectrum with $x=0.24$ (Fig. 17) and both the cathodic and anodic samples' spectra with $x=0.35$ (Fig. 18). It also has a faint presence in all samples with $x=0.45$ (Fig. 19). The low intensity for this resonance is likely to be due to a very high equilibrium constant K_2 for reaction (3) that provides a very low relative concentration of the $\text{AlCl}_2(\text{NTf}_2)_2^-$ ion in $[\text{C}_3\text{mpip}][\text{NTf}_2]-[\text{AlCl}_3]_x$ mixtures.

The broad resonance at around $\delta=66$ ppm in all spectra is due to aluminium in the solid material used in the probe and is not associated with the sample mixtures. This is consistent with the electrode reactions being:

Cathode:

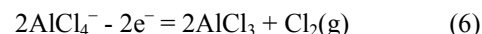


Anode:



although the chlorine ion is very likely to be part of an aluminium complex ion coordination, so the anode reaction is more likely to be of the form:

Anode:



The tetrahedral AlCl_4^- ($\delta=104$) resonance decreased in intensity for anodic samples with $x=0.24$ and 0.45 . The AlCl_3 product is expected to be consumed by reaction (1) and partially sublimes as was noted earlier with DSA anodes.

No aluminium was deposited on the graphite rod cathode during the tests suggesting that another cathodic reaction is occurring at the set potential that would explain a decrease in resonance intensities for both tetrahedral AlCl_4^- and octahedral $\text{Al(NTf}_2\text{)}_3$ ions and the presence of $\text{AlCl}_2(\text{NTf}_2)_2^-$ resonance in the cathodic samples, namely:

Cathode:



Alternatively, a plausible reason for the absences of aluminium deposits is the hydrolysis of the electro-active ion $[\text{AlCl}_3\text{-(NTf}_2\text{)}]^-$ and possible electrode passivation. A more rigorous drying procedure both in preparation and testing of these liquids should prevent deactivation of the $[\text{C}_3\text{mpip}][\text{NTf}_2]-[\text{AlCl}_3]_x$ mixtures, but this would be a significant additional cost on an industrial scale.

4. Conclusion

In the present study of the deposition of aluminium and other cathodic reactions, the ionic liquid was not stable since decomposition products co-deposited on the electrode at the Al deposition potential investigated of -3.7 V. In addition, the deposition of aluminium from $[\text{C}_3\text{mpip}][\text{NTf}_2]-[\text{AlCl}_3]_x$ mixtures was generally found to be highly inconsistent and it is thought that sensitivity of the ionic liquid mixtures to moisture and exposure of the electrode substrate to a deposition voltage in which decomposition of the ionic liquid is occurring simultaneously is at least partly responsible for the presence of passivation products on the electrode surface during deposition.

In the present study of the anodic reactions taking place in $[\text{C}_3\text{mpip}][\text{NTf}_2]-[\text{AlCl}_3]_x$ mixtures using glassy carbon electrodes and dimensionally stable anodes (DSA) (Ir_2O_3 on Ti) at various compositions and temperatures indicated that some decomposition of the ionic liquid was occurring at least under the conditions investigated. Formation of Cl_2 was confirmed to take place at dimensionally stable anodes as a part of the anodic reaction of $[\text{C}_3\text{mpip}][\text{NTf}_2]-[\text{AlCl}_3]_x$ mixtures (at least when $x=0.35$); however analysis of the mixture indicated that at temperatures near to a potential operating temperature of the $[\text{C}_3\text{mpip}][\text{NTf}_2]-[\text{AlCl}_3]_x$ the mixture at least partially decomposes into fluoro-carbons (at least when $x=0.24$) and other chloro-compounds (at least when $x=0.35$). It would appear therefore, that the formation of fluorocarbons, at least for the ionic liquids investigated in this study, may be difficult to avoid under the operating

temperature required for Al electro-deposition from a $[\text{C}_3\text{mpip}][\text{NTf}_2]-[\text{AlCl}_3]_x$ mixture. The formation of these anodic decomposition products has the further disadvantage that the $[\text{C}_3\text{mpip}][\text{NTf}_2]$ liquid may be difficult to reuse.

In summary, the ionic liquids may have a poor usage life and may need to be regularly replaced under industrial operation due to the potential anodic reactions as illustrated in the present study by the decomposition reactions found to be occurring at a DSA electrode at a potential of around 2 V vs Ag triflate under typical conditions envisaged for aluminium deposition. Given this and the apparent additional disadvantages of moisture sensitivity of Al electro-deposition in these ionic liquids, the inconsistency of Al deposition and the potential for the cathodic decomposition of the ionic liquid and the co-deposition of the resultant electrolyte decomposition products on the cathode as has been shown to occur when the potential of the cathode is made too negative, a commercial process of electro-deposition of Al from $[\text{C}_3\text{mpip}][\text{NTf}_2]-[\text{AlCl}_3]_x$ mixtures may prove to be difficult to develop and perform satisfactorily on an industrial scale.

5. Acknowledgement

This work was conducted as part of a research cluster entitled "Breakthrough technologies for primary aluminium" established between five Australian universities and the CSIRO Light Metals Flagship and was funded by the CSIRO National Research Flagships Collaboration Fund.

6. References

- Hall C. M., *US* 400664, **1889**.
- Welch B. J., *J. of Minerals, Metals and Materials Society*, **1999**, 51, 24.
- Gielen D. J., *Methodological Aspects of Resource-Oriented Analysis of material Flows, Workshop. The Future of the European Aluminium Industry: A MARKAL Energy and Material Flow Analysis*, **1998**.
- Zhang M., Kamavaram V., Reddy R.G., *J. Organomet. Chem.*, **2003**, 11, 54.
- Kamavaram V., Mantha D., Reddy R.G., *Electrochim. Acta*, **2005**, 50, 3286.
- Kamavaram V., Mantha D., Reddy R.G., *J. Min Metall.*, **2003**, B39(1-2), 43.
- Reddy R.G., *J. of Physics: Conference Series*, **2005**, 165, 012076.
- Lehmkuhl H., Mehler K., Landau U., in: *Gerischer H., Tobias C.W., (Eds.), Advances in Electrochemical Science and Engineering, Vol. 3, VCH Verlagsgesellschaft, Weinheim*, **1990**, 165.
- Zhao Y., VanderNoot T. J., *Electrochim. Acta*, **1997**, 42, 1639.
- Liao Q., Pitner W. R., Stewart G., Hussey C. L., Stafford G. R., *J. Electrochem. Soc.*, **1997**, 144, 936.
- Zell C. A., Endres F., Freyland W., *Phys. Chem. Chem. Phys.*, **1999**, 1, 697.
- Endres F., Bukowski M., Hempelmann R., Natter H., *Angew. Chem.*, **2003**, 115, 3550; *Angew. Chem. Int. Ed.*, **2003**, 42, 3428.
- Lu J., Dreisinger D., in *Ionic Liquids as Green Solvents: Progress and Prospects (Eds.: R. D. Rogers, K. R. Seddon)*, American Chemical Society, Washington, DC, **2003**, 495.
- Abbott P., Eardley C. A., Farley N. R. S., Griffith G. A., Pratt A., *J. Appl. Electrochem.*, **2001**, 31, 1345.
- Kamavaram V., Reddy R. G., *Metal Separation Technologies III, Engineering Conferences International*, Brooklyn, NY, **2004**, 143.
- Jiang T., Chollier Brym M. J., Dub G., Lasia A., Brisard G. M., *Surf. Coat. Technol.*, **2006**, 201, 1.
- Welch B. J., Osteryoung R. A., *J. Electroanal. Chem.*, **1981**, 118, 455.
- Chum H. L., Osteryoung R. A., in *Ionic Liquids (Eds: Inman D., Lovering D. G.)*, Plenum Press, New York, **1981**, 407.
- Auborn J. J., Barberio Y. L., *J. Electrochem. Soc.*, **1985**, 132, 598.
- Jones S. D., Blomgren G. E., *J. Electrochem. Soc.*, **1989**, 136, 424.
- Carlin R. T., Crawford W., Bersch M., *J. Electrochem. Soc.*, **1992**, 139, 2720.
- Jiang T., Chollier Brym M. J., Dube G., Lasia A., Brisard G. M., *Surf. Coat. Technol.*, **2006**, 201, 10.
- Gao L., Wang L., Li Y., Chu J., Qu J., *Acta Phys. Chim. Sin.*, **2008**, 24, 939.
- Robinson J., Osteryoung R. A., *J. Electrochem. Soc.*, **1980**, 127, 122.
- Rocher N. M., Izgorodina E. I., Ruther T., Forsyth M., MacFarlane D. R., Rodopoulos T., Horne M. D., Bond A. M., *Chem. Eur. J.*, **2009**, 15, 3435.
- Rodopoulos T., Smith L., Horne M. D., Ruther T., *Chem. Eur. J.*, **2010**, 16(12), 3815.
- Zein El Abedin S., Moustafa E. M., Hempelmann R., Natter H., Endres F., *Electrochemistry Communications*, **2005**, 7(11), 1111.
- Horne M. D., Rodopoulos T., Smith L., Ruether T., *Proceedings of 2nd International Congress on Ionic Liquids (COIL-2)*, Yokohama, Japan, August 5th - 10th, **2007**, 3P07-076, 385.
- Zein El Abedin S., Moustafa E. M., Hempelmann R., Natter H., Endres F., *Chem. Phys. Chem.*, **2006**, 7, 1535.
- Carlin R. T., Osteryoung R. A., *J. Electrochem. Soc.*, **1989**, 136, 1409.
- Lai P. K., Skyllas-Kazacos M., *J. Electroanal. Chem.*, **1988**, 248, 431.
- Rocher N. M., Clare R., Izgorodina E. I., Bond A., Forsyth M., MacFarlane D., Horne M., Rodopoulos T., *Proceedings of 2nd International Congress on Ionic Liquids (COIL-2)*, Yokohama, Japan, August 5th - 10th, **2007**, 243.
- Katase T., Imashuku S., Murase K., Hirato T., Awakura Y., *Science and Technology of Advanced Minerals*, **2006**, 7, 502.
- Endres F., Zein El Abedin S., *Phys. Chem. Chem. Phys.*, **2006**, 8, 2101.
- Zhang M., Kamavaram V., Reddy R. G., *Minerals and Metallurgical Processing*, **2006**, 23(4), 177.
- Takahashi S., Saboungi M. L., Klinger R. J., Chen M. J., Rathke J. W., *J. Chem. Soc. Faraday Trans.*, **1993**, 89, 3591.
- Franzen G., Gilbert B. P., Pelzer G., DePauw E., *Org. Mass. Spectrom.*, **1986**, 21, 443.

Received: 31.10.2012.

Accepted: 09.11.2012.



SORPTION CHARACTERISTICS OF ACTIVATED SLUDGE FOR Co-Zn BINARY SYSTEM

Vladimír Frišták^[a], Martin Pipiška^[a], Miroslav Horník^[a], Juraj Lesný^[a]

Paper was presented at the 4th International Symposium on Trace Elements in the Food Chain, Friends or Foes, 15-17 November, 2012, Visegrád, Hungary

Keywords: sorption, activated sludge, Co-Zn system, ⁶⁰Co, ⁶⁵Zn

Toxic and radiotoxic metals of liquid wastes are sorbed by the sludge of Waste Water Treatment Plants (WWTPs) with a high efficiency. Sludges with low toxic metals concentrations can be temporarily stored or utilized as soil conditioners in agriculture. Other possible and economically acceptable way is repeated utilization of the sludge as heavy metals sorbent. Since effluents can contain several metals, it is necessary to study the simultaneous sorption of two or more metal ions and also to quantify the mutual effect of one metal on the other. In the present study, we have undertaken the study on the sorption characteristics of Dried Activated Sludge (DAS) from industrial WWTP for sorption Co²⁺ and Zn²⁺ ions from their binary aqueous system in batch experiments using radiotracers ⁶⁰Co and ⁶⁵Zn technique. Values of maximum sorption capacity (Q_{max}) of DAS at pH 6 calculated from extended Langmuir adsorption isotherm were $247 \pm 15 \mu\text{mol g}^{-1}$ for Co²⁺ and $479 \pm 32 \mu\text{mol g}^{-1}$ for Zn²⁺ ions. Results revealed that the sorption capacity of DAS for both the metals increases with increased initial concentration in the range 100 – 4000 $\mu\text{mol dm}^{-3}$ CoCl₂ and ZnCl₂, respectively. Presence of Zn²⁺ ions as co-ions caused more significant decrease of Co²⁺ uptake in binary Co-Zn system than vice versa. Experimental data Co and Zn sorption in binary system were well described by extended Langmuir model and affinity parameter b indicate higher affinity of DAS to Zn²⁺ in comparison with Co²⁺ ions. Prediction of total Co-Zn sorption by DAS using extended Langmuir model was less suitable due to dissimilarity of Q_{max} value of DAS for Co²⁺ and Zn²⁺ in single systems.

* Corresponding Authors

Fax: 033/ 5921 403

E-Mail: vladimir.fristak@ucm.sk

[a] Department of Ecochemistry and Radioecology, University of SS. Cyril and Methodius in Trnava, Nám. J. Herdu 2, SK-917 01 Trnava, Slovak Republic

Introduction

Industrial effluents treated with wastewater treatment plants (WWTPs) contain high amounts of organic matter and pollutants including metals such as Co, Cd, Zn etc.¹ Toxic metals of liquid wastes are sorbed by the sludge of WWTPs with a high efficiency. Liquid part of sludge is being dispersed to an aqueous recipient but solid part is processed for the next disposal (e.g. temporarily storing, landfilling, incineration). The increased amount of sewage sludges (which are not having a tendency to settle) are a global environmental problem.

Sludges with a low toxic metals concentration can be temporarily stored or utilized as soil conditioners in agriculture processes. Activated sludges produce high amounts of extracellular polymeric substances (EPS) which are metabolic products of bacteria accumulated on the cell surface.² EPS as soil beneficial substances are mainly composed from polysaccharides, proteins and humic substances, containing high concentration of ionizable functional groups.³ The matrix of extracellular polymers is involved in the processes of microbial aggregation in flocs, stabilization of biofilms, water retention and uptake of exogenous organic compounds.⁴ Organic polymers play also crucial role in the sorption process of heavy metals by biomass of activated sludge. Composition of activated sludge as a consortium of bacteria, microalgae, fungi and protozoa and metal sorption characteristics varies depending

on type of waste waters and technology used. Reversibility of metals binding represents the condition of metals entry to the food chain.

Other possible and economically acceptable way is repeated utilization of the sludge as heavy metals sorbent. Biological materials have effective sorption capacity and cheaper regeneration cost as compared to conventional sorbents and ion-exchange resins.⁵ For instance, diverse variety of microorganisms were used extensively for toxic and radiotoxic metals sorption and accumulation studies.⁶ Bivalent metal ions such as Co²⁺ and Zn²⁺ can be removed from aqueous solutions not only by inorganic sorbents, such as zeolites but also by sorbents prepared from microbial biomass.⁷⁻⁸ Adsorption and precipitation on sorbent surface are predominant in the process of metal uptake. Only small fraction of Me²⁺ ions is localized intracellularly.⁸ The bio-sorption is largely attributed to the binding of metals onto the bacterial cell surface due to the presence of active functional binding sites.⁹ Moreover, sorption in multicomponent systems is complicated, because of the possible interactions among the metals. Different adsorption characteristics of metal ions as one of the major sorption process parameter can affect metal positions on surface binding sites of sorbents. Competitive effect of metal components can be evaluated by many statistics and mathematics tool.¹⁰ Marešová et al.¹¹ used extended Langmuir type equations to describe the sorption of Co²⁺ and Sr²⁺ in binary system by sorbent prepared from moss biomass. On the basis of that, the objective of our study was to investigate sorption characteristics of DAS from industrial WWTP for sorption Co²⁺ and Zn²⁺ ions from their binary aqueous system. To obtain reliable experimental data, radiotracer technique with ⁶⁰CoCl₂ and ⁶⁵ZnCl₂ was used. Binary equilibrium isotherm data of Co-Zn system were described using extended Langmuir model.

Experimental

Material

Samples of activated sludge were obtained from aerobic phase of WWTP in Enviral Inc, the plant producing bioethanol (Leopoldov, Slovak Republic). After washing twice in deionised water, the sludge was oven dried at 90 °C for 72 h, ground and sieved. Powdered dried activated sludge (DAS) of particle size <450 µm was used for metal sorption studies.

Standardized $^{60}\text{CoCl}_2$ solution (5.181 MBq cm⁻³; 20 mg dm⁻³ CoCl₂ in 3 g dm⁻³ HCl) and $^{65}\text{ZnCl}_2$ solution (0.8767 MBq cm⁻³; 50 mg dm⁻³ ZnCl₂ in 3 g dm⁻³ HCl) were obtained from the Czech Institute of Metrology. Chemicals used were of analytical reagents grade.

Sorption experiments

Batch sorption experiments were carried out by suspending of DAS biomass (2.5 g dm⁻³ d.w.) in 8 cm³ water solutions of CoCl₂ and ZnCl₂ in variable molar concentration range 100 - 4000 µmol dm⁻³ in molar ratios 2:1, 1:1, 1:2 spiked with $^{60}\text{CoCl}_2$ (65 kBq dm⁻³) and $^{65}\text{ZnCl}_2$ (63 kBq dm⁻³). The reaction pH was adjusted to 6.0 ± 0.1 with 0.1 mol dm⁻³ NaOH and 0.1 mol dm⁻³ HCl. Flasks were agitated on reciprocal shaker (120 rpm) at 22 °C and samples were taken for equilibrium study. Biomass was filtered out, washed twice in deionised water and radioactivity of both activated sludge and liquid phase was measured. All experiments were performed thrice. Presented data are arithmetic mean values. The metal uptake was calculated as:

$$Q_{eq} = (C_0 - C_{eq}) \frac{V}{M} \quad (1)$$

where Q is the uptake (µmol g⁻¹), C_0 and C_{eq} are the liquid-phase concentrations of metal at initial and equilibrium (µmol dm⁻³), V is the volume (dm³), and M is the amount of dried bio-sorbent (given in grams).

Analytical equipments

The gamma spectrometric assembly using well type scintillation detector 54BP54/2-X, NaI(Tl) (Scionix, the Netherlands) and the data processing software Scintivision 32 (ORTEC, USA) were used for ^{60}Co and ^{65}Zn determination in DAS and supernatant liquids at the energy of γ- photons: ^{60}Co - 1173.24 keV and ^{65}Zn - 1115.52 keV.

Determination of initial cobalt and zinc content in sorbent was made by atomic absorption spectrometry (ETAAS) device Shimadzu AA-6300 (USA) with an electrothermal atomization equipment Shimadzu GFA-EX7i using a Shimadzu autosampler ASC6100 and background correction method of Smith-Hieftje, after decomposition samples of

high-pressure digestion mineralization equipment DAH406 Berghof (DE).

Sorption isotherm models

$$Q_{eq}(Me_1) = \frac{Q_{maxMe_1} b_{Me_1} C_{eq}(Me_1)}{1 + b_{Me_1} C_{eq}(Me_1) + b_{Me_2} C_{eq}(Me_2)} \quad (2)$$

Analysis of sorption equilibrium data was done using extended Langmuir adsorption isotherms equations:

$$Q_{eq}(Me_2) = \frac{Q_{maxMe_2} b_{Me_2} C_{eq}(Me_2)}{1 + b_{Me_1} C_{eq}(Me_1) + b_{Me_2} C_{eq}(Me_2)} \quad (3)$$

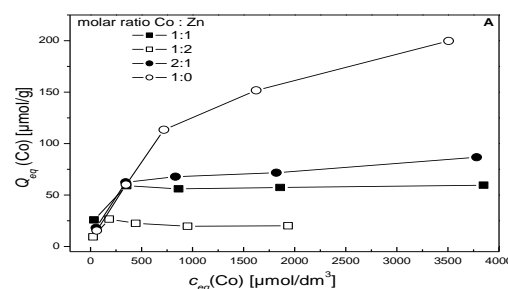
$$b_{Me_1} = \frac{1}{K_{Me_1}} \quad \text{and} \quad b_{Me_2} = \frac{1}{K_{Me_2}}$$

where $c_{eq}(Me_1)$ and $c_{eq}(Me_2)$ represent concentration of metals in equilibrium and Q_{maxMe_1} and Q_{maxMe_2} represent the maximum sorption capacity for both metal present in reaction solution, b_{Me_1} and b_{Me_2} represent affinity constants of Langmuir model for both metals and K_{Me_1} and K_{Me_2} are constants of equilibrium for surface binding sites of sorbent available for metals Me_1 and Me_2 .

To calculate maximum sorption capacity of the sorbent and the corresponding parameters of adsorption isotherms ORIGIN 8.0 Professional (OriginLab Corporation, Northampton, USA), GraphPad PRISM 5.0 (GraphPad Software Inc., USA) and Table Curve 3D 4.0 (Systat Software, Inc., Chicago, USA) were used.

Results and discussion

In comparison to the single metal solutions sorption in binary systems is complicated, because of possible interactions among the metals.



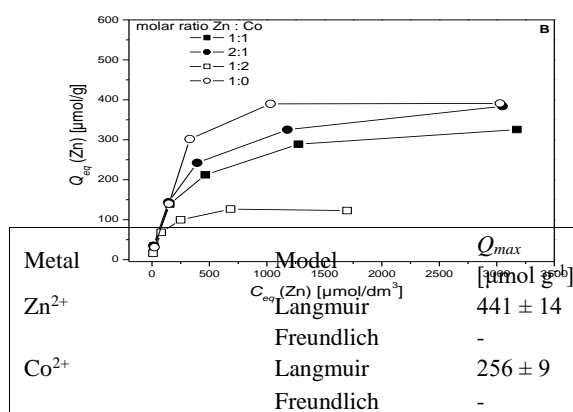


Figure 1. Cobalt (A) and zinc (B) sorption from binary system Co-Zn at variable initial molar [Co]: [Zn] ratios by dried activated sludge (2.5 g/dm³, d.w.) at 22°C and pH 6.0.

Table 1. Comparison of Langmuir and Freundlich equilibrium parameters (\pm SD) for Co²⁺ and Zn²⁺ sorption by dried activated sludge from single system at pH 6 obtained by non-linear regression analysis¹⁰

Metal	Model	Q_{max} [$\mu\text{mol g}^{-1}$]	B [$\text{L } \mu\text{mol}^{-1}$]	K [L g^{-1}]	$1/n$	R^2
Zn ²⁺	Langmuir	441 \pm 14	0.0045 \pm 0.0015	-	-	0.96394
	Freundlich	-	-	40.6 \pm 15.31	0.29 \pm 0.10	0.81961
Co ²⁺	Langmuir	256 \pm 9	0.0010 \pm 0.0001	-	-	0.99353
	Freundlich	-	-	4.29 \pm 1.36	0.48 \pm 0.04	0.96704

Table 2. Extended Langmuir isotherm parameters for Co²⁺ and Zn²⁺ sorption in binary Co-Zn system by dried activated sludge calculated by non-linear regression analysis.

Sorption	Q_{max} [$\mu\text{mol g}^{-1}$]	b_{Co} [$\text{dm}^3 \mu\text{mol}^{-1}$]	b_{Zn} [$\text{dm}^3 \mu\text{mol}^{-1}$]	R^2	RMSE
$Q_{max Co}$	247 \pm 15	0.001 \pm 0.0002	0,005 \pm 0,001	0,975	8,15
$Q_{max Zn}$	479 \pm 32	0.002 \pm 0.001	0,004 \pm 0,001	0,949	32,89

Sorption of cobalt and zinc ions by dried activated sludge from binary Co-Zn system increased with an increasing initial concentration of both metals in the range of 0 – 4 000 $\mu\text{mol dm}^{-3}$ CoCl₂ and ZnCl₂, respectively. Obtained results are shown in Fig. 1A, B. The presence of co-ion in solution caused significant decrease of uptake of primary ion. Zn²⁺ as co-ion caused the decrease about 85% of Co²⁺ ions sorption from 200 $\mu\text{mol g}^{-1}$ to 25 $\mu\text{mol g}^{-1}$ d.w. of sludge. The competitive effect of zinc increased with increasing of its solution concentration. On the other hand Co²⁺ as co-ion in sorption of Zn²⁺ ions caused decrease about only 68% from 390 $\mu\text{mol g}^{-1}$ to 125 $\mu\text{mol g}^{-1}$ d.w. of sludge. At equimolar concentration of both metal ions (ratio 1:1) maximum sorption capacity of activated sludge was 325 $\mu\text{mol g}^{-1}$ for zinc and 60 $\mu\text{mol g}^{-1}$ for cobalt. For a description of Co²⁺ and Zn²⁺ sorption equilibrium in single-component systems was more suitable Langmuir adsorption model (Table 1).

Experimental data from two-component system (Co-Zn) were fitted and evaluated by extended Langmuir competitive model.¹¹ For determination of sorption equilibrium of Co²⁺ and Zn²⁺ ions we used Eqs. 3 and 4. Parameters of extended Langmuir model for single and binary metal uptake calculated by non-linear regression analysis are shown in Table 2.

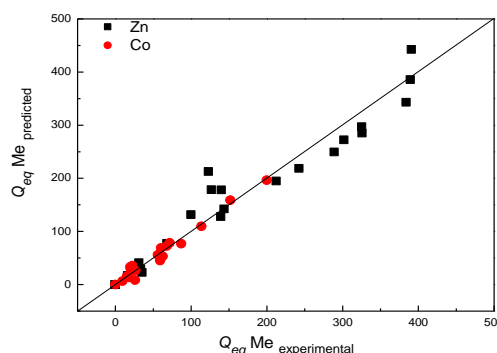


Fig. 2. Comparison of experimentally observed data with predicted data obtained using the extended Langmuir model.

The degree of affinity is expressed in the form of the parameter b , which is the Langmuir constant. The relationship between value and its affinity for metal sorbent is proportional, based on Arrhenius equation to express energy of sorption process. Parameter b_{Zn} is higher than b_{Co} that indicates higher affinity of sorbent prepared from activated sludge to zinc ions in comparison with cobalt ions in sorption process from binary system Co-Zn.

The correlation between predicted and experimental values of metal sorption by DAS is shown in Fig. 2. Since most of the points are distributed around the line, this indicates that equation used described the sorption data well. The adequacy of model was also compared by coefficient of determination and by RMSE (Table 2). It is evident that extended Langmuir model fits the data well.

The extended Langmuir model can be represented by adsorption isotherms in 3-D space (Fig. 3 A,B). X and Y axes represent the concentrations of cobalt and zinc in equilibrium (C_{eqCo} , C_{eqZn}), while the Z axis represents plotted

value of sorbed cobalt and zinc (Q_{eq}). Experimental sorption values of metal uptake are presented as individual points.

The Fig. 3 shows that at higher concentrations of the metal ions, binding sites of sorbent can be easily saturated what is presented by the plateau of sorption surface. This adsorption model is suitable and has a high efficiency for the description and prediction of single metal sorption. For determination of binary metal sorption, the method has proved to be less effective. It is mainly due to the different values of maximal sorption capacities of Co^{2+} and Zn^{2+} ions. Extended Langmuir model is suitable for description of metal cations sorption processes for which parameters (Q_{max}) are approximately similar.¹¹ The sorption capacity of activated sludge for zinc was higher about 50% as compared to cobalt sorption.

This difference in affinity of sorbent for Me^{2+} ions could be because of different physico-chemical characteristics of metal ions.¹² Remenárová et al.¹³ showed different sorption capacity of DAS for Cd^{2+} and Zn^{2+} ions. Metal ions can be classified according to covalent index that reflects different ligand affinities.¹⁴

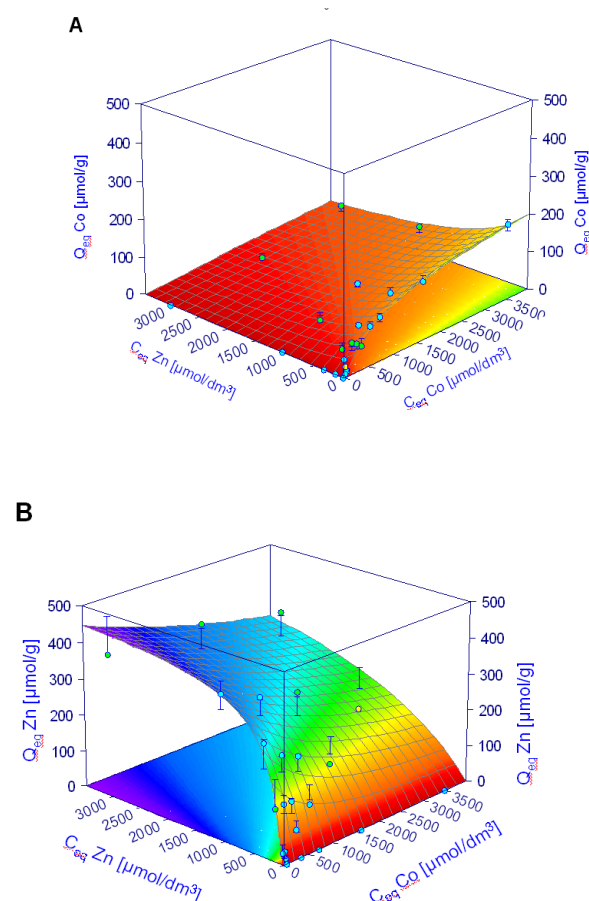


Fig. 3. 3-D sorption isotherm surfaces of Co^{2+} - Zn^{2+} binary system: (A) Co^{2+} sorption ($\mu mol g^{-1}$); (B) Zn^{2+} sorption ($\mu mol g^{-1}$). The sorption surfaces are predicted by the competitive Langmuir model (Eqs. 2 and 3) and the points present experimental data obtained at pH 6 and 22 °C. Error-bars represent 90% confidence interval.

Higher affinity of reactive sites on sludge surface for zinc ions in binary sorption system is also related to the covalent index, ionic radius and electronegativity (Table 3). Ionic index is responsible for the preference of the metal ion binding to the oxygen ligands. Co^{2+} ion has higher value of

covalent index that indicates a covalent binding to the active sites of sulfo and nitro functional groups.

Table 3. Physico-chemical properties of Co^{2+} and Zn^{2+} ions

Properties	Co^{2+}	Zn^{2+}
Atomic weight	58.93	65.39
Ionic radius r (pm)	72	74
Electronegativity (Pauling) X_m	1.88	1.65
Covalent index ($X_m^2 r^{-1}$)	2.5	2.04
Ionic index ($z^2 r^{-1}$)	5.4	5.4

Conclusion

Sorbent prepared from DAS from industrial WWTP has an ability to remove cobalt and zinc from binary aqueous system. Experimental data of batch metal sorption were obtained using radiotracer technique with ^{60}Co and ^{65}Zn .

Values of maximum sorption capacity (Q_{max}) of DAS at pH 6 calculated from extended Langmuir adsorption isotherm were $247 \pm 15 \mu mol g^{-1}$ for Co^{2+} and $479 \pm 32 \mu mol g^{-1}$ for Zn^{2+} ions. Results revealed that the sorption capacity of DAS for both metals increases with an increase in initial concentration in the range 100 – 4000 $\mu mol/dm^3$ $CoCl_2$ and $ZnCl_2$, respectively. Presence of Zn^{2+} ions as co-ions caused more significant decrease of Co^{2+} uptake in binary Co-Zn system than vice versa. Experimental data Co and Zn sorption in binary system were well described by extended Langmuir model and affinity parameter b indicate higher affinity of DAS to Zn^{2+} in comparison with Co^{2+} ions. Prediction of total Co-Zn sorption by DAS using extended Langmuir model was less suitable due to dissimilarity of Q_{max} value of DAS for Co^{2+} and Zn^{2+} in single systems. Determination of binding mechanisms of cobalt and zinc from binary system to active sites of sludge surface as content variable microbial mass will require detailed study for further storage or disposal this material. Zinc and cobalt as metals included to the borderline class bind to the residues of histidine and free amino groups of proteins.

References

- Souza Pereira, M., Kuch, M. *Chemosphere*, **2005**, 60, 844.
- Morgan, J.W., Forster, C.F., Evison, L.M. *Water Res.*, **1990**, 6, 743.
- Guibaud, G., Van Hullebusch, E., Bordas, F. *Chemosphere*, **2006**, 64, 1955.
- Liu, Y., Fang, H.P.P. *Crit.Rev. Env. Sci. Tec.*, **2003**, 33, 237.
- Singh, D.K., Tiwari, D.P., Saksena, D.N. *Indian J. Environ. Health*, **1993**, 35, 169.
- Tišáková, L., Pipiška, M., Godány, A., Horník, M., Vidová, B., Augustín, J. *J. Radioanal. Nucl. Chem.*, **2012**, in press.
- Závodská, L., Lesný, J., Szákal, P., Schmidt, R. *Cereal Res. Commun.*, **2006**, 34, 109.
- Pipiška, M., Horník, M., Vrtoch, L., Augustín, J., Lesný J. *Biologia*, **2007**, 62, 276.
- Cox, J.S., Smith, D.S., Warren, L.A., Ferris, F.G. *Environ. Sci. Technol.*, **1999**, 33, 4514.

- ¹⁰Frišták, V., Remenárová, L., Lesný, J. *J. Microbiol., Biotechnol. Food Sci.*, **2012**, *1*, 1235.
- ¹¹Marešová, J., Pipiška, M., Rozložník, M., Horník, M., Remenárová, L., Augustín, J. *Desalination*, **2011**, *266*, 134.
- ¹²Pérez-Marín, A.B., Ballester, A., Gonzáles, F., Blázquez, M.L., Muñoz, J.A. *Bioresour Technol.*, **2008**, *99*, 8101.
- ¹³Remenárová, L., Pipiška, M., Horník, M., Rozložník, M., Augustín, J., Lesný, J. *J. Taiwan. Inst. Chem. E.*, **2012**, *43*, 433.
- ¹⁴Nieboer, E., Richardson, D.H.S. *Environ. Pollut.*, **1980**, *1*, 3.

Received: 15.10.2012.

Accepted: 10.11.2012.



REACTION CONDITIONS AND KINETICS FOR SYNTHESIZING *n*-BUTYL ACETATE

Cong Yufeng^[a]

Keywords: reaction conditions; kinetics; *n*-butyl acetate; synthesis

Effects of different reaction conditions on the synthetic method of *n*-butyl acetate have been reviewed in the present paper. Different catalysts consisting inorganic salt like $(\text{Ce}(\text{S}_2\text{O}_8)_2/\text{SBA-15})$, $\text{NH}_4\text{Fe}(\text{SO}_4)_2 \cdot 12\text{H}_2\text{O}$ and oxide ($\text{MoO}_3/\text{SiO}_2$) have also been introduced. Kinetics equations have also been applied on *n*-butyl acetate system. The results showed that kinetic equations may predict the distribution of product and the experimental data are in agreement with the quantitatively analytical conclusions drawn from the calculated data.

* Corresponding Author

Fax: 86-24-56860869

E-Mail: congyufeng2012@hotmail.com

[a] Liaoning Shihua University, Fushun, Liaoning, P.R. China.

Introduction

n-Butyl acetate is one of the important fine chemical products. It is widely used in different areas such as solvent, plasticizer, resin, painting, perfume, cosmetics, medicine, surfactant and other organic syntheses¹ Acetic acid and *n*-butanol are used as feedstock to manufacture *n*-butyl acetate in the industry. Concentrated sulphuric acid is one of the main catalysts. Apart from several advantages, concentrated sulphuric acid has a lot of disadvantages also, such as tainted products due to strong oxidizing nature, it is very difficult to purify, even after several washings, due to complicated process lot of waste water is discharged which is also an environmental pollution problem and equipments are corroded.² Inorganic salt like $(\text{Ce}(\text{S}_2\text{O}_8)_2/\text{SBA-15})$, $\text{FeNH}_4(\text{SO}_4)_2 \cdot 12\text{H}_2\text{O}$ and oxide ($\text{MoO}_3/\text{SiO}_2$) are the best catalysts. They have high catalytic performance, selectivity and non-corrosive in nature.³

In the present paper, different catalysts such as inorganic salt ($\text{Ce}(\text{S}_2\text{O}_8)_2$, $\text{NH}_4\text{Fe}(\text{SO}_4)_2 \cdot 12\text{H}_2\text{O}$) and oxide ($\text{MoO}_3/\text{SiO}_2$) have been discussed. Effects of different reaction conditions on the synthetic method of *n*-butyl acetate have also been reviewed. Furthermore, kinetics equations have also been applied.

Discussion

Effects of the reaction time on the yields of *n*-butyl acetate by the addition of $\text{Ce}(\text{S}_2\text{O}_8)_2$ -SBA-15 as a catalyst

Yin Yanlei⁴ has reported the preparation of *n*-butyl acetate and the effect of the reaction conditions on its yield. $\text{Ce}(\text{S}_2\text{O}_8)_2$ and SBA-15 catalysts were ground and roasted to generate *n*-butyl acetate. It was supposed that molar ratio (1.0:1.2) and amount (0.0375g) of acetic acid to *n*-butanol and the amount of catalyst kept constants. Effects of the reaction time on the yield of *n*-butyl acetate,

has also been discussed. Table 1 showed effects of the reaction time on the yields of *n*-butyl acetate. The yields of *n*-butyl acetate increased with an increase of the reaction time. The maximum yield of *n*-butyl acetate was 96.58%, when the reaction time was about three hours. The experimental results showed that $\text{Ce}(\text{S}_2\text{O}_8)_2$ and SBA-15 had good catalytic performance and were reused several times.

Table 1. effects of the reaction time on the yields of *n*-butyl acetate

Reaction time, h	0.5	1.0	1.5	2.0	2.5	3.0
Yield, %	30.00	69.98	83.21	95.13	96.01	96.58

Effect of the AcOH/*n*-BuOH ratio on the yield in the presence of $\text{NH}_4\text{Fe}(\text{SO}_4)_2 \cdot 12\text{H}_2\text{O}$ catalyst

Kong Xiangwen⁵ explained why $\text{NH}_4\text{Fe}(\text{SO}_4)_2 \cdot 12\text{H}_2\text{O}$ as a catalyst replaced concentrated sulfuric acid to generate *n*-butyl acetate. It was found that the reaction time and the amount of catalyst kept at constants were 0.75 hours and 1.1g, respectively. Effects of the molar ratio of acetic acid to *n*-butanol on the yields of *n*-butyl acetate had been discussed. Results are recorded in Table 2. First the yields of *n*-butyl acetate increased and then decreased with an increase in the molar ratio of acetic acid to *n*-butanol. When the molar ratio of acetic acid to *n*-butanol was 1.0:1.2, the maximum yield of *n*-butyl acetate reached 98.1%. $\text{NH}_4\text{Fe}(\text{SO}_4)_2 \cdot 12\text{H}_2\text{O}$ one of the best catalysts was used to synthesise *n*-butyl acetate because it was very economic, stable and insoluble in organic acids and alcohol. After the reaction, $\text{NH}_4\text{Fe}(\text{SO}_4)_2 \cdot 12\text{H}_2\text{O}$ became insoluble material and was easily separated from the reaction system. It had high catalytic performance and selectivity and non-corrosive.

Table 2. effects of the molar ratio of acetic acid to *n*-butanol on the yields of *n*-butyl acetate

Molar ratio of AcOH to <i>n</i> -BuOH	1.0:1.0	1.0:1.1	1.0:1.2	1.0:1.3	1.0:1.4
Yield (%)	90.7	93.6	98.1	94.3	90.4

Effects of the amount of MoO₃/SiO₂ catalyst catalyst on the yields of *n*-BuOAc

Li Shuchang⁶ described the preparation of MoO₃/SiO₂ and the effect of the reaction conditions such as the reaction time, the molar ratio of acetic acid to *n*-butanol, the amount of catalyst and number of reuse of catalyst on the yield of *n*-butyl acetate. It was found that the reaction time and the molar ratio of acetic acid to *n*-butanol kept at constants were 3 hours and 1.0:4.0, respectively. Effects of the amount of catalyst on the yields of *n*-butyl acetate had been discussed. Table 3 presented effects of the amount of catalyst on the yields of *n*-butyl acetate. The yields of *n*-butyl acetate firstly increased and then decreased with an increase in the amount of catalyst. When the amount of catalyst was 1.0, the maximum yield of *n*-butyl acetate arrived at 95.6%.

Table 3. effects of the amount of catalyst on the yields of *n*-butyl acetate

Catalyst amount, g	0.6	0.8	1.0	1.2	1.4
Yield, %	62.3	78.6	95.6	91.7	84.5

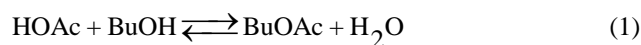
Kinetics equations of *n*-butyl acetate

Qiu Ting⁷ used cation exchange resin as a feedstock and described effects of the reaction conditions such as the stirring speed, the catalyst particle size (cation exchange resin), the reaction temperature, the molar ratio of acetic acid to *n*-butanol and the amount of catalyst on the yield of *n*-butyl acetate. The kinetic model LHHW was used to calculate the experimental data. The experimental results showed that the surface reaction was the main control step of acetic acid and *n*-butanol. Its reaction enthalpy was -1.838×10^4 J/mol. The activation energies of the forward and reverse reaction were 5.238×10^4 J/mol and 3.929×10^4 J/mol, respectively. The pre-exponential factors were 1.015×10^4 mol/(g·s) and 3.148 mol/(g·s), respectively.

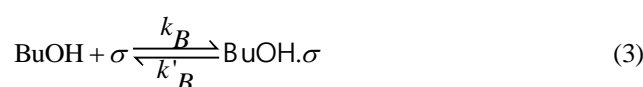
The reaction of acetic acid and *n*-butanol was the heterogeneous catalytic liquid-solid reaction. It consisted of several steps such as the reactant was diffused from the liquid phase to the external surface area of the catalyst, and then spread from the external surface area of the catalyst to the internal surface area. The reactant was absorbed and the reaction took place at the same time. The product was desorbed and diffused to the external surface area of the catalyst, and then spread from the external surface area of the catalyst to the liquid phase. The real reaction process was absorption, the surface reaction and desorption in advance of ignoring the internal and external diffusion. Based on the principle of LHHW model, it was supposed that (1) catalytic and active centres were their acid parts. (2) The reactant competed to be absorbed on catalytic and active centres with the product whose absorptions totally were single layer. (3) Acetic acid absorbed on one catalytic and active centre reacted with *n*-butanol absorbed on another catalytic and active centre. *n*-Butyl acetate was obtained

from the internal surface area of the catalyst. (4) The surface reaction was the main control step.

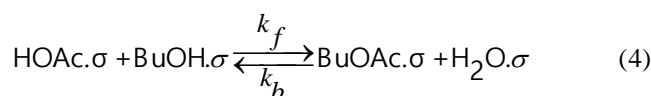
The reaction of acetic acid and *n*-butanol was listed as follows:



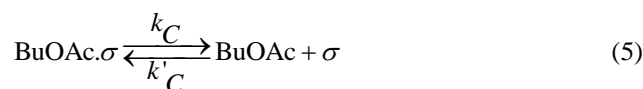
Absorptions:



The surface reactions:



Desorptions:



where σ means the adsorption site. HOAc. σ , BuOH. σ , BuOAc. σ and H₂O. σ are the adsorption state of acetic acid, *n*-butanol, *n*-butyl acetate and water, respectively.

It is supposed that

$$\begin{aligned} K_{\text{SHOAc}} &= k_A/k'_A, \\ K_{\text{SBuOH}} &= k_B/k'_B, \\ K_{\text{SBuOAc}} &= k'_C/k_C \text{ and} \\ K_{\text{SH}_2\text{O}} &= k'_D/k_D. \end{aligned}$$

Furthermore, K_{SHOAc} , K_{SBuOH} , K_{SBuOAc} and $K_{\text{SH}_2\text{O}}$ are adsorption equilibrium constants of acetic acid, *n*-butanol, *n*-butyl acetate and water, respectively. The total reaction rate, r is written as follows:

$$r = \frac{-ndx_{BuOH}}{dt} = \frac{M_{cat}(K_f K_{sHOAc}^x HOAc K_{sBuOH}^x BuOH - K_b K_{sBuOAc}^x BuOAc K_{sH_2O}^x H_2O)}{(1 + K_{HOAc}^x HOAc + K_{sBuOH}^x BuOH + K_{sBuOAc}^x BuOAc + K_{sH_2O}^x H_2O)^2} \quad (7)$$

where

r - the reaction rate, mol s⁻¹

x_i - the molar fraction of substance

M_{cat} - the amount of catalyst, g

n - the amount of substance, mol.

K_f - the positive reaction rate, mol g⁻¹·s⁻¹

K_b - the negative reaction rate, mol g⁻¹·s⁻¹

When the reaction equilibrium constant K_s is equal to $K_f K_{sHOAc} K_{sBuOH} / K_b K_{sBuOAc} K_{sH_2O}$, Eqn. (7) can be simplified to Eqn. (8)

$$r = \frac{M_{cat} K_f K_{HOAc} K_{sBuOH} \left[x_{HOAc} x_{BuOH} - \frac{x_{BuOAc} K_{sH_2O} x_{H_2O}}{K_s} \right]}{(1 + K_{sHOAc}^x HOAc + K_{sBuOH}^x BuOH + K_{sBuOAc}^x BuOAc K_{sH_2O}^x H_2O)^2} \quad (8)$$

The experimental data are calculated by using the particle swarm optimization algorithm. The above model parameters are shown in Table 4. The reaction equilibrium constants (K_s) decrease with an increase in the reaction temperature, however, the positive and

negative reaction rate gradually increase with the increase in the reaction temperature. This proves that this particular reaction is an exothermic in nature. The higher the reaction temperature shorter is the time to reach reaction equilibrium.

Table 4. parameters of kinetic model

T (°C)	K_{sHOAc}	K_{sBuOH}	K_{sBuAc}	K_{sH_2O}	$K_f \times 10^4$ (mol/(g·s))	$K_b \times 10^6$ (mol/(g·s))	K_s
75	4.2051	5.8754	14.9870	8.6886	1.2530	4.0149	5.9215
80	4.1115	4.3115	12.8400	7.8040	1.4862	4.8346	5.4383
85	4.0884	2.9421	11.0160	7.2986	1.9465	5.8273	4.9973
90	3.9753	1.8702	9.5009	6.4785	2.6502	7.0350	4.5502

Based on the above the experimental data, the regression Eqn. (9), (10), (11) and (12) are written as follows:

$$K_{sHOAc} = 1.188 \times \exp(3.658 \times 10^3 / RT) \quad (9)$$

$$K_{sBuOH} = 5.80 \times 10^{-12} \times \exp(8.014 \times 10^4 / RT) \quad (10)$$

$$K_{sBuOAc} = 2.40 \times 10^{-4} \times \exp(3.197 \times 10^4 / RT) \quad (11)$$

$$K_{sH_2O} = 8.941 \times 10^{-3} \times \exp(1.991 \times 10^4 / RT) \quad (12)$$

Conclusion

Using acetic acid and n-butanol as feed stocks and (Ce(S₂O₈)₂/SBA-15, FeNH₄(SO₄)₂·12H₂O) and oxide (MoO₃/SiO₂) as catalysts, effects of the reaction time, acetic acid/ n-butanol ratio and the amount of catalyst have been discussed. The experimental results obtained are as follows:

The maximum yield of n-butyl acetate reached 96.58% in three hours by the addition of Ce(S₂O₈)₂/SBA-15.

The maximum yield of n-butyl acetate arrived at 98.1% under the condition of acetic acid/n-butanol ratio (1.0:1.2).

The maximum yield of n-butyl acetate was 95.6% when the amount of catalyst was 1.0.

The reaction speed rate Eqn. was obtained and predicted the distribution of product.

References

- ¹Li, M. H., Zhu, M. and Liu, N. *J. Dalian Polytechnic Univ.*, **2009**, 28(5), 347.
- ²Jiang, H. B. *Chem. Eng.*, **2011**, 6, 14.
- ³Cong, Y. F. *Eur. Chem. Bull.*, **2012**, 1(8), 336.

⁴Yin, Y. L., Tian, Z. M., Deng, Q. G. and Ding, K. P. *J. Qiqihar Univ.*, **2008**, 24(1), 4.

⁷Qiu, T., Huang, Z. X., Cheng, C. B. and Wu, Y. X. *Chem. React. Eng. Technol.*, **2009**, 25(4), 355.

⁵Kong, X. W., Yu, L., Zhang, J. and Shu, Y. *Res. Exploration Lab.*, **2011**, 30(2), 21.

⁶Li, S. C., Sun, D. and Du, C. H. *Chem. Eng.*, **2010**, 10, 61.

Received: 29.10.2012.

Accepted: 11.11.2012.



EFFECT OF COBALT-EDTA ON IRON CONTENT IN SPLEEN AND LIVER OF IMMATURE MICE

Yordanka Gluhcheva^[a], Ekaterina Pavlova^[a], Vasil Atanasov^[b], Juliana Ivanova^[c], Ivelin Vladov^[a], Sonja Ganeva^[b], Mariana Mitewa^[b]

Paper was presented at the 4th International Symposium on Trace Elements in the Food Chain, Friends or Foes, 15-17 November, 2012, Visegrád, Hungary.

Keywords: Co-EDTA, iron content, in vivo model, immature mice, spleen, liver

Cobalt (Co) is an essential trace element and its accumulation affects the concentrations of other elements also. Co(II) is shown to compete with iron (Fe) for the transferrin receptor and to form a stable complex with haemoglobin thus affecting haematopoiesis. There are lack of data regarding the effect of chronic exposure to Co compounds on Fe content in spleen and liver of mice. The study deals with the effect of long-term treatment with cobalt-EDTA (Co-EDTA) on iron content in the spleen and liver of immature mice. Pregnant ICR mice were subjected to chronic treatment with daily dose of 75 mg/kg Co-EDTA which continued until day 25pnd of the newborn pups. Results show accumulation of Co(II) and altered Fe content in the spleen and liver of treated mice compared to age-matched controls with significantly increased Fe concentration in the livers of treated mice. The changes could explain impaired haematopoiesis and immune responses of exposed to Co(II) immature mice.

* Corresponding Author Yordanka Gluhcheva

Fax: + 359 2 871 0107

E-Mail: ygluhcheva@hotmail.com;

- [a] Institute of Experimental Morphology, Pathology and Anthropology with Museum, Bulgarian Academy of Sciences Acad. Georgi Bonchev Str., Bl. 25, 1113 Sofia, Bulgaria
- [b] Author Address line 2 Faculty of Chemistry and Pharmacy, Sofia University "St. Kliment Ohridski" 1164 - Sofia, Bulgaria
- [c] Author Address line 3 Faculty of Medicine, Sofia University "St. Kliment Ohridski" 1407 Sofia, Bulgaria

The aim of the present study is to investigate the effect of long-term treatment with cobalt-EDTA (Co-EDTA) on iron content in the spleen and liver of immature mice.

Methods

Synthesis of Co-EDTA complex

All chemicals and solvents used were of AR grade. Co-EDTA was synthesized according to modified literature procedures^{11,12} as already described¹³.

Introduction

Cobalt (Co) is an essential trace element and its accumulation in blood plasma and other organs affects the concentrations of other elements¹. The wide use of cobalt alloys in medical devices requires full elucidation of its biological role in cells, tissues and organs after long-term exposure^{2,3}. Co(II) is shown to compete with iron (Fe) for the transferrin receptor and to form a stable complex with haemoglobin⁴ thus affecting haematopoiesis. Barany et al. found higher concentrations of Co in blood at low body iron storages⁵.

Iron is another essential micronutrient required for erythropoietic function, DNA synthesis, oxidative metabolism and cellular immune response^{6,7}. Spleen and liver are the main sites of iron storage in the body.

There are lack of data regarding the effect of chronic exposure to Co compounds on Fe content in spleen and liver of mice. Data show that cobalt is transferred from food into human milk⁸. Added cobalt caused an increase in cobalt concentration in the milk during late gestation and early lactation in cows⁹. According to Shingfield et al. ruminal infusion of Co-EDTA alters milk fatty acid composition in lactating cows¹⁰.

In vivo animal model

Pregnant ICR mice in late gestation were subjected to cobalt EDTA (Co-EDTA) treatment at daily doses of 75 mg/kg that continued until day 25 of the newborn mice. Cobalt compound was dissolved and obtained from drinking tap water. Each pregnant mouse received 1.7 mg Co-EDTA dissolved in 8 ml tap water. Our studies have shown that this is the amount of water that an adult mouse drinks per day. Pure tap water was used as control. Animals were fed a standard diet and had access to food *ad libitum*. Mice were maintained in the institute's animal house at 23°C ± 2°C and 12:12 h light-dark cycle in individual standard hard bottom polypropylene cages to ensure that all experimental animals obtained the required dose.

The newborn pups (n=3 per group) were sacrificed on days 18 and 25. Mice were weighed weekly and the experimental cobalt concentration was adjusted accordingly. Spleen and liver were excised and used for measuring cobalt bioaccumulation and Fe content.

The studies were approved by the Ethics Committee of the Institute of Experimental Morphology, Pathology and Anthropology with Museum – Bulgarian Academy of Sciences.

Analysis of cobalt content in spleen and liver

Cobalt and iron contents in the spleen and liver were determined after nitric acid wet digestion by flame atomic absorption spectrometry (FAAS) using Perkin Elmer AAnalyst 400, flame: air – acetylene.

Statistical analysis

The obtained results are presented, as mean value \pm SD. Statistical significance between the experimental groups was determined using Student's *t*-test. Difference was considered significant at $p < 0.05$.

Results

Since cobalt is transferred from food into the mother's milk the newborn pups were exposed to it as well. Co concentration in the milk was not measured in this study. The pups showed no differences regarding number and viability when compared to control ones. Reduction in food or water consumption was not observed and all animals survived the experiment.

Preliminary results indicate that chronic exposure of immature mice to Co-EDTA increased Co(II) content in the spleen and liver of treated animals (Figs. 1 and 2).

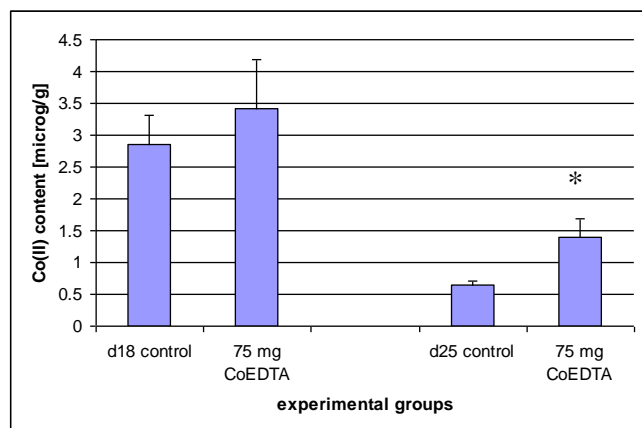


Figure 1. Cobalt(II) content in the spleen of experimental animals. Each column represents mean \pm SD, $n = 3$. Asterisk (*) represents statistical differences ($p < 0.05$).

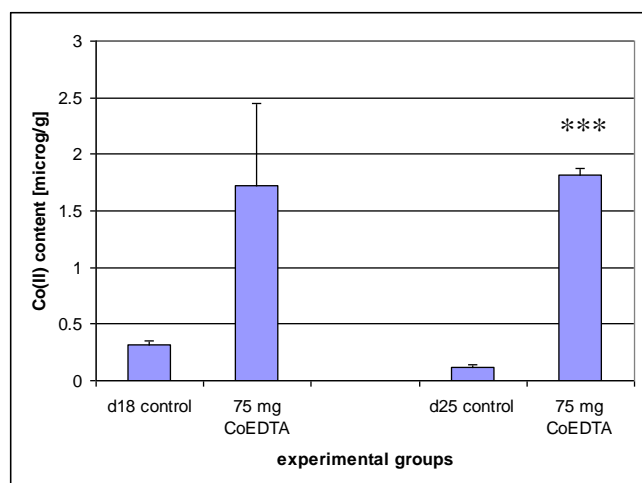


Figure 2. Cobalt(II) content in the liver of experimental animals. Each column represents mean \pm SD, $n = 3$. Triple asterisk (***) represents statistical differences ($p < 0.001$).

Livers of treated mice accumulated up to ~ 15 -fold Co(II) compared to untreated controls. Spleens accumulated less which indicates that liver is more sensitive to Co(II) exposure than spleen.

The Co(II) measured in the organs of the control mice could be due to cobalt containing supplements in the food they obtained.

Exposure to Co-EDTA induced changes in the iron content as well. Surprisingly, spleen of day18 Co-EDTA-treated mice had less Fe compared to the controls (Fig.3).

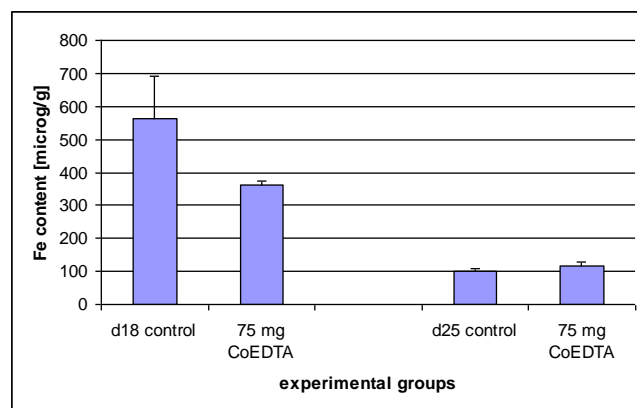


Figure 3. Iron content in the spleen of experimental animals. Each column represents mean \pm SD, $n = 3$.

Iron was significantly increased in the liver of treated mice compared to age-matched controls (Fig.4).

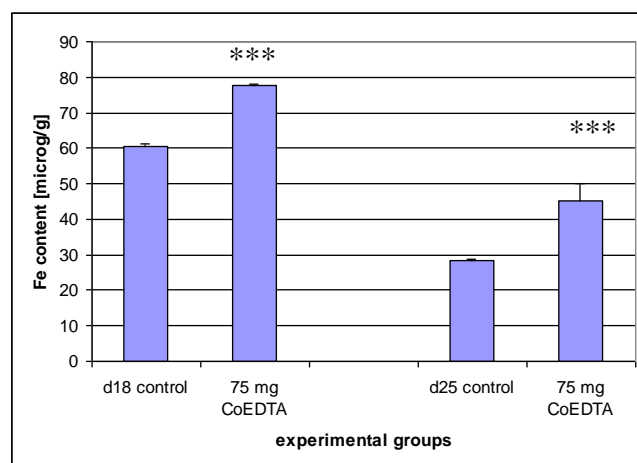


Figure 4. Iron content in the liver of experimental animals. Each column represents mean \pm SD, $n = 3$. Triple asterisk (***) represents statistical differences ($p < 0.001$).

Discussion

As inorganic and complex compounds (with organic ligand) cobalt(II) is used as nutritional supplement, preservative, in drinks, as therapeutic agent for treating different diseases, etc. Co(II) compounds are shown to induce DNA damage, gene mutations, sister chromatid exchanges and aneuploidy in *in vitro* studies on animal and human cells¹⁴. On the other hand, treatment with EDTA

alone has shown to induce severe biochemical and histopathological changes in bone marrow, liver, kidneys and testes of treated rats¹⁵. The compound led to a higher incidence of micronucleated polychromatic erythrocytes and chromosome aberrations in bone marrow cells in mice and Syrian hamster embryo cells^{15,16}. The lowest EDTA dose reported to cause a toxic effect in animals was 750 mg/kg/day. The dose of Co-EDTA used in the present study is 75 mg/kg/day or 10-fold less and toxic effects on the experimental animals should not be expected.

In our studies chronic exposure to Co-EDTA resulted in accumulation of Co(II) ions in the spleen and liver of treated mice which affected iron content as well. The results are in good agreement with WHO report that spleen and liver are sensitive to cobalt treatment and accumulate the metal ions¹⁷. Korf et al. also show significant uptake of radioactive cobalt in rat spleen 24h after injection¹⁸.

Under physiological conditions there is a balance between iron absorption, transport and storage in the human body⁷. TfR1 and TfR27 mediate the uptake of transferrin-bound Fe by the liver from blood plasma.

Surprisingly, day18 mice had less Fe in their spleen compared to the controls. This is possibly the reason for the decreased haemoglobin content and other erythrocytic indices of the treated mice (data not shown). Hypoxia increases iron storage in the spleen¹⁹. Day 25 mice show increased Fe content in their spleen that may be due the prolonged treatment and the effect of hypoxia induced by Co-EDTA. The results could explain our previous observation about disturbed extramedullary haematopoiesis in the spleen (reduced number of megakaryocytes), after long-term treatment of mice with low (75 mg/kg) or high (125 mg/kg) dose Co-EDTA²⁰.

Liver plays a key role in body's detoxification which explains the high amount of Co(II) accumulated. Hpcidin, produced mainly by the hepatocytes is responsible to liver iron levels, inflammation, hypoxia and anemia and is the key Fe regulatory hormone for iron absorption and recirculation⁷. Anemia and hypoxia trigger a decrease in hepcidin levels²¹. Cobalt is a hypoxia inducing agent and this could explain the increased Fe content in the liver due to suppressed hepcidin levels. Garoui et al. find that exposure of rats to cobalt chloride during pregnancy and early postnatal periods affects antioxidant enzyme activities and lipid peroxidation in the liver of treated mothers and their offspring²². Possible effects may be suggested for Co-EDTA as well.

Co-EDTA treatment affects early postnatal mouse development altering Fe homeostasis. Administration of the complex in the animal feed requires full elucidation of its effects on key physiological processes.

Acknowledgements

The work is supported by a grant No DMU 03/25 for Young scientists from the Bulgarian National Science Fund.

References

- ¹Zaksas N., Gluhcheva Y, Sedykh S, Madzharova M, Atanassova N, Nevinsky G., *J Trace Elem. Med. Biol.*, **2012** (in press)
- ²Guildford, A.L., Poletti, T., Osbourne, L.H., Di Cerbo, A., Gatti, A.M., Santin M., 2009. *J. Roy. Soc. Interface*, **2009**, 6(41), 1213.
- ³Tanaka, Y., Kurashima, K., Saito, H., Nagai, A., Tsutsumi, Y., Doi, H., Nomura N., Hanawa, T., *J. Artificial Organs.*, **2009**, 12, 182.
- ⁴Simonsen, L.O., Brown, A.M., Harbak, H., Kristensen, B.I., Bennekou, P. 2011. *Blood Cells Mol. Dis.*, **2011**, 46(4), 266.
- ⁵Bárány, E., Bergdahl, I.A., Bratteby, L.-E., Lundh, T., Samuelson, G., Skerfving, S., Oskarsson, A., *Environ. Res.*, **2005**, 98, 215.
- ⁶Harrison-Findik, D., *World J Hepatol.*, **2010**, 2(8), 302.
- ⁷Muñoz, M, Villar, I, García-Erce, JA., *World J. Gastroenterol.*, **2009**, 15(37), 4617.
- ⁸Wappelhorst, O., Kühn, I., Heidenreich, H., Markert, B., *Nutrition*, **2002**, 18 (4), 316.
- ⁹Kincaid, R.L., Socha, M. T., *J. Dairy Sci.*, **2007**, 90(4), 1880.
- ¹⁰Shingfield, K., Arola, A., Ahvenjarvi, S., Vanhatalo, A., Toivonen, V., Griinari, J., Huhtanen, P., *J. Nutrition*, **2008**, 710.
- ¹¹Gomez-Romero, P., Jameson, G. B., Casan-Pastor, N., Coronado, E., Beltran, D., *Inorg. Chem.*, **1986**, 25, 3171.
- ¹²McCandlish, E. F. K., Michael, T. K., Neal, J. A., Lingafelter, E. C., Rose N. J., *Inorg. Chem.*, **1978**, 17, 1383.
- ¹³Gluhcheva, G., Madzharova, M., Atanasov, V., Zhorova, R., Mitewa, M., Pavlova, E., Ivanova, Ju., *Acta Morphol. Anthropol.*, **2011**, 17, 89.
- ¹⁴Lison, D., De Boeck, M., Verougstraete, V., Kirsch-Volders, M., *Occup. Environ. Med.*, **2001**, 58, 619.
- ¹⁵Khalil, W., Ahmed, K., Park, M., Kim, Y., Park, H., Abdel-Wahhab, M., *Arch Toxicol*, 2008, 82, 183.
- ¹⁶Hagiwara, M., Watanabe, E., Barrett, J. C., Tsutsui, T., *Mutat Res.*, 2006, 603, 111.
- ¹⁷World Health Organization. In: *Concise Int. Chem. Assessment Document* **2006**, 69, 13.
- ¹⁸Korf, J., Veenma-van der Duin, L., Brinkman-Medema, R., Niemarkt, A., De Leij, L., *J. Nucl. Med.*, **1998**, 39(5), 836.
- ¹⁹Borch-Iohansen, B., Myhre, K., Norheim, G., *Eur J. Haematol.*, **1990**, 44(1), 56.
- ²⁰Gluhcheva, Y., Atanasov, V., Ivanova, Ju., Mitewa, M., *JTEH, Part A*, **2012** (in press)
- ²¹Rossi, E. *Clin. Biochem. Rev.*, **2005**, 26, 47.
- ²²Garoui el, M., Fetoui, H., Ayadi Makni, F., Boudawara, T., Zeghal, N., *Exp. Toxicol. Pathol.*, **2011**, 63(1-2), 9.

Received: 15.10.2012.

Accepted: 11.11.2012.

